

# **The role of CCR10 in cutaneous carcinogenesis**

Inaugural-Dissertation

zur Erlangung des Doktorgrades  
der Mathematisch-Naturwissenschaftlichen Fakultät  
der Heinrich-Heine-Universität Düsseldorf

vorgelegt von

**Stephanie Müller**  
aus Essen

Düsseldorf, August 2019

aus der Klinik für Dermatologie,  
Forschungslabor für Dermato-Immunologie und Onkologie  
Medizinische Fakultät  
der Heinrich-Heine-Universität Düsseldorf

Gedruckt mit der Genehmigung der  
Mathematisch-Naturwissenschaftlichen Fakultät der  
Heinrich-Heine-Universität Düsseldorf

Berichterstatte:

1. Univ.-Prof. Dr. med. Bernhard Homey
2. Univ.-Prof. Dr. rer. nat. Johannes Hegemann

Tag der mündlichen Prüfung: 26.06.2020

*Meinen Eltern  
in Liebe und großer Dankbarkeit  
gewidmet*

## Table of contents

|  |    |
|--|----|
| Abbreviations .....  | VI |
| Summary .....  | 1  |
| Zusammenfassung .....  | 2  |
| 1 Introduction .....   | 3  |
| 1.1 The natural function of the skin .....                                 | 3  |
| 1.2 The structure of the skin .....  | 4  |
| 1.2.1 Epidermis .....  | 4  |
| 1.2.2 Dermis .....   | 7  |
| 1.2.3 Subcutis .....   | 8  |
| 1.2.4 Mouse skin .....   | 9  |
| 1.3 Cutaneous squamous cell carcinoma (SCC) .....                          | 10 |
| 1.4 Chemokines and chemokine receptors .....                               | 12 |
| 1.4.1 The Chemokine receptor CCR10 .....                                   | 15 |
| 1.4.2 The chemokine CCL27 .....  | 17 |
| 1.5 Chemokines and chemokine receptors in cancer .....                     | 18 |
| 1.6 The DMBA/TPA two-stage carcinogenesis model .....                      | 21 |
| 1.7 The UVB-irradiation model of cutaneous carcinogenesis .....            | 24 |
| 1.8 Aims .....   | 26 |
| 2 Material and Methods .....   | 28 |
| 2.1 Mice .....   | 28 |
| 2.2 Buffers and solutions .....  | 28 |
| 2.2.1 Reagents .....   | 28 |
| 2.2.2 DNA Ladder .....   | 29 |
| 2.2.3 Kits .....   | 30 |
| 2.2.4 Instruments .....  | 30 |
| 2.3 Methods .....  | 31 |
| 2.3.1 DMBA/TPA two-stage skin carcinogenesis model. ....                   | 31 |
| 2.3.2 Detailed listing of animal numbers used in DMBA/TPA experiments .... | 32 |
| 2.3.3 Minimal Erythema Dose .....  | 36 |
| 2.3.4 UVB-irradiation of mice .....  | 37 |
| 2.3.5 Detailed listing of animal numbers used in UVB experiments .....     | 38 |
| 2.3.6 Measurement of epidermal thickness .....                             | 41 |

|        |   |     |
|--------|---|-----|
| 2.3.7  | Total DNA Isolation of murine tail tips .....   | 43  |
| 2.3.8  | Polymerase chain reaction (PCR).....  | 44  |
| 2.3.9  | Agarose gel electrophoresis.....  | 46  |
| 2.3.10 | Statistical analysis .....  | 47  |
| 3      | Results .....   | 48  |
| 3.1    | Analysis of the role of CCR10 in cutaneous carcinogenesis in two model systems.....   | 48  |
| 3.2    | Tumor progression in <i>Ccr10</i> -deficient mice is significantly reduced compared to WT controls after DMBA/TPA treatment ..... | 48  |
| 3.3    | Absence of CCR10 signaling decreases cutaneous carcinogenesis in an 'inflammation'-dependent (DMBA/TPA) tumor model.....          | 50  |
| 3.4    | <i>Ccr10</i> -deficiency induces different tumor morphologies compared to WT controls .....                                       | 52  |
| 3.5    | <i>Ccr10</i> -deficient mice do not exhibit reduced nuchal fold thickness to DMBA/TPA administration .....                        | 55  |
| 3.6    | Chronic UVB-irradiation causes a decreased overall survival in <i>Ccr10</i> -deficient mice .....                                 | 58  |
| 3.7    | UVB-irradiation increases tumor burden in the absence of CCR10 signaling<br>60  |     |
| 3.8    | Loss of <i>Ccr10</i> results in morphologically different tumors compared to WT mice in a photocarcinogenesis model .....         | 61  |
| 3.9    | Decreased epidermal thickness in <i>Ccr10</i> -deficient mice is associated with an increased tumor burden .....                  | 64  |
| 4      | Discussion .....  | 67  |
| 5      | References .....  | 86  |
| 6      | List of figures .....   | 103 |
| 7      | List of tables .....  | 104 |
| 8      | Vita .....  | 105 |
| 9      | Publications .....  | 106 |
| 9.1    | Scientific articles.....  | 106 |
| 9.2    | Poster .....  | 106 |
| 10     | Acknowledgements.....   | 107 |
| 11     | Declaration.....  | 108 |

## Abbreviations

### A

|      |  |
|------|--|
| AIDS | acquired immune deficiency syndrome            |
| Arnt | aryl hydrocarbon receptor nuclear translocator |
| ASC  | antibody secreting cell                        |

### B

|        |                      |
|--------|----------------------|
| Balb/c | Bagg albino c        |
| BCC    | basal cell carcinoma |
| B cell | B lymphocyte         |
| bp     | base pair            |
| BSA    | bovine serum albumin |

### C

|                             |   |
|-----------------------------|---|
| C                           | cysteine                                |
| °C                          | degree Celsius                          |
| CAF                         | cancer-associated fibroblast            |
| CCL                         | CC-motif chemokine ligand               |
| CCR                         | CC-motif chemokine receptor             |
| <i>Ccr10</i> <sup>-/-</sup> | <i>Ccr10</i> -deficient                 |
| CD                          | cluster of differentiation              |
| CE                          | cornified envelope                      |
| CI                          | confidence interval                     |
| CLA                         | cutaneous lymphocyte-associated antigen |
| CLL                         | chronic lymphocytic leukemia            |
| cm                          | centimeter                              |
| cm <sup>2</sup>             | square centimeter                       |
| CO <sub>2</sub>             | carbon dioxide                          |
| CTACK                       | cutaneous T cell-attracting chemokine   |
| CTL                         | cytotoxic T lymphocyte                  |
| CX26                        | connexin 26                             |
| CXCL                        | CXC-motif chemokine ligand              |
| CXCR                        | CXC-motif chemokine receptor            |

---

|                     |   |
|---------------------|---|
| CX3CL               | CX <sub>3</sub> CL-motif chemokine ligand   |
| CX3CR               | CX <sub>3</sub> CR-motif chemokine receptor |
| <b>D</b>            |   |
| Δ                   | delta                                       |
| d-x                 | day x                                       |
| Da                  | Dalton                                      |
| DC                  | dendritic cell                              |
| DEPC                | diethylpyrocarbonate                        |
| Dept.               | Department                                  |
| dH <sub>2</sub> O   | distilled water                             |
| DLN                 | draining lymph node                         |
| DMBA                | 7,12-Dimethylbenz(a)anthracene              |
| DNA                 | deoxyribonucleic acid                       |
| DNFB                | 2,4-Dinitro-1-fluorbenzol                   |
| dNTP                | deoxyribonucleotide triphosphate            |
| DSO                 | Düsseldorf School of Oncology               |
| <b>E</b>            |   |
| ECM                 | extracellular matrix                        |
| EDC                 | epidermal differentiation complex           |
| EDTA                | Ethylenediaminetetraacetic acid             |
| e.g.                | for exsample                                |
| EGF                 | epidermal growth factor                     |
| EGFP                | enhanced green fluorescent protein          |
| EGFR                | epidermal growth factor receptor            |
| EGFR <sup>Δep</sup> | EGFR deletion in the epidermis              |
| EGFRI               | epidermal growth factor receptor inhibitor  |
| ELR                 | glutamic acid-leucine-arginine              |
| EPI                 | envoplakin, periplakin, and involucrin      |
| Erk                 | extracellular-signal regulated kinase       |
| ESDR                | European Society for Dermatology Research   |
| <i>et al.</i>       | et alii, and others                         |

**F**

|       |                          |
|-------|--------------------------|
| fg    | femtogram                |
| FGF   | fibroblast growth factor |
| Fig.  | Figure                   |
| FoxP3 | Forkhead-Box-Protein P3  |

**G**

|                    |                                     |
|--------------------|-------------------------------------|
| g                  | gram                                |
| $\gamma\delta$ TCR | gamma delta t cell receptor         |
| GGT                | $\gamma$ -glutamyl transpeptidase   |
| Glu-Leu-Arg        | glutamic acid-leucine-arginine      |
| GPCR               | G protein-coupled receptor          |
| G-protein          | guanine nucleotide-binding-proteins |

**H**

|                  |                                   |
|------------------|-----------------------------------|
| h                | hour                              |
| HCL              | hydrogen chloride                 |
| H&E              | hematoxylin and eosin             |
| HEV              | high endothelial venules          |
| HIV              | human immunodeficiency virus      |
| H <sub>2</sub> O | hydrogen oxide, water             |
| HPV              | human papillomasvirus             |
| HRAS             | Harvey rat sarcoma viral oncogene |
| HYA              | hyaluronan                        |

**I**

|                |                           |
|----------------|---------------------------|
| Ig             | immunoglobulin            |
| IL             | interleukin               |
| ILC            | innate lymphoid cell      |
| INF- $\gamma$  | interferon gamma          |
| INF $\gamma$ R | interferon gamma receptor |

**K**

|   |         |
|---|---------|
| K | keratin |
|---|---------|



---

|                   |                                    |
|-------------------|------------------------------------|
| kDa               | kilodalton                         |
| kg                | kilogram                           |
| KO                | knockout                           |
| <b>L</b>          |                                    |
| L                 | ligand                             |
| LC                | Langerhans cell                    |
| LE                | lupus erythematosus                |
| <b>M</b>          |                                    |
| μ                 | micro                              |
| M                 | molar                              |
| m <sup>2</sup>    | square meter                       |
| MAPK              | mitogen-activated protein kinases  |
| max               | maximum                            |
| mCCL27            | mouse CC-motif chemokine ligand 27 |
| MED               | minimal erythema dose              |
| μg                | microgram                          |
| mg                | milligram                          |
| MgCl <sub>2</sub> | magnesium chloride                 |
| min               | minute/ minimum                    |
| mJ                | millijoule                         |
| μl                | microliter                         |
| ml                | milliliter                         |
| μm                | micrometer                         |
| mm                | millimeter                         |
| mm <sup>3</sup>   | cubic millimeter                   |
| mM                | millimolar                         |
| mRNA              | messenger RNA                      |
| MSC               | mesenchymal stem cell              |
| mW                | milliwatt                          |
| <b>N</b>          |                                    |
| n                 | number                             |

---

|       |                            |
|-------|----------------------------|
| NaCl  | sodium chloride            |
| NK    | natural killer             |
| nm    | nanometer                  |
| NMSC  | nonmelanoma skin cancer    |
| n.s.  | not significant            |
| NSCLC | non-small cell lung cancer |

**O**

|        |                             |
|--------|-----------------------------|
| O.C.T. | optimal cutting temperature |
| OTR    | organ transplant recipient  |

**P**

|                  |                                |
|------------------|--------------------------------|
| %                | percentage                     |
| P                | probability                    |
| PAS              | Per-Arnt-Sim                   |
| PCR              | Polymerase chain reaction      |
| pDC              | plasmacytoid dendritic cell    |
| PDGF             | platelet-derived growth factor |
| pErk             | phosphor-Erk                   |
| PGE <sub>2</sub> | prostaglandin E <sub>2</sub>   |
| pH               | potential hydrogenii           |
| pmol             | picomole                       |

**R**

|      |   |
|------|---|
| R    | receptor                                    |
| Rag2 | recombination activating gene 2 protein     |
| RAGE | receptor for advanced glycation endproducts |
| Ras  | rat sarcoma                                 |
| RNA  | ribonucleic acid                            |
| ROS  | reactive oxygen species                     |
| rpm  | revolutions per minute                      |
| RT   | room temperature                            |

**S**

|       |  |
|-------|--|
| SCC   | squamous cell carcinoma                          |
| SD    | standard deviation                               |
| sec   | second   |
| SEM   | standard error of the mean                       |
| shRNA | small hairpin RNA                                |
| STAT  | signal transducer and activator of transcription |

**T**

|               |                                      |
|---------------|--------------------------------------|
| Tab.          | table                                |
| TAE           | Tris-acetate-EDTA                    |
| TAM           | tumor-associated macrophage          |
| TAN           | tumor-associated neutrophil          |
| Taq           | Thermus aquaticus                    |
| T cell        | T lymphocyte                         |
| Teff          | effector T cell                      |
| TGF           | transforming growth factor           |
| Th            | T helper cell                        |
| TNF- $\alpha$ | tumor necrosis factor- $\alpha$      |
| TPA           | 12-0-Tetradecanoylphorbol-13-acetate |
| Treg          | regulatory T cell                    |

**U**

|     |                          |
|-----|--------------------------|
| U   | unit                     |
| UCA | urocanic acid            |
| USA | United States of America |
| UV  | ultraviolet              |

**V**

|       |                                      |
|-------|--------------------------------------|
| V     | volt                                 |
| VEGF  | vascular endothelial growth factor   |
| VEGFA | vascular endothelial growth factor A |
| Vol.  | volume                               |

**W**

WT                      wildtype

**X**

XCL                    XC-motif chemokine ligand

XCR                    XC-motif chemokine receptor

**Z**

ZETT                   *Zentrale Einrichtung für Tierforschung und  
Tierschutzaufgaben*

## Summary

The activation of the EGFR/Ras signaling pathway plays an important role in cutaneous carcinogenesis. In particular, it regulates the expression of several chemokines, which in turn modulate the tumor microenvironment. Chemokines and their receptors are interesting pharmacological targets.

In this work the role of CCR10 signaling was investigated by taking advantage of an inflammation-driven cutaneous carcinogenesis 7,12-Dimethylbenz(a)anthracene/12-O-Tetradecanoylphorbol-13-acetate (DMBA/TPA) model compared to an immunomodulation-associated UVB-induced skin carcinogenesis model. *Ccr10*-deficient mice in a DMBA/TPA carcinogenesis model show a significantly lower number of tumors and the tumor growth is inhibited. Hence, the tumor-free survival of *Ccr10*-deficient mice in the inflammation-driven DMBA/TPA skin carcinogenesis model is significantly increased. Skin thickness measurements as a marker for cutaneous inflammation show no significant differences in *Ccr10*-deficient versus wildtype mice.

In contrast to the inflammation-driven DMBA/TPA model, *Ccr10*-deficiency resulted in an increased tumor growth, accompanied with decreased overall survival, in an immunomodulation-associated UVB-induced skin carcinogenesis model. In further analyses, *Ccr10*-deficient mice showed a reduced UVB-induced epidermal thickening (acanthosis) when compared to wildtype mice.

Taken together, results of the present study demonstrate a context-dependent role of CCR10 in cutaneous carcinogenesis. Further analyses have to unravel the underlying mechanisms of CCR10. Finally, findings of the present study suggest that potential pharmacological targets should be evaluated in different tumor models and context-dependent indications could be relevant.

## Zusammenfassung

Für die Entstehung von Plattenepithelkarzinomen der Haut ist die Aktivierung des EGFR/Ras Signaltransduktionswegs von großer Bedeutung, unter anderem werden dadurch zahlreiche Chemokine reguliert, die das Tumormikromilieu modulieren. Chemokine und ihre Rezeptoren stellen interessante pharmakologische Ziele dar.

In dieser Arbeit wurde die Rolle des Chemokinrezeptors CCR10 auf die spontane, kutane Karzinogenese in zwei *in vivo*-Mausmodellen untersucht. In einem entzündungsgetriebenen 7,12-Dimethylbenzo(a)anthracen/12-O-Tetradecanoylphorbol-13-acetat (DMBA/TPA)-Modell zeigen die *Ccr10*-defizienten Mäuse im Vergleich zu Wildtyptieren eine signifikant reduzierte Tumoranzahl und eine signifikant reduzierte Tumorgroße. Dies resultiert in einer signifikant erhöhten tumorfreien Überlebensrate der *Ccr10*-defizienten Mäuse im DMBA/TPA-Modell. In der Hautdickenmessung, als Maß für die lokale Entzündungsreaktion in der Haut, zeigen *Ccr10*-defiziente im Vergleich zu Wildtyptieren keinen Unterschied.

Im Gegensatz zum entzündungsgetriebenen DMBA/TPA-Modell zeigten die *Ccr10*-defizienten Mäuse in einem immunmodulationsgetriebenen UVB-induzierten kutanen Kanzerogenesemodell ein erhöhtes Tumorwachstum, begleitet von einer signifikant niedrigeren Gesamtüberlebensrate. In weiteren Untersuchungen zeigte sich in *Ccr10*-defizienten im Vergleich zu Wildtyptieren eine geringere Zunahme der Epidermisdicke (Akanthose) unter chronischer UVB-Bestrahlung.

Zusammenfassend unterstreichen die Ergebnisse der vorliegenden Arbeit eine kontextabhängige Rolle von CCR10 in der kutanen Kanzerogenese. Weiterführende Untersuchungen müssen nun die zugrundeliegenden CCR10-vermittelten Mechanismen aufklären. Abschließend weisen die Daten der Arbeit daraufhin, dass potentielle pharmakologische Ziele in unterschiedlichen Tumormodellen getestet werden sollten und kontextabhängige Indikatoren relevant sein können.

# 1 Introduction

## 1.1 The natural function of the skin

The skin (cutis) is the largest organ of the human body with a total area of 1.5 - 2 m<sup>2</sup>, a weight of 3 - 10 kg, and a skin thickness of 1.5 - 4 mm [1, 2]. It has several important functions, which can be divided into passive and active functions (Tab. 1.1) [1]. The skin is able to offer protection against mechanical influences through its elasticity and against ultraviolet radiation (UV-radiation) through reflection and absorption [2, 3]. Other physiological protections against UV-radiation are the formation of a light callus by acanthosis and hyperkeratosis of the epidermal compartment, melanin synthesis, antioxidants, and the repair of DNA damage due to UV-radiation [2]. The controlled release of fluid, salts, and minerals by glands protect the skin against dehydration [2, 4]. Body temperature regulation takes place by vasoconstriction of blood vessels in the skin followed by diffusion of fluid to the skin surface and through sweating [2, 4]. Additionally, the protection of the skin against chemical and microbial influences by cornification of the epithelial tissue and the glandular secretion (e.g. the fat content of the skin and the acid mantle of the skin pH 5.7) is one of the most important functions [1, 2, 4]. If this protective barrier of the skin is destroyed and pathogens or molecules are able permeate the body, the skin can initiate immune responses [2]. The first step is, the initiation of innate immune responses by activation of macrophages and granulocytes to create an inflammatory reaction [2]. This is followed by the initiation of adaptive and specific immune responses characterized by T- and B-lymphocytes after antigen presentation in draining lymph nodes [2].

| Passive functions of the cutis                        | Active functions of the cutis  |
|---|--|
| Protection against chemical and mechanical influences | Sensory perception of contact, pressure, vibration, pruritus, temperature and pain |
| Protection against radiation                          | Resorption of active substances  |
| Protection against dehydration                        | Delivery of sebum and sudor  |
| Temperature regulation                                | Thermoregulation by blood circulation  |
| Protection against viruses, bacteria and allergens    | Initiation of immune responses   |

**Table 1.1** Passive and active functions of the skin.

## **1.2 The structure of the skin**

The human skin is an organ, which is structured in three compartments: (1) the epidermis characterized by multilayered keratinized squamous epithelium, (2) the dermis consisting of concentric sheets of collagen and elastic fibers, and (3) the subcutis, which is firmly connected to the dermis (Fig. 1.2) [1, 4]. The epidermis and the dermis are also collectively referred to as cutis [4]. Normal skin contains abundant stores of T lymphocytes [5] as well as resident populations of dendritic cells (DCs) [6], suggesting its potential for mediating immune responses [7]. During inflammation, keratinocytes release various immune related cytokines and chemokines, which can activate the immune system and induce the recruitment of additional T cells and DCs [7].

### **1.2.1 Epidermis**

The epidermis of the skin is located at the surface of the body and functions as a protective barrier, where pathogens like microbes and toxic substances are kept out and necessary body fluids are retained inside [8, 9]. The epidermis is a multilayered, keratinized, squamous epithelium formed by keratinocytes [1] with a thickness of 30 - 300  $\mu\text{m}$  (Fig. 1.1) [2]. Additionally, pigmented cells (melanocytes), skin-associated immunocompetent cells (Langerhans cells) as well as occasional Merkel disks, specialized on pressure reception, are located in the basal membrane [1, 10]. Additionally, stem cells of the epidermal basal membrane are important for proliferation and, therefore, skin renewal [1, 2]. Epithelia are classified into three main classes based on their morphology and differentiation program [11]. The three main classes are defined by (1) the keratinization of stratified squamous epithelia, which can be found in the epidermis, palate, and in the gingival tissue of the oral cavity; (2) stratified epithelia without any keratinization like the buccal oral mucosa and the esophagus; or (3) as simple, non-stratified cell layers which can be observed in the kidney and liver [11]. In contrast to the keratinized epithelium of the skin, the mucosa holds neither a horny layer nor hair [1]. Moreover, mucosae provide secretion and resorption processes, contain lymphocytes and are able to produce and secrete immunoglobulin and thereby create a protective barrier against pathogens [1]. The epidermis contains many nerve endings, however it has no blood or lymph vessels [2]. Therefore, nutrients need to diffuse from the dermis into the epidermis [2]. The epidermis consists of a multilayered epithelium [1], containing the following structures



from the outside to the inside: The stratum corneum, which forms the major barrier of the epidermis [9] and which consists of dead corneocytes [2]. The lowest cell layer of the stratum corneum is the one-layered stratum lucidum, which is markedly thicker at the hairless skin of the palm and the bottom of the feet [2]. Next, is the stratum granulosum with keratinocytes containing basophilic keratohyalin granules, which produce important structural proteins of the cornified envelope (CE) [1], followed by the stratum spinosum consisting of spinous cells, which contain a cytoskeleton of K1/K10 filament bundles to provide the mechanical strength necessary to resist physical trauma [8, 9]. The spinous cells are connected to each other through desmosomes [8]. The lowest layer of the epidermis is the one-layered stratum basale, which contains epidermal stem cells and functions as the barrier between the epidermis and the underlying dermis [1]. Environmental cues are the reason for epidermal stem cells to differentiate and form a stratified epidermis, hair follicles or sebaceous glands [8]. Moreover, the stem cells undergo continual self-renewal to repair damaged tissue and replace old cells, received through harmful assaults like UV-radiation, scratches, and wounds [8]. Epidermal growth and proliferation is a complex system, which is tightly balanced: inadequate proliferation results in thinning of the skin followed by the loss of protection, while excessive proliferation is characteristic for hyperproliferative disorders, for example psoriasis and cancers [8]. Under homeostatic conditions, the epidermis must be able to sense damage to the basal layer and when gaps occur through wounding, cells are recruited to the damaged tissue and proliferate to establish wound healing [8]. After wound healing has occurred, the epidermis has to sense the wound closure and give a signal to cease proliferation [8]. Finally, the SOS system of the epidermis is able to balance between the activation and recruitment of immune cells during infection and its impact in wound repair on the one hand, but on the other hand it has to stop signaling to turn off the recruitment of immune cells once the wound is closed [8]. In the basal layer, stem cell proliferation seems to be asymmetric, leading to one proliferative daughter cell [8], which migrates from the stratum basale outwards to the stratum corneum, and one detached suprabasal daughter cell, which remains in the basal layer and proliferates again [4]. During the process of continual skin self-renewal, the dividing cells undergo programs of terminal differentiation, while they move outwards and are sloughed from the skin [8]. Terminal differentiation ends with the deconstruction of cellular organelles like the nucleus, and lipid membranes are

packaged in lamellar granules to transport them to the cornified envelope [8]. During terminal differentiation, when cells migrate from the basal layer towards the skin surface, they change their expression pattern from the expression of keratins K14 and K5 to K1 and K10 [8, 12]. In humans, the epidermal self-renewal takes place every 4 weeks [1, 8]. A key to basal cell proliferation is the basal membrane, located between the epidermis and the dermis, which contains extracellular matrix (ECM) proteins and growth factors [8]. Basal cells adhere to one another through desmosomes and adherens junctions [8]. Adherens junctions act as sensors for basal cell density, which is important for mediating cell migration and proliferation and the recruitment of immune cells in the case of low basal cell density, e.g. in a wound [8]. After wound closure and the re-establishment of optimal junction formation, cell migration is stopped and proliferation returns to homeostatic levels [8]. Melanocytes migrate originally from the neural crest to the basal membrane of the epidermis and the hair follicle [2]. These cells form dendrites and contain melanosomes in which they synthesize and store melanin [2]. Melanocytes deliver their synthesized melanin to neighboring keratinocytes [2]. They can be activated through various factors but the most important inductor is radiation from the sun [1]. Especially UVB-irradiation leads to increased pigmentation, damaged DNA, and induction of DNA repair mechanisms [1]. While the number of melanocytes is always the same regardless of skin type [1], pigmentation of the skin is determined by their ability to produce melanin [1]. Merkel disks also originally migrate from the neural crest to the basal membrane and contain neurosecretory granules [1, 2]. They are attached to neighboring keratinocytes via desmosomes [1] and mediate tactile sensation [2]. Langerhans cells (LCs) are immunocompetent cells of the epidermis [1]. They are important for antigen presentation and the activation of T cells [1]. They are characterized by Birbeck granules and express CD1a on their cell surface [2]. There are also a few T cells in the epidermis, but they are predominately located in the stratum papillare of the dermis and interact with LCs [2].

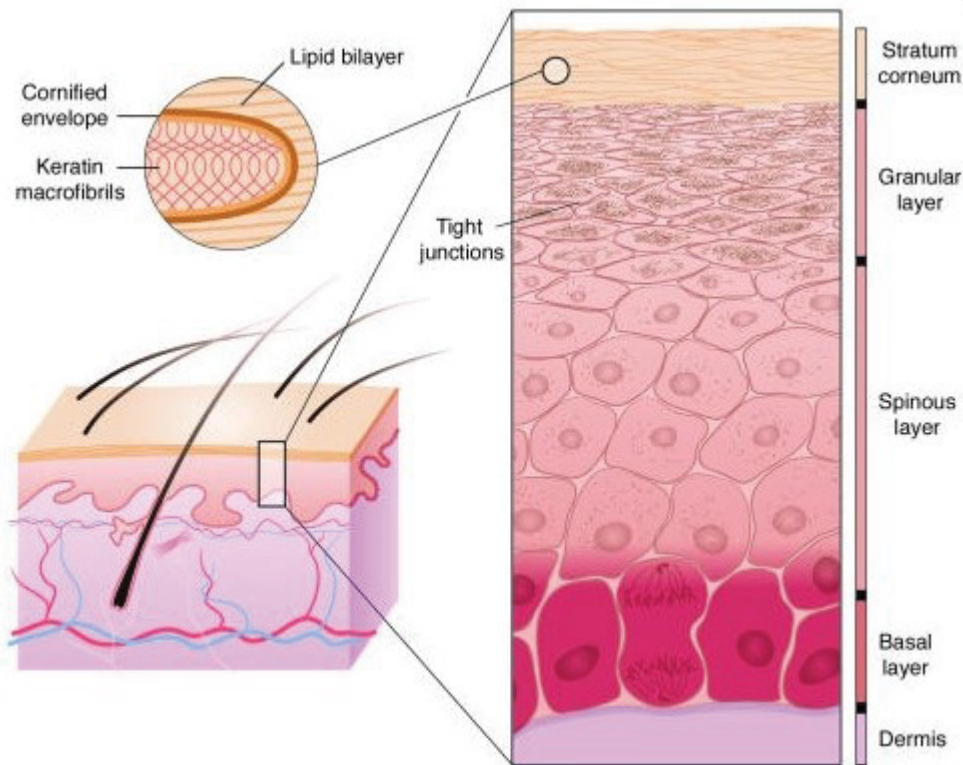


**Figure 1.1** Epidermal layers of human skin. Adapted from [9] with kind permission from the author.

### 1.2.2 Dermis

The dermis (corium) is located between the epidermis and adipose connective tissue of the subcutaneous layer [1, 2]. It consists of fibroelastic tissue [13]. The area between the epidermis and the dermis is called dermo-epidermal junction [1]. In this area, the basal membrane of the epidermis, consisting of the lamina lucida and the lamina densa, is connected to the dermis by rete ridges and anchoring fibrils [1]. The dermis consists of two layers, the stratum papillare (papillary layer) and the stratum reticulare (reticular layer) [1, 2]. The stratum papillare forms the upper part of the dermis, which is directly attached to the basal membrane of the epidermis [1, 2]. The connective tissue matrix is composed of loose elastic fibers intermixed with fibroblasts and collagen (consisting mainly of collagen type III), additionally a network of capillaries functions as regulatory system for body temperature and supply the cells of the epidermal compartment with essential nutrients [13]. Furthermore the stratum papillare contains many cells: (1) histiocytes are tissue macrophages which have an immunological function [2], (2) Mast cells are immunocompetent cells which store histamine, serotonin, and heparin in their granules and mediate allergic and inflammatory reactions [2], and (3) Meissner corpuscles, located in some papillae and

especially numerous in the lips, external genitalia, and nipples, which contain mechanoreceptors mediating tactile stimuli of slight deformations of the epidermal compartment [13]. The stratum reticulare is located under the stratum papillare and is a mixture of dense connective tissue, mainly type I collagen fibers bundles with elastic fibers and fibroblasts [1, 13]. Whereas there are many cells in the stratum papillare, the stratum reticulare contains fewer cells, mainly a few melanocytes and T-lymphocytes [2]. Additionally, hair follicles, sebaceous glands, and sweat glands are located in this layer [1]. The mechanoreceptors of Pacinian corpuscles are located in deeper parts of the dermis close to the subcutis and signal to pressure stimuli [13]. The ECM of the connective tissue is established by fibroblasts [1]. It consists of collagen fibers, reticulin fibers, and elastic fibers [1, 2]. Collagen fibers are important for the mechanical stability of the dermis [2] and elastic fibers are important for the elasticity of the dermis [1]. Hyaluronan (HYA), a straight chain of glycosaminoglycan polymer is a component of the ECM [14] in loose connective tissues [15]. Bindings of HYA with proteoglycans stabilize the structure of the ECM and interactions of both kinds with cell surfaces modify cell behavior [15]. Because of its osmotic activity, HYA has an important impact on the distribution of water in tissue and plays a major role in water homeostasis [15, 16]. An important property of hyaluronan in its hydrated state is its visco-elasticity [15]. Moreover, hyaluronan is located in small volumes of liquid in the serous cavities and in regions of tissue movement between muscle bodies and skin [15, 16]. The enrichment of HYA in the ECM is closely related to embryonic development, some forms of tissue injury, immune reactions, inflammation, and cancer development [15, 16]. The reduction of elastic fibers during aging causes the age-related atony of the skin [2].

### **1.2.3 Subcutis**

The subcutis, also called hypodermis, is the deepest layer of the skin and is mainly composed of large pads of adipose tissue [13]. It is located beneath the stratum reticulare of the dermis and serves as thermal insulation, storage of energy, and mechanical protection [1, 13]. It is only loosely attached to the deep fascia or periosteum and therefore it gives the skin its ability to slide over them [13]. Adipose tissue cannot be found in the subcutis of the eyelids, clitoris, or penis [13]. Situated between the hypodermis and the cutis is a broad capillary network [4, 13] to supply

the skin with nutrients and to regulate temperature and blood pressure of the body [2].

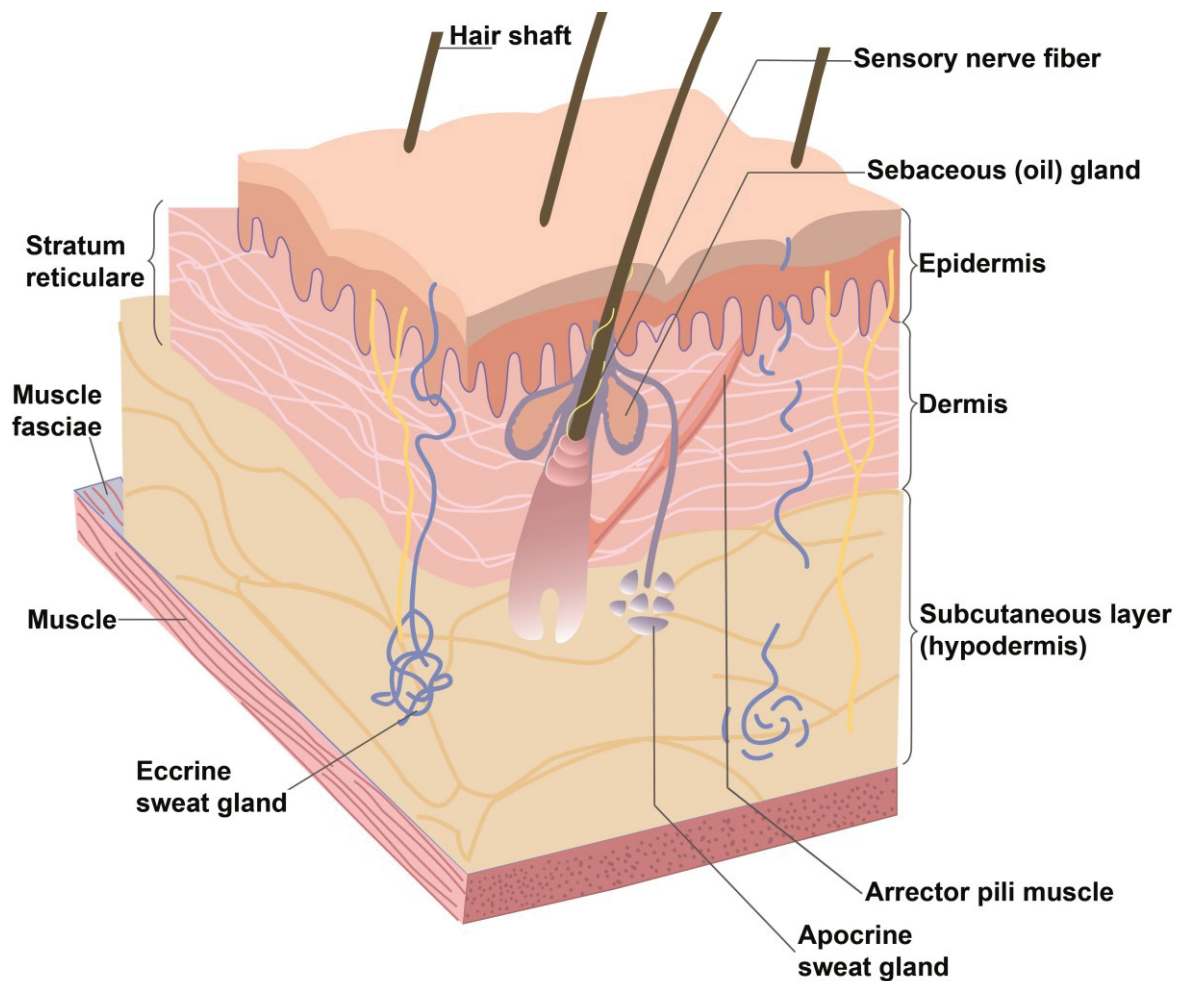


**Figure 1.2** Structure of the human skin.

#### 1.2.4 Mouse skin

Although the general structure of mouse skin is comparable to human skin, there are a few differences, mainly in the number of cell layers in the epidermis and dermis [7]. In the stratum corneum, in contrast to human skin (16 to 18 layers), mouse skin has only 6 to 7 layers [17]. The squames in the upper layer of the dorsal mouse epidermis constitute of ordered columns that are connected to cells in the basal layer [18]. Characteristic for dorsal mouse epidermis is that it has only a few (2) living cell layers and therefore it is accordingly flat, whereas human epidermis consists of many cell layers, the skin surface is also flat, but the basal layer undulates [18]. Additionally, the epidermal rete of human epidermis is absent in mouse skin [7]. In contrast to human skin, mouse skin is tightly packed with hair follicles (Fig. 1.3) [7]. The repair



mechanism of the skin barrier is much shorter in mice (24h) compared to humans (60 – 80h) [17]. Moreover, skin barrier homeostasis is more robust in mice than in humans, because environmental influences on the skin are less harmful for survival in humans [17]. Reasons for this are the ability of humans to protect their skin against environmental influences through clothing and additionally, humans can control their macroenvironment by their choice of housing, which can alleviate the effect of radiation, temperature, and humidity [17]. Increasing skin care and better living conditions lead to an enhanced development of sensitive skin [17]. Even though there are some structural differences of mouse skin compared to human skin, animal models are important to determine complex immune reactions to skin carcinogenesis.

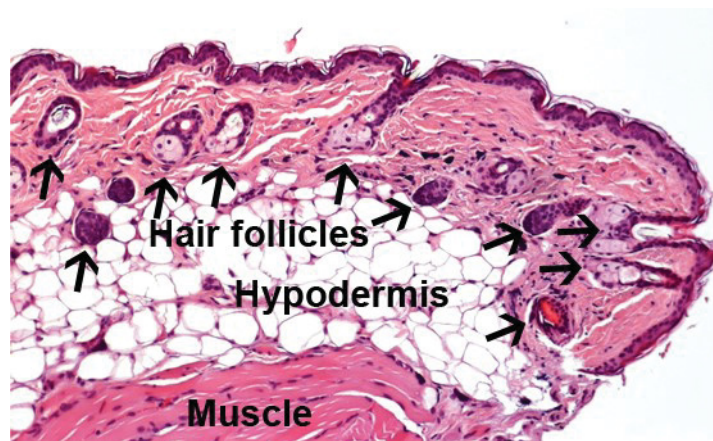


**Figure 1.3** Normal mouse skin. Image of a normal Balb/c mouse skin. Haematoxylin & eosin staining (paraffin section in a 100x magnification). Hair follicles are marked with black arrows.

### 1.3 Cutaneous squamous cell carcinoma (SCC)

Squamous cell carcinoma (SCC) and basal cell carcinoma (BCC) belong to the nonmelanoma skin cancers (NMSCs) and represent the most common cancers in fair skinned populations [19]. The incidence of NMCSs are valued at over 150 cases per 100.000 inhabitants in Germany [20, 21] and represent the most common form of cancer in North Rhine-Westphalia (Datenreport 2012, epidemiologisches Krebsregister Nordrhein-Westfalen). Observations over the last 40 years show that the incidence rates of NMSCs have increased over time [19]. Cell damage conducive to the initialization of SCC is introduced by the exposure to UV-radiation, followed by long-term sun exposure resulting in SCC development [19, 22, 23]. In addition, low levels of sun protection (clothing, sunscreen), latitude, use of sunbeds, specific

carcinogens (e.g. arsenic, tobacco), chronic wounds, and inflammatory skin diseases (e.g. ulcers, burns, scars, lichenoid diseases, and bullous skin disease) or immunosuppression (e.g. human immunodeficiency depending on viral infections or organ transplantation) increase the risk of NMSC and especially of SCCs development [19, 24-27]. Furthermore, fair skin types with reduced tanning ability have an increased risk to develop skin cancer [28, 29]. Interestingly, the highest incidence rates of skin cancer is found in Australia [30]. This effect is caused by (1) depletion of the ozone layer with the most impact at the polar regions, which is responsible for an increase in UVB-radiation [30], and (2) an unnatural migration of fair skin people to subtropical regions [30]. UV-radiation is directly associated with the climate [30, 31]. Populations living in middle latitudes, like Australia, tend to spend more time outside with inappropriate clothes due to the pleasant temperature followed by increased UV-exposure [30, 31]. People living in climate zones with temperatures under 18°C or over 27°C have a different behavior of clothing, spend more time inside or seek shade [30, 31]. This effect can be observed for example in the incidence rates of NMSC development between Australia and Scotland with a difference of 10-fold according to their latitude [19, 29, 32]. Additionally, the incidence rates for developing a NMSC are significantly higher in men than in women and increase with age, which might be a result of traditional role differences whereby men spend much more time outside either by choosing outdoor professions or hobby activities and use less sunscreen than women, leading to higher UV-radiation of the skin and NMSC development [19, 33]. 20% of NMSCs are represented by SCC [34], the second most common tumor in the Caucasian population in which 5% of cancer patients are observed with metastatic formations [26, 35]. The risk of SCC metastasis formation significantly increases in tumors with a thickness larger than 2.0 mm [22]. In tumors with a thickness over 6.0 mm the risk for metastasis formation is high and local relapse is a common occurrence [22]. The beginning of SCC development is characterized by the disorganization of the epidermal compartment and morphological changes of cells [26]. In the development of human cutaneous SCC, alterations in the following genes are known: *ras*, *c-jun*, *c-fos*, *c-myc* gene mutations [36], and, especially, a mutation of the *p53* tumor suppressor gene is observed in 40 – 50% of patients [34, 37, 38]. All the genes mentioned above are key players in the regulation of important cell signaling pathways, controlling cell proliferation, differentiation, survival or apoptosis and are found to be mutated in response to

chronic UVB-irradiation, the major risk factor for SCC development [36]. Moreover, solid organ transplant patients, who are immune-compromised due to immunosuppressive regimens against rejection reactions, have a 65-fold to 250-fold higher risk to develop SCC and metastasis [22, 39-41]. Lymphatic cellular infiltrates with SCCs have been associated with smaller tumors, whereas lack of inflammation was detected in invasive and aggressive tumors as mentioned in cases of chronic lymphocytic leukemia (CLL) [42]. Pivarcsi *et al.* showed that NMSCs inhibit T cell-mediated antitumor immune responses through activation of the EGFR-Ras-MAPK-signaling pathway, leading to downregulation of CCL27 mRNA and protein expression [43]. Furthermore, they reported that blocking of CCL27 function results in decreased leukocyte migration into the tumor environment and significantly increase tumor growth [43]. Other groups associated chronic skin inflammation with the development of SCCs and tumor progression [44]. Based on this understanding that the host immunity regulates tumor growth and progression in SCC, it is important to understand the mechanism of tumor-associated immune regulation [45].

#### **1.4 Chemokines and chemokine receptors**

Chemokines are a group of small, secreted molecules (8-14 kDa) that regulate, along with adhesion molecules, cell trafficking of specific leukocyte subpopulations to sites of tissue damage, through interactions with a subset of seven-transmembrane, G protein-coupled receptors (GPCRs) [46-48]. They are abundantly produced by cells that express them and mainly act on neutrophils, monocytes, lymphocytes, and eosinophils and play fundamental roles in host defense mechanisms, development, homeostasis, and in functions of the immune system [47, 48]. Chemokines are often highly expressed and build concentration gradients, along which specific responding cell populations migrate [48]. However, chemokines and their receptors are also important in lymphoid organ development, lymphoid trafficking, wound healing, Th1/Th2 development and responses, angiogenesis, and disease processes, including inflammation, autoimmune disease, infectious disease (such as HIV/AIDS and HPV) and cancer (in regulating tumor growth and metastasis formation) [46, 48]. The human chemokine superfamily includes at least 50 chemokines [49] and is classified into four subclasses of chemokines, due to the location of their first N-terminal cysteine residues, which are CC, CXC, XC and CX3C, where the X in the classification name denotes the position and number of other amino acid residues in



relation to the cysteines [50]. The nomenclature of chemokines uses the subclass name, followed by an R for receptor or an L for ligand and then a number specific to a single chemokine [47]. The two major chemokine subfamilies (CC and CXC) are composed of several family members, whereas the other two chemokine classes contain only two family members in the case of the XC family and only one in the case of the CX3C family, where CX3CL1 is the only known family member (Fig. 1.4) [47, 50, 51]. Moreover, the chemokine genes are located in distinct chromosomal sites, which assemble into two large gene clusters, one for CXC chemokines, which is located at chromosome 4q13.3 in humans, and another for CC chemokines clustered in the human chromosome 17q12 [50]. The majority of these chemokines are characterized as inflammatory, due to their important roles during inflammatory processes, where they recruit leukocytes to sites of tissue damage [50]. An explanation for the redundancy of the ligands to receptor pairings could be that, during inflammation, multiple chemokines might be needed to induce a robust inflammatory response [48]. Furthermore, chemokines are differentially expressed based on the site of tissue origin and are able to orchestrate the recruitment of leukocytes to the specific tissues, thereby allowing for a customization of inflammatory responses [48]. In contrast, non-cluster or mini-cluster chemokines, whose genes are located separately in unique chromosomal locations are conserved between species and many of them exhibit highly restricted ligand-receptor relationships [48, 50]. These homeostatic chemokines are constitutively expressed and their expression is restricted to specific cells or organs, so that each human chemokine of this type has a clearly identifiable mouse counterpart, as in the case of CCL27 [48, 50]. Homeostatic chemokines recruit subsets of lymphocytes or dendritic cells to specific healthy tissues, where they act as surveillance as part of the acquired immunity, while inflammatory chemokines are expressed after activation and mainly attract macrophages or neutrophils [50]. Additionally, homeostatic chemokines recruit leukocytes under steady state conditions, whereas inflammatory chemokines are produced at sites of infection and disease and are able to react to stimuli with the recruitment of effector cells [52]. Homeostatic chemokines are known to play major roles in organogenesis of immune specific organs such as lymph nodes [50]. Other important examples for homeostatic chemokines are CXCL12 and CCL21. CXCL12 is the only ligand for CXCR4 [53-55]. This ligand-receptor pair is crucial for organogenesis, homing and repopulation of human stem cells into the bone marrow

[54, 56-58]. This is exemplified in mice, where *Ccxr4*- and *Cxcl12*-deficiency is lethal and results in abortion due to defects in organs such as the heart, brain or bone marrow during organogenesis [48]. CXCL12 also has a pivotal role in homing of immune cells to the skin due to its ubiquitous tissue expression and that its only receptor is expressed on all circulating leukocytes [52]. The chemokines CCL19 and CCL21 are both binding to chemokine receptor CCR7 and play an important role for the recruitment of lymphocytes and dendritic cells into secondary lymphoid organs, where CCL19 and CCL21 are expressed [50, 54]. Moreover, both are expressed in T cell zones of secondary lymphatic tissues, whereas only CCL21 is expressed by high endothelial venules (HEV) and on afferent lymphatic vessels [50]. In contrast, only CCL19 is able to desensitize and internalize CCR7 [50]. Therefore, CCR7 expressing lymphocytes and dendritic cells are recruited into lymph nodes by a gradient of CCL21 and T cell zones via HEVs and afferent lymphatics [50]. CCL19 has to override CCL21-mediated cell recruitment, followed by CCR7 downregulation to guide B and follicular helper T cells into B cell zones via CXCL13/CXCR5 signaling [50, 59]. The effects of chemokines are mediated through GPCRs and, they are grouped in to their respective chemokine subfamilies [50]. Just like the chemokines themselves, chemokine receptors also tend to be present in gene clusters [50]. The largest chemokine receptor cluster is found on human chromosome 3 [50]. Chemokine receptors of inflammatory chemokines tend to be promiscuous, meaning that one chemokine can interact with several receptors, while a single chemokine receptor can mediate signals for more than one chemokine [47, 50]. 18 chemokine receptors have been found in humans and mice [50]. Additionally, 5 atypical chemokine receptors were discovered [50]. The interaction of chemokine receptors and adhesion molecules enable a distinct tissue recruitment and provide 'distinct address codes' deciding which leukocytes subsets remain in circulation, are recruited to secondary lymphoid organs or to peripheral tissues [52]. Taken together, chemokines are mediators to control immune and inflammatory responses and as a consequence have a strong therapeutic potential, mainly in cancer [46, 47]. To date, there are two main therapeutic areas of application for chemokine receptor inhibition, (1) targeting of CCR5 to reduce HIV infection and (2) targeting of CXCR4 to release bone marrow stem cells into the bloodstream for harvesting cells for bone marrow transplants [55].

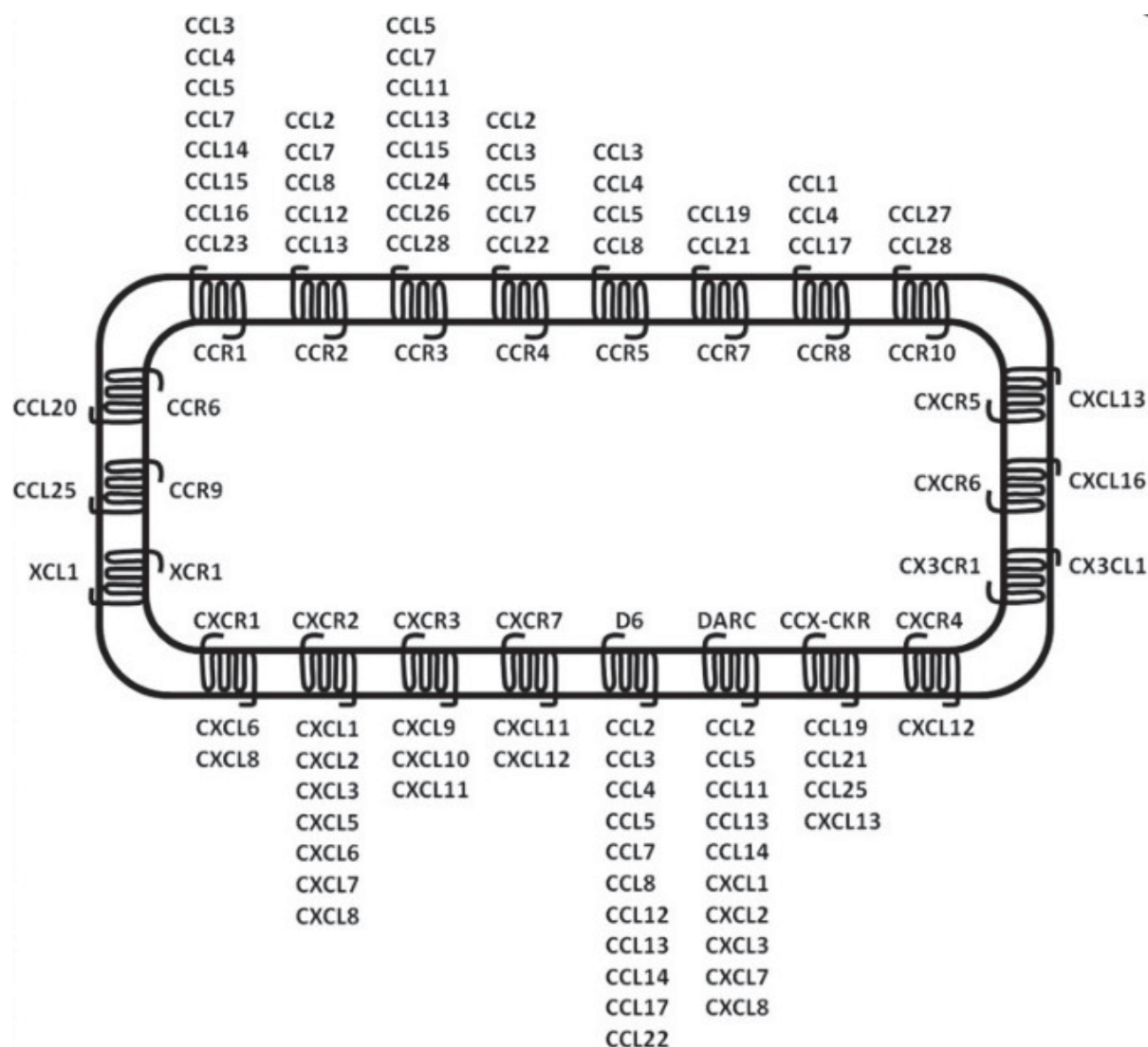


**Figure 1.4** The chemokine superfamily. Most inflammatory chemokines can bind to several receptors and a single chemokine receptor can bind to several chemokines. There are some chemokine clusters identified for the CC and CXC chemokine subfamilies. Decoy receptors (atypical chemokine receptors) can also interact with several chemokines but they do not signal, whereas a minority of chemokine receptors are restricted to only one ligand [60]. Adapted from [60] with kind permission from the author.

#### 1.4.1 The Chemokine receptor CCR10

The chemokine receptor CCR10 also called GPR-2 (G protein-coupled receptor-2) plays an important role in the mechanisms of skin homeostasis, inflammation and carcinogenesis [54, 61, 62]. The chemokine receptor ligand of CCR10 in the skin is CCL27 [63], while CCL28 recruits CCR10-positiv cells to the intestine mucosa [64, 65]. CCR10 is expressed by various cells types among them immune cells as well as structural cells [63]. Concentrating on cutaneous tissue, CCR10 is described to be expressed by melanocytes, dermal microvascular endothelial cells, melanocytes, T

cells and Langerhans cells [61]. The recruitment of skin-homing CCR10<sup>+</sup> CLA<sup>+</sup> memory T cells are connected to homeostatic and inflammatory conditions [66, 67] (Figure 4.1 A). Cutaneous inflammatory diseases like psoriasis, atopic dermatitis and allergic-contact dermatitis are linked to CCR10<sup>+</sup> lymphocyte recruitment [67].

Inflamed skin samples of patients suffering from psoriasis or verrucae vulgaris show migration of CCR6<sup>+</sup> CCR10<sup>+</sup> plasmacytoid dendritic cells (pDC) [68]. The authors suggest that activated pDCs migrate from the blood into lymphoid tissue by expressing CCR7 [68]. Afterwards the pDCs change their receptor expression profile by acquiring CCR6 and CCR10 expression through IL-3 stimulation released from local T cells, which allows the pDCs to migrate into inflamed epithelial sites of the skin or the mucosa where they release IFN- $\alpha$  [68]. In addition, another subset of CCR6<sup>+</sup> CCR4<sup>+</sup> CCR10<sup>+</sup> CD4<sup>+</sup> T cells are recruited to the skin in homeostasis [69, 70]. These T cell subsets secrete IL-22 but not IL-17 or IFN- $\gamma$  and are characterized as Th22 cells [69, 70]. Another immune cell population expressing CCR10 are the innate lymphoid cells (ILCs) [71]. In skin-draining lymph nodes ILCs are programmed for the expression of CCR10 by T cells and B cells [71]. The expression of CCR10 on ILCs allows them to migrate into the skin, where they are responsible for maintaining homeostatic levels of Treg cells and effector T cells [71]. In turn T cells are important for the maintenance of CCR10<sup>+</sup> ILCs in the skin, suggesting a crosstalk between these two different cell types [71] (Figure 4.1 A). By Using a *Ccr10*-deficient/ *EGFP*-knock-in mouse model Fu *et al.* showed that CCR10 is required for CD8<sup>+</sup> T cell migration into the skin and that the loss of CCR10 results in an altered CD4<sup>+</sup> T cell homeostasis including Treg cells and Teff cells [72]. These results suggest a role for CCR10 in balancing Treg and Teff (Th17 cells) immune homeostasis [72, 73]. The same mouse model showed that CCR10 is also required for the migration of  $\gamma\delta$ T cells into the epidermal regions of the skin and the maintenance of their dendritic shape [72, 73]. *Ccr10*-deficiency resulted in impaired skin homing and an altered morphology of  $\gamma\delta$ T cells [72]. *Ccr10*-deficient/ *EGFP*-knock-in mice are also reported to acquire an increased immune response to 2,4-Dinitro-1-flourbenzol (DNFB) challenging [73]. In contrast, the reaction to topical TPA treatment was comparable in *Ccr10*-deficient mice and control mice [73]. After infection with *Leishmania major* *Ccr10*-deficient mice react with an enhanced Th17 response accompanied by increased secretion of TNF- $\alpha$  and IL-1 $\beta$  which resulted in more efficient pathogen clearance compared to control mice indicating an important role for CCR10 in

balancing Treg and Th17 immune responses for skin homeostasis and inflammation [73]. Analyzing the expression pattern of CCR10 in T cells of mice and human by flow cytometric analysis, resulted in comparable CCR10 expression pattern which leads to the expectation that CCR10 has a similar function in mice and human [73]. The *Ccr10*-deficient mice used in this study are describes first by Morteau *et al.* [74]. This *Ccr10*-deficient mice strain had an insertion of a EGFP/NeoR cassette within the start codon of *Ccr10* [74]. Morteau *et al.* reported an impact for CCR10 in lymphocyte recruitment of IgA-ASCs to mucosal tissue via the CCR10-CCL28 axis [74]. A recently published paper analyzes the role of CCR10 on structural cells [75, 76]. Human dermal fibroblasts and primary dermal microvascular endothelial cells express both CCR10 on their cell surface [75]. Both cell types promoted wound repair by migration via a CCL27-CCR10 axis [75]. In the case of cancer progression, CCR10 expressed on lymphatic endothelial cells promotes lymphatic vessel development via CCL27/CCL28-CCR10 interactions during tumor lymphangiogenesis [76]. Another paper reported increased *CCR10* mRNA expression in malignant melanoma cells showing an impact of CCR10 in support of skin metastasis development through its ligand CCL27 [54].

#### 1.4.2 The chemokine CCL27

Homeostatic chemokines are constitutively expressed and regulate tissue-specific leukocyte migration [77]. The homeostatic chemokine CCL27 also called CTACK (cutaneous T cell-attracting chemokine) is specifically expressed by human epidermal keratinocytes in the skin [67, 78]. CCL27 is expressed in large amounts in basal cells of the epidermis [67]. During the process of epidermal cell differentiation from the basal layer to the skin surface, the expression levels of CCL27 decrease [67]. CCL27 binds to its receptor CCR10 and recruits CLA<sup>+</sup> skin-homing memory T cells predominantly to the epidermis [61, 78] (Figure 4.1 A). During cutaneous inflammation the proinflammatory cytokines TNF- $\alpha$  and IL-1 $\beta$  can induce an increased expression of CCL27, accompanied by an upregulation of the vascular ligand E-selectin [78]. The TNF- $\alpha$ /IL-1 $\beta$ -induced CCL27 expression can be partially inhibited by IL-10 treatment [61]. In inflammatory skin diseases, like psoriasis, allergic-contact dermatitis, and atopic dermatitis, the inflammatory infiltrate is dominated by lymphocytes [67]. Interestingly, these inflammatory skin diseases also show an increased expression of CCL27 and CCR10 [67]. In a lymphocyte-driven *in*

*vivo* mouse model induced by epicutaneous ovalbumin exposure, mice showed an upregulation of CCL27 in inflamed skin [67]. When mice were treated with neutralizing antibodies against CCL27, histological analysis indicated a suppression of inflammation-induced skin thickening, and a substantially decreased leukocyte recruitment into the skin [67]. In previous experiments, Pivarcsi *et al.* could show the progressive loss of CCL27 expression during cutaneous carcinogenesis (actinic keratosis, basal cell carcinoma, squamous cell carcinoma) by activation of the EGFR/Ras signaling pathway [43]. The epidermal growth factor receptor (EGFR) induces Ras signaling, which is activated in a variety of tumors [43, 79]. In cell culture experiments, it was observed that oncogenic Ras down-regulates CCL27 but increases CXCL8 expression in keratinocytes [43]. Immunohistochemical analysis of skin tumor samples showed a significantly increased phosphor-Erk1/2 (p-Erk1/2) expression, suggesting a role for MAPK pathway activation in skin tumors [43]. Furthermore, in the case of an enhanced response rate to an epidermal growth factor receptor inhibitor (EGFRI) treatment such as Erlotinib<sup>®</sup>, tumor patients are observed with inflammatory skin lesions (rash) [43, 80, 81]. These patients also presented with an up-regulated CCL27 expression in lesional skin and, additionally, an increased inflammatory infiltrate with clustering macrophages, intraepidermal LCs, and CD4<sup>+</sup> and CD8<sup>+</sup> T cells [43, 81]. Mutant mice, which bore a specific EGFR deletion in the epidermis (EGFR<sup>Δep</sup>), developed a severe skin inflammation three weeks after birth, characterized by an increased amount of DCs, granulocytes, monocytes, degranulated mast cells, and T cells [81]. In accordance to these results, other studies were able to show in an *in vivo* tumor mouse model of injected murine B16/F10 tumor cells into the dermis and additional treatment with CCL27-neutralizing antibody that tumor growth is significantly enhanced by inhibition of leukocyte recruitment (CD4 and CD8) to sites of tumor formation [43].

### **1.5 Chemokines and chemokine receptors in cancer**

Chemokines have diversified roles in malignancies: some chemokines have a role in combatting tumor development by their activation and recruitment of immune responses or by impairment of angiogenesis, whereas other chemokines promote tumor development and growth, followed by induction of angiogenesis and the metastatic spread [82, 83].



The prominent role of chemokines in metastasis has been a focus of research in the last years [84]. Chemokine receptors expressed by tumor cells are implicated to be responsible for specific metastasis into target organs, e.g. CXCR4 into the liver, lung and bone marrow, and CCR7 into lymph nodes [54]. Tumors consist of a variety of different cells (malignant cells, resident fibroblasts, endothelial cells, pericytes, and leukocytes), the interaction of these cells with each other constitute the tumor microenvironment [85, 86]. Inflammation is one of the hallmarks of cancer [85]. The tumor stroma and tumor-associated inflammatory processes play a leading role in tumor development, growth, and progression [86]. During carcinogenesis, chemokines are produced by cancer cells as well as by different cells of the tumor microenvironment, such as cancer-associated fibroblasts (CAFs), mesenchymal stem cells (MSCs), endothelial cells, tumor-associated macrophages (TAMs), and tumor-associated neutrophils (TANs) [83]. Tumor cells themselves and the cells of the tumor microenvironment influence each other through stimuli, which promote tumor growth and metastasis [83]. Chemokines are key players, not only in the recruitment of cancer cells to distinct metastatic organs, but they also guide a variety of different cells to sites of tumor development for the establishment of a favorable tumor microenvironment [83]. Chemokines expressed by tumor-infiltrating cells can influence tumor growth, cell survival, senescence, angiogenesis, and metastasis [83]. The upregulation of chemokines and chemokine receptors on cancer epithelial cells can induce the release of cytokines, which create a strong inflammatory response by recruiting immune cells, like macrophages, neutrophils, and lymphocytes, to establish an anti-tumor or a tumor-promoting environment [83]. Infiltrating leukocytes, endothelial cells, and CAFs are carrying chemokine receptors, such as CXCR1, 2 and CCR2, 4, 5 and 6 [83]. In turn, these cells, after recruitment to sites of tumor development, express chemokines, which have an impact on tumor growth, angiogenesis, metastasis, as well as the continued development of the tumor microenvironment [83]. Indeed, epithelial tumors are often enriched with many immune cells [82]. In contrast, effector cells have the potential to recognize tumor cells and eliminate them and therefore they are very important for a possible rejection of tumor cells [87]. For example, the infiltration of CD4<sup>+</sup> and CD8<sup>+</sup> T cells and natural killer (NK) cells, recruited after detection by these effector cells through specific chemokine expression, is correlated with the protection against tumor growth [87-89]. The expression of CCL2 within the tumor microenvironment is restricted to epithelial areas

and was found to be correlated with the amount of infiltrating lymphocytes and macrophages [90]. CCL5 recruits CD8<sup>+</sup> T-lymphocyte into the tumor microenvironment [90]. To avoid this fate, some tumors developed the ability to evade immunosurveillance by suppressing immune responses [87]. Additionally, tumors hijack the direct growth stimulatory activity of some chemokines by changing their chemokine receptor profile to include receptors for these stimulatory chemokines [82, 91]. Another leading role of chemokines is the induction of angiogenesis to ensure the nourishment of the tumor in case of tumor growth [82, 91]. Therefore, it is important to balance the inflammatory responses [92].

Chemokines can affect angiogenesis by releasing promoting or inhibitory stimuli [93, 94]. Two sets of angiogenesis-modulating chemokines have been discovered. They are distinguished by either containing or missing a so-called ELR motif in their amino acid sequence. ELR motif-containing chemokines that contain the three amino acid (Glu-Leu-Arg) motif are angiogenic and enhance tumor growth by induction of angiogenesis, while chemokines that do not contain the ELR motif are interferon  $\gamma$  (IFN- $\gamma$ )-inducible and inhibit angiogenesis [82, 93, 94]. The ELR-positive chemokine CXCL8 is correlated with angiogenesis in ovarian carcinoma, while ELR-positive CXCL5 is an important regulator of angiogenesis in non-small cell lung cancer (NSCLC) [93, 95]. In contrast, ELR motif-negative chemokines like CXCL9 and CXCL10 are associated with spontaneous regression due to decreased angiogenesis in human lymphoma and human NSCLC xenograft mouse models [93, 94]. Therefore, the balance between angiogenic and angiostatic chemokines in the tumor microenvironment decides the strength and occurrence of angiogenesis initiation and defines the metastatic potential of a tumor [82].

In most cases, the main problem for cancer patients is not the primary tumor, but the metastatic spread of cancer cells to distant organs, which is often the cause of treatment failure [96]. At the beginning of the last century, scientist discovered that secondary tumors developed from tumor cells migrated from the original tumor into other organ systems by lymphatic and blood vessels [96]. 15 years ago, Müller *et al.* reported that tumor cell migration and metastatic spread are comparable to the migration of leukocytes, which is mediated by chemokines and their receptors as mentioned before [54]. The authors demonstrated that tumor cells also express a distinct and non-random pattern of chemokine receptors [54]. After analyzing human malignant breast tumors and metastases, they showed that CXCR4 and CCR7



signaling pathways are regulators for actin polymerization and pseudopodia formation and induce the response of tumor cells to chemotactic signals which leads to metastasis development [54]. Additionally, they observed that distinct organs are the main locations of breast cancer metastasis (bone-marrow, lung, liver, and lymph node) and these organs express the ligands for chemokine receptors expressed by breast cancer cells (CXCL12 and CCL21) [54]. In *in vivo* experiments, they demonstrated that inhibition of CXCL12/CXCR4 signaling resulted in a significant inhibition of lymph node and lung metastasis development [54]. Another example is CCR10, which is expressed on normal melanocytes and malignant melanoma cells [54, 55, 61]. The skin-specific expression of its ligand CCL27 might explain the high incidence of melanoma skin metastases [54, 55]. Interestingly, if a shift in the receptor expression of melanoma cells from CCR10 to CCR9 occurs, melanoma metastasis formation is redirected to the small intestine, where the ligand of CCR9, CCL25, is expressed [55, 97]. Therefore, chemokines and their receptors play a dual role by not only mediating leukocyte trafficking and organogenesis, but by also guiding tumor cells to their metastatic destination [54].

### **1.6 The DMBA/TPA two-stage carcinogenesis model**

The DMBA/TPA two-stage carcinogenesis model is well established [98]. It is based on an initiation-promotion protocol [99]. In the initiation stage, the induction of skin carcinogenesis by topical application of the carcinogen 7,12-dimethylbenz(a)anthracene (DMBA) causes an activated *Hras* gene mutation at codon 61, which leads to an irreversible change of some epidermal cells [99-101]. Activation of Hras signaling leads to altered gene expression in cells through increased gene expression of ras-inducible genes [102-104]. This is followed by the promotion stage, in which repetitive topical applications of the tumor promoting agent 12-O-tetradecanoylphorbol-13-acetate (TPA) is carried out to induce cutaneous inflammation and epidermal hyperplasia in the treated area by induction of the EGFR [99, 105]. The combination of the promotion and the induction of epidermal cell proliferation induced by TPA gives initiated cells the possibility of selective clonal expansion into papillomas and some papillomas progress irreversibly to carcinomas [99, 100, 104]. Signaling through the EGFR is an essential component of skin tumor promotion during chemically induced mouse skin carcinogenesis [106]. The expression of EGFR ligands, such as the growth factors TGF- $\alpha$  and EGF, have been

identified to be overexpressed during two-stage carcinogenesis and to activate the EGFR [104, 106]. Additionally, there are also other factors which have an altered expression pattern during chemically induced skin carcinogenesis. The growth inhibitor TGF- $\beta$  and keratin 1 (K1) are suppressed, while the cell cycle protein cyclin D1,  $\alpha_6\beta_4$  integrin, keratin 13 (K13),  $\gamma$ -glutamyl transpeptidase (GGT) and the gap-junctional protein connexin 26 (Cx26) are overexpressed [103, 104, 107, 108]. *Hras* mutations appear to be an initiation-dependent event in mouse skin by DMBA, while in contrast, v-fos has been implicated in later stages [104]. Immune responses play an important role during tumor promotion and rejection [109, 110]. As mentioned before, the topical application of TPA onto the skin induces an inflammatory response in the skin [98, 99, 111], therefore in the following paragraph the role of immune responses after DMBA/TPA treatment will be elucidated. The importance of immune responses for the control of tumor incidence and progression is a key mechanism which is reduced in immunosuppressive conditions such as in case of organ transplantations, autoimmune disease and atopic dermatitis [112]. All these diseases are treated with immune suppressive drugs which increase the risk of tumor development as a recent study of skin carcinogenesis in Swiss albino mice showed [112]. In this study, DMBA/TPA-induced skin carcinogenesis was enhanced by additional topical treatment with immunosuppressant tacrolimus accompanied by reduced levels of CD4<sup>+</sup>/CD8<sup>+</sup> T cells [112]. The tumor-promoting effect of tacrolimus was also previously shown by Niwa *et al.* [113]. The role of T cell mediated immune response during skin carcinogenesis induction was also shown in another study of DMBA/TPA-induced carcinogenesis [114]. Here, *EPI*-deficient mice are observed with significantly reduced tumor development [114]. *EPI*-deficient mice have defects in the epidermal barrier accompanied by an enhanced inflammatory response which presented with an altered immune response leading to reduced  $\gamma\delta$ TCR<sup>+</sup> CD3<sup>+</sup> cells and a prominent dermal infiltrate of CD4<sup>+</sup> T cells [114]. Additionally, these mice showed an increased recruitment of dermal mast cells and eosinophils which are also presented together with CD4<sup>+</sup> T cells in acute atopic dermatitis [114]. In contrast to the two studies above, DMBA/TPA carcinogenesis in FVB/N-*Cd4*-deficient mice exhibit significantly reduced tumor multiplicity compared to wildtype littermates [115]. In accordance with that observation, *Cxcr3*-deficient mice are found with reduced tumor development accompanied with a general increase of the inflammatory infiltrate but markedly decreased epidermal proliferation whereas the infiltration of

CD4<sup>+</sup> and CD8<sup>+</sup> T cells was significantly reduced after DMBA/TPA treatment [116]. Schioppa *et al.* found out that *Tnf*-deficient mice are resistant to DMBA/TPA induced papilloma development which was associated with a decrease of tumor-promoting IL10-producing B cells and an increased recruitment of IFN- $\gamma$ -producing CD8<sup>+</sup> T cells [117]. When DMBA/TPA-treated *Tnf*-deficient mice were transferred with B cells from DMBA/TPA treated wildtype mice the effect was an enhanced infiltrate of F4/80<sup>+</sup> macrophages, but a decreased amount of CD8<sup>+</sup> T cells, accompanied by significantly increased papilloma development compared to *Tnf*-deficient mice [117]. They also reported that C57BL/6 *Rag2*-deficient mice are resistant to DMBA/TPA-induced papilloma development indicating a role for B and T cells for skin tumor development [117]. Furthermore B cell-deficient *Jh* mice showed reduced tumor development [117]. Surprisingly, *INF $\gamma$ R*-deficient mice are also resistant to papilloma development after DMBA/TPA treatment [118]. The analysis of the immune infiltrate of these mice exhibited a decreased amount of CD11b<sup>+</sup> and Gr1<sup>+</sup> cells, but predominantly, the number of IL-17<sup>+</sup> CD4<sup>+</sup> T cells was reduced in *INF $\gamma$ R*-deficient mice compared to the wildtype mice [118]. The same level could be observed for the amount of Th17 cells in *INF $\gamma$ R*-deficient mice compared to the wildtype controls [118]. A study by Yusuf *et al.* impressively showed that *Cd8*-deficient mice developed only a reduced contact hypersensitivity to DMBA treatment whereas *Cd4*-deficient mice showed a strong reaction to DMBA-induced contact hypersensitivity [119]. When these mice were treated with DMBA/TPA, *Cd8*-deficient mice developed significantly more tumors compared to wildtype controls whereas *Cd4*-deficient mice presented with a decreased number of tumors compared to wildtype mice [119]. These results suggest an anti-tumor role for CD8<sup>+</sup> effector T cells compared to CD4<sup>+</sup> T cells which seem to have an inhibitory effect and promote tumor development [119]. A further characterization of the distinct T cell subpopulations from tumor-bearing mice demonstrated that CD4<sup>+</sup> T cells mainly produced IL-4, IL-10 and IL-17 in contrast CD8<sup>+</sup> T cells produced IFN- $\gamma$  [119]. As all the studies above show, the inflammatory infiltrate of DMBA/TPA-induced carcinogenesis is complex and not easy to understand. Complex processes orchestrate the immune infiltrate, which can have pro-tumor or anti-tumor effects. Inflammation is a hallmark of cancer [85] and the obvious conclusion would be that a reduction of the inflammatory infiltrate would reduce tumor development, but this reduction is a double-edged sword and depending on the mechanism of immune inhibition, might lead to a tumor-favorable

modulation of the inflammatory infiltrate. Studies above showed also a decrease in tumor development, if the immune response of the inflammatory infiltrate is altered from Th2 to Th1. Inflammation is a multifactorial process, therefore it is important to consider that not only a reduction of the inflammatory response can be beneficial, but also an alteration of the inflammatory infiltrate to a Th1 response.

### **1.7 The UVB-irradiation model of cutaneous carcinogenesis**

It is well known that UV-irradiation impairs the immune system and is responsible for tumor progression and cutaneous carcinogenesis [120]. Chronic UV exposure leads to inflammation of the irradiated skin, oxidative stress, DNA damage, and impairment of immune responses [121]. These events play an important role during skin carcinogenesis [121]. In 1977, Fortner and Kripke could show in *in vivo*-transplantation studies that UV-induced tumors grow progressively when transplanted onto UV-irradiated mice, whereas all were rejected in control mice, who had never been exposed to UVB [120]. They also suggested a reduction of cytotoxic lymphocytes, which is responsible for the progressive growth of tumors in UVB-irradiated mice [120]. Previous studies suggested the importance of a change in a subpopulation of T cells and an increased induction of CD4<sup>+</sup> regulatory T cells (Tregs) and inhibition of CD8<sup>+</sup> effector T cells [122, 123]. Another group could show in a UVB-induced murine tumor model that a markedly increased recruitment of CD8<sup>+</sup> T cell into the tumor microenvironment correlate with significantly decreased skin carcinogenesis and spontaneous rejection of developed tumors [124]. In contrast, inhibition of CD8-signaling was followed by tumor development and strong tumor growth [124]. To validate the impact of CD4<sup>+</sup> and CD8<sup>+</sup> T cells in UVB-induced skin carcinogenesis, a study by Nasti *et al.* took advantage of *Cd8*-deficient and *Cd4*-deficient mouse strains [125]. *Cd4*-deficient mice show reduced skin carcinogenesis compared to wildtype mice, while *Cd8*-deficient mice presented with increased tumor induction and progression [125]. Additionally, they reported a higher secretion of TGF- $\beta$  and a higher expression of CD25 and FoxP3 in Tregs of *Cd8*-deficient mice compared to the wildtype control [125]. The results of this study suggest that CD8<sup>+</sup> and CD4<sup>+</sup> T cells seem to have opposing roles during skin carcinogenesis. While CD4<sup>+</sup> T cells have a pro-tumor effect by producing IL-4, IL-10, and IL-17, CD8<sup>+</sup> T cells reduce tumor development through the release of INF- $\gamma$  [125]. In their work, Wang *et al.* showed that a significant increase of CD1<sup>+</sup> DCs, which are antigen-

presenting cells important for the activation of the T cell immune response and a significant increase of CD4<sup>+</sup> and CD8<sup>+</sup> T cells markedly decrease skin carcinogenesis of UVB-induced SCCs [126]. This was accompanied by a strong enhancement of TNF- $\alpha$  expression [126]. Meanwhile, Hatton *et al.* reported a significantly increased recruitment of CD4<sup>+</sup> T cells into the epidermal compartment after UVB-irradiation, whereas they detected no change in the amount of CD8<sup>+</sup> T cells [127]. Interestingly, an inhibition of CD4-signaling resulted in a significant enhancement of CD8<sup>+</sup> T cells in the epidermal compartment, while inhibition of CD8-signaling had no effect on the amount of CD4<sup>+</sup> T cells in the epidermis after UVB-exposure [127]. Furthermore, an inhibition of CD4-signaling was followed by a significantly increased recruitment of neutrophils into the irradiated skin, which led to increased tumor induction compared to mice injected with the isotype control [127]. The amount of neutrophils did not alter after the impairment of CD8-signaling [127]. Taken together, this study indicated a complete novel role for CD4<sup>+</sup> T cells in maintaining skin homeostasis, where an inhibition of CD4-signaling would lead to increased tumor development by shaping the immune response after UVB-irradiation to an increased inflammatory response characterized by significantly enhanced recruitment of CD8<sup>+</sup> T cells and neutrophils [127]. The studies of Nasti *et al.* and Hatton *et al.* have contrary results, which might be due to experimental differences. While Nasti *et al.* used *Cd4*-deficient and *Cd8*-deficient mice on a C3H/HeN background, Hatton *et al.* used Skh-1 hairless mice and used antibodies against CD4<sup>+</sup> and CD8<sup>+</sup> cells to induce a CD4- and CD8-depletion. Furthermore, Nasti *et al.* irradiated the mice for 40 weeks with 200 mJ/cm<sup>2</sup>, whereas Hatton *et al.* irradiated the mice only for 25 weeks with 224 mJ/cm<sup>2</sup>. Moreover, Hatton *et al.* did not examine the impact of CD8-depletion during skin carcinogenesis and the CD4-depletion was first induced after 11 weeks of UVB-irradiation. In addition, for CD4-depletion, mice had to be injected with the antibody or the control two times a week every third week, which might cause also differences in inflammatory responses.

UV-radiation is capable of isomerizing *trans*-urocanic acid (UCA) to *cis*-UCA [123]. *Cis*-UCA impairs the function of keratinocytes, LCs, fibroblasts, T lymphocytes, NK cells, and macrophages [123]. In addition, mast cells seem to play a role in UVB-induced immunosuppression related to BCC development, too [128]. The effect of UVB-induced immunomodulation is manifested by damage to skin-specific antigen presenting cells, like LCs in the epidermis and DCs and macrophages in the dermis,

whose antigen presenting function is impaired by *cis*-UCA [123, 129], which is accompanied by the induction of immunomodulatory cytokines, for example TNF- $\alpha$  and IL-10 [123]. These cytokines, together with IL-1, IL-6, IL-8 and PGE<sub>2</sub>, are responsible for the establishment of an inflammatory response by releasing chemotactic signals to immune competent cells, such as neutrophils and macrophages in the skin [123, 130, 131]. IL-10 seems to be a major player in UVB-induced immunomodulation [123]. There are also other factors with important roles in cutaneous carcinogenesis. UVB light (280-320 nm) is absorbed by chromophores of the skin, producing “signature” mutations in DNA, which induce the development of cutaneous carcinogenesis [132]. How does radiation cause mutations in skin cells? UVB-radiation causes an increased reactive oxygen species (ROS) production [123, 133]. ROS production induces the migration of LCs from the epidermal compartment into the draining lymph node (DLN) after UVB-irradiation [123, 134]. Additionally, oxygen radicals are responsible for base substitutions and alter single pyrimidines [135]. Interestingly, such mutations have also been found in the *p53* tumor suppressor gene in UV-induced SCC [135, 136]. The mutation of the *p53* tumor suppressor gene seems to be an early event from sun exposure, primarily in childhood, followed by other events: development of dysplasia, actinic keratosis, or carcinoma *in situ* with a possible end result of SCC [136, 137]. SCCs arise from mutated epithelial keratinocytes in the upper layers of the epidermal compartment, are characterized by increased cornification and the development of horn beads, and have a risk to metastasize [135, 138].

## 1.8 Aims

During carcinogenesis, the activation of the EGFR/Ras signaling pathway on transformed cells is important for modulating tumor immune escape and tumor progression [43, 139]. In particular, the expression of the chemokine CCL27 is regulated by the EGFR/Ras signaling pathway [43]. The chemokine CCL27 and its receptor CCR10 play an important role during the maintenance of cutaneous homeostasis and inflammation [63, 67, 87]. This study investigates the role of CCR10 in cutaneous carcinogenesis in two distinct skin tumor models.

- The focus of this study involves the role of CCL27/CCR10 signaling during cutaneous carcinogenesis. In a previous study, it was discovered that loss of

CCL27 expression during cutaneous carcinogenesis leads to tumor immune escape [43]. This mechanism will be further elucidated in the present study by taking advantage of a *Ccr10*-deficient mouse strain and two distinct murine cutaneous carcinogenesis models, using either chemicals (DMBA/TPA) or UVB-radiation. The aim of the present study is to address the following questions:

- Does the loss of *Ccr10* in the skin during skin carcinogenesis result in increased tumor growth and progression?
- Which tumor phenotypes develop in the different models and does *Ccr10*-deficiency influence the ratio of developing tumor types?
- Does *Ccr10*-deficiency have an impact on alterations of skin morphology?
- Does a difference in the mechanism of carcinogenesis induction lead to different roles of CCL27/CCR10 signaling?



## 2 Material and Methods

### 2.1 Mice

The study involved two different models of carcinogenesis induction. In each experiment, female Balb/c wildtype (WT) and Balb/c-*Ccr10*-deficient mice at the age of 12-16 weeks were used. WT mice were purchased from Janvier Labs (France, Europe). *Ccr10*-deficient mice were originally provided by Craig Gerard and were a kind gift from Dr. M. Steinhoff (Dept. of Dermatology, University Hospital Münster, Münster, Germany). All mice received food and water *ad libitum* and were housed on a 12-hour light/dark cycle within an air-conditioned facility at the *Zentrale Einrichtung für Tierforschung und Tierschutzaufgaben* (ZETT) of the Heinrich-Heine-University Düsseldorf (Düsseldorf, Germany). All animal experiments were performed according to the guidelines of the Animal Care and Use Committee of the Heinrich-Heine-University and Bezirksregierung Düsseldorf, animal license number 84-02.04.2011. Genotypes of all mice were validated by PCR.

### 2.2 Buffers and solutions

Distilled water (dH<sub>2</sub>O) was used for the production of all solutions.

|  |  |  |
|--|--|--|
| EDTA (Ethylenediaminetetraacetic acid) | 0.5 M EDTA                               | adjust to pH 8.0                               |
| Oligonucleotide primer                 | 10 pmol/μl dH <sub>2</sub> O             |  |
| TAE (Tris-acetate-EDTA) buffer, 50x    | 2.0 M Tris acetate<br><u>0.05 M EDTA</u> | ad 1000 ml ddH <sub>2</sub> O adjust to pH 8.3 |

#### 2.2.1 Reagents

|                                |                                 |
|--------------------------------|---------------------------------|
| Acetone                        | Merk (Darmstadt, Germany)       |
| Agarose Low EEO                | Sigma-Aldrich (St. Louis, USA)  |
| Bovine Serum Albumin (BSA)     | Sigma-Aldrich (St. Louis, USA)  |
| DEPC water                     | Carl Roth (Karlsruhe, Germany)  |
| 7,12-Dimethylbenz[a]anthracene | Sigma-Aldrich (St. Louis, USA)  |
| dNTP mix [10 mM]               | Bioline USA Inc. (Taunton, USA) |
| 4% formalin                    | Sigma-Aldrich (St. Louis, USA)  |



|   |   |
|---|---|
| Hematoxylin                             | Sigma-Aldrich (St. Louis, USA)          |
| MgCl <sub>2</sub>                       | Qiagen (Hilden, Germany)                |
| Orange DNA Loading Dye (6x)             | Thermo Fisher Scientific (Waltham, USA) |
| Phorbol 12-myristate 13-acetate [10 mg] | Sigma-Aldrich (St. Louis, USA)          |
| PCR buffer without MgCl <sub>2</sub>    | Qiagen (Hilden, Germany)                |
| RedSafe™                                | iNtRON Biotechnology (Korea)            |
| RNA/ater                                | Qiagen (Hilden, Germany)                |
| Tissue-Tek®-O.C.T.                      | Sakura (Zoeterwoude, Netherlands)       |
| Veet Enthaarungscreme — Sensible Haut   | Veet (Reckitt Benckiser, Slough, UK)    |
| Xylene                                  | Merk (Darmstadt, Germany)               |

### 2.2.2 DNA Ladder

For genotyping PCRs the Thermo Scientific O'GeneRuler 100 bp DNA Ladder was used (Thermo Fisher Scientific, Waltham, USA).

**O'RangeRuler 100 bp DNA Ladder, ready-to-use**

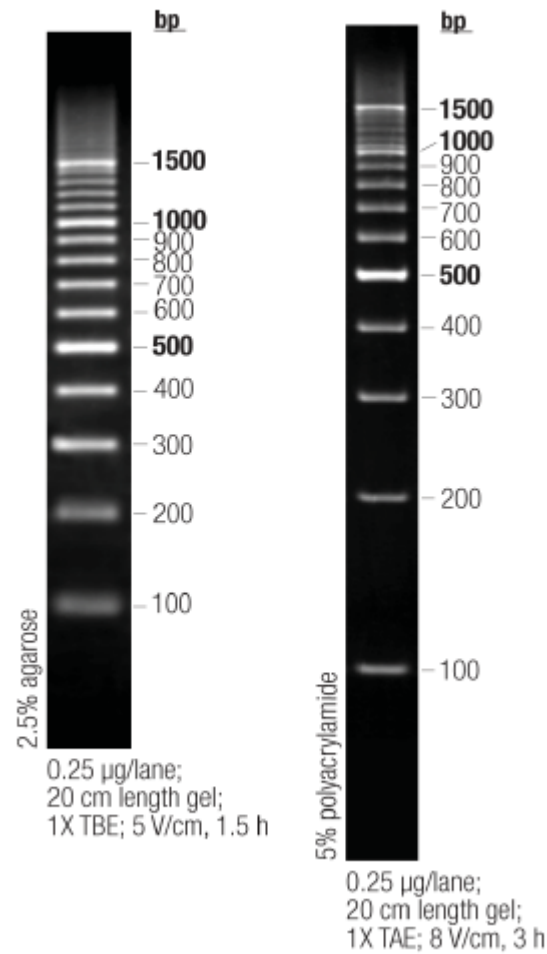


**Figure 2.1** Thermo Scientific O'GeneRuler 100 bp DNA Ladder (<https://tools.thermofisher.com/content/sfs/manuals/MAN0013023ORangeRuler100bpDNALadderRTUUG.pdf>).

### 2.2.3 Kits

DNeasy Blood & Tissue Kit

Qiagen (Hilden, Germany)

HotStarTaq DNA Polymerase (250 U)

Qiagen (Hilden, Germany)

### 2.2.4 Instruments

Axioskop 40

Carl Zeiss (Oberkochen, Germany)

AxioCam MRc

Carl Zeiss (Oberkochen, Germany)

Bio Vortex V1

Biosan (Riga, Latvia)

Canon EOS 1100D

Canon (Tokyo, Japan)

Centrifuge 5415R

Eppendorf (Hamburg, Germany)

Cryostat Leica CM3050 S

Leica Biosystems (Wetzlar, Germany)

|                                   |  |
|-----------------------------------|--|
| Irradiation chamber               | Saalmann GmbH (Herford, Germany)               |
| Isis GT420                        | Aesculap Suhl GmbH (Suhl, Germany)             |
| Oditest 00T6                      | Kroeplin GmbH (Schlächtern, Germany)           |
| peqSTAR 96x Thermocycler Gradient | PEQLAB Biotechnologie GmbH (Erlangen, Germany) |
| Caliper                           | Fine Science Tools (Heidelberg, Germany)       |
| Thermomixer 5437                  | Eppendorf (Hamburg, Germany)                   |
| UV-meter                          | Waldmann (Villingen-Schwenningen, Germany)     |

## 2.3 Methods

### 2.3.1 DMBA/TPA two-stage skin carcinogenesis model.

Groups of 10 WT and 10 *Ccr10*-deficient mice were included for an early time point, ending the experiment after 12 weeks of DMBA/TPA treatment. Additionally, 40 WT mice and 40 *Ccr10*-deficient mice were included in the experiment for a late time point, ending the experiment after 40 weeks of DMBA/TPA treatment. The dorsal area of the mice was shaved with an electric razor (Isis GT420, Aesculap Suhl GmbH, Suhl, Germany) in conjunction with topical hair removal cream for sensitive skin (Veet, Slough, UK) 3 days prior to administration of the initiating agent DMBA (Sigma-Aldrich, St. Louis, USA). Mice received a single application of 25 µg DMBA dissolved in 200 µl acetone. One week after DMBA application, the promoting agent TPA (5 µg/ 200 µl) (Sigma-Aldrich, St. Louis, USA) was administered once a week for either 12 or 40 weeks. The shaving of mice was repeated every other week with an electric razor and mice were additionally treated with hair removal cream for sensitive skin (Veet, Slough, UK) every five weeks. The mice were observed daily and pictures of the mice were taken weekly (Canon EOS 1100D, Tokyo, Japan). Additionally, emerging tumors were counted weekly. At the end of the experiment, either after 12 or 40 weeks or due to a tumor diameter over 1 cm per tumor, mice were photographed (Canon EOS 1100D, Tokyo, Japan) and afterwards sacrificed by CO<sub>2</sub> exposure. After measuring the nuchal fold thickness with dial caliper gage (Oditest 00T6, Kroeplin GmbH, Schlächtern, Germany), tumors were excised and measured manually with a caliper (Fine Science Tools, Heidelberg, Germany) and weighed.

Nuchal fold thickness was measured as a marker for inflammation-induced skin thickening. A larger thickness denotes a stronger induction of an inflammatory response. Additionally, the tumor volume was calculated by measuring the three-dimensional size (height, length and width). Developed tumors showed a hemi-ellipsoid shape and ellipsoid tumor volume was calculated by:

$$\text{Vol.} = \frac{\pi}{6} \times (\text{length}) \times (\text{width}) \times (\text{height})$$

The spleen and the lymph nodes (inguinal, axillary and mandibular) were collected, and a 5 mm skin biopsy of the back and the abdominal region was also collected by using a skin biopsy punch (pfm medical ag, Cologne, Germany).

### 2.3.2 Detailed listing of animal numbers used in DMBA/TPA experiments

For the early time point (12 weeks) of DMBA/TPA treatment, 10 WT mice and 10 *Ccr10*-deficient mice were used in the experiment. In the WT group, one mouse was excluded from the experiment, due to a premature death, independent of tumor size or cancer development. As this death might be unconnected to the treatment, it was decided to exclude the mouse from this analysis. Therefore, only 9 WT mice reached the end of experiment after 12 weeks of DMBA/TPA treatment. In contrast, all *Ccr10*-deficient mice survived until the end of DMBA/TPA treatment after 12 weeks.

| Group                       | Start of experiment [n] | Death due to other causes [n] | Death due to tumor size [n] | End of experiment [n] |
|-----------------------------|-------------------------|-------------------------------|-----------------------------|-----------------------|
| WT                          | 10                      | 1                             | 0                           | 9                     |
| <i>Ccr10</i> <sup>-/-</sup> | 10                      | 0                             | 0                           | 10                    |

**Table 2.1** Number of total mice used for the 12-week early time point analysis after DMBA/TPA treatment.

For analysis of early morphological changes of the skin, changes in the epidermal thickness were analyzed after 12 weeks of DMBA/TPA treatment. In this experiment mice were only included, if they survived the end of experiment (n = 9 WT and n = 10 *Ccr10*-deficient mice).

| Analysis                     | Start of experiment [n] | Animals not measured [n] | Death due to other causes [n] | Death due to tumor size [n] | End of experiment [n] | Animals measured [n] |
|------------------------------|-------------------------|--------------------------|-------------------------------|-----------------------------|-----------------------|----------------------|
| $\Delta$ epidermal thickness | 10                      | 1                        | 1                             | 0                           | 9                     | 9                    |

**Table 2.2** Number of WT mice used in the analysis of epidermal thickness after 12 weeks of DMBA/TPA treatment.

| Analysis                     | Start of experiment [n] | Animals not measured [n] | Death due to other causes [n] | Death due to tumor size [n] | End of experiment [n] | Animals measured [n] |
|------------------------------|-------------------------|--------------------------|-------------------------------|-----------------------------|-----------------------|----------------------|
| $\Delta$ epidermal thickness | 10                      | 0                        | 0                             | 0                           | 10                    | 10                   |

**Table 2.3** Number of *Ccr10*-deficient mice used in the analysis of epidermal thickness after 12 weeks of DMBA/TPA treatment.

For the late time point after 40 weeks of DMBA/TPA treatment, 40 WT mice and 40 *Ccr10*-deficient mice were used in the experiment. In the WT group, six mice had to be taken out of the experiment earlier than the designated 40 weeks, due to a tumor diameter over 1 cm per tumor, resulting in 34 mice reaching the endpoint of the experiment after 40 weeks of DMBA/TPA treatment. In contrast, four *Ccr10*-deficient mice developed a cardiac degeneration and had to be sacrificed due to this cause. These mice were examined by the veterinarian at the ZETT of the Heinrich-Heine-University Düsseldorf. Only one mouse of the *Ccr10*-deficient group developed a tumor with a diameter over 1 cm and had to be sacrificed earlier. Therefore, 35 mice survived until the end of the experiment after 40 weeks of DMBA/TPA treatment in the *Ccr10*-deficient group.

| Group                       | Start of experiment [n] | Death due to other causes [n] | Death due to tumor size [n] | End of experiment [n] |
|-----------------------------|-------------------------|-------------------------------|-----------------------------|-----------------------|
| WT                          | 40                      | 0                             | 6                           | 34                    |
| <i>Ccr10</i> <sup>-/-</sup> | 40                      | 4                             | 1                           | 35                    |

**Table 2.4** Number of animals used for the late time point after 40 weeks of DMBA/TPA treatment.

All mice sacrificed due to a tumor diameter over 1 cm and all mice surviving to the end of the experiment after 40 weeks of DMBA/TPA treatment were included into the analysis of the tumor burden (WT mice  $n = 40$  and *Ccr10*-deficient mice  $n = 36$ ). 40 WT mice and all 40 *Ccr10*-deficient mice were included into the evaluation of overall survival and tumor-free survival. Four mice in the *Ccr10*-deficient group died due to cardiac degeneration and were censored in the two survival statistics. Censored animals (*Ccr10*-deficient mice  $n = 4$ ) are shown by a vertical line in the figures (Fig. 3.1 C and D). All mice sacrificed due to their tumor size and all mice surviving to the end of the experiment after 40 weeks of DMBA/TPA treatment were included (WT mice  $n = 40$  and *Ccr10*-deficient mice  $n = 36$ ) in the analysis of tumors per mouse and tumor size per mouse. All mice, which survived the end of experiment or were sacrificed due to their tumor size, except one individual, where the tumor weight was not measured, were included in the analysis of tumor weights. Therefore 39 WT mice and 36 *Ccr10*-deficient mice were included in this analysis. For the evaluation of tumor size distribution, only those mice were included in the analysis, which developed tumor. This included mice sacrificed based on their tumor size ( $n = 6$  WT and  $n = 1$  *Ccr10*-deficient mice) and those developing tumors smaller than 1 cm till the endpoint of the experiment after 40 weeks (WT mice  $n = 28$  and *Ccr10*-deficient mice  $n = 21$ ). Excluded were mice that died due to causes other than tumor size (*Ccr10*-deficient mice  $n = 4$ ). Therefore, 34 WT mice and 22 *Ccr10*-deficient mice were analyzed in the tumor size distribution, altogether. The huge difference between the numbers of tumors, which developed in both groups, was the reason for the evaluation of the data as a percentage. For an investigation of tumor morphology, only mice with intermediate and large tumors ( $> 50 \text{ mm}^3$ ) were included in the analysis (WT mice  $n = 9$  and *Ccr10*-deficient mice  $n = 3$ ). Mice with smaller tumors than  $> 50 \text{ mm}^3$ , mice without tumors or mice, which died due to cardiac degeneration, were excluded from the evaluation. In this analysis, data were also shown as a percentage due to the difference in the tumor number. For the measurement of the nuchal fold thickness, all mice surviving to the end of the experiment and all mice sacrificed sooner due to tumor size greater than 1 cm were included in the analysis (WT mice  $n = 40$  and *Ccr10*-deficient mice  $n = 36$ ). Moreover, the nuchal fold thickness in control mice (WT mice  $n = 4$  and *Ccr10*-deficient mice  $n = 4$ ), was measured. Finally, changes in epidermal thickness were measured in eight randomly picked mice from each group (WT mice  $n = 8$  and *Ccr10*-deficient mice  $n = 8$ ) out of

all the mice, which survived till the end of the experiment and/or which were sacrificed earlier due to their tumor size. Furthermore, the epidermal thickness was measured in control mice (WT mice  $n = 2$  and *Ccr10*-deficient mice  $n = 2$ ) to calculate the epidermal changes.

| Analysis                      | Start of experiment [n] | Animals not measured [n] | Death due to other causes [n] | Death due to tumor size [n] | End of experiment [n] | Animals measured [n] |
|-------------------------------|-------------------------|--------------------------|-------------------------------|-----------------------------|-----------------------|----------------------|
| Tumor burden                  | 40                      | 0                        | 0                             | 6                           | 34                    | 40                   |
| Survival                      | 40                      | 0                        | 0                             | 6                           | 34                    | 40                   |
| Tumor-free survival           | 40                      | 0                        | 0                             | 6                           | 34                    | 40                   |
| Tumors/mouse                  | 40                      | 0                        | 0                             | 6                           | 34                    | 40                   |
| Tumor weight                  | 40                      | 1                        | 0                             | 6                           | 34                    | 39                   |
| Tumor size/mouse              | 40                      | 0                        | 0                             | 6                           | 34                    | 40                   |
| Tumor size distribution       | 40                      | 6                        | 0                             | 6                           | 34                    | 34                   |
| Tumor morphology distribution | 40                      | 31                       | 0                             | 6                           | 34                    | 9                    |
| Nuchal fold thickness         | 40                      | 0                        | 0                             | 6                           | 34                    | 40                   |
| $\Delta$ epidermal thickness  | 40                      | 32                       | 0                             | 6                           | 34                    | 8                    |

**Table 2.5** Number of WT mice used for the listed analyses after 40 weeks of DMBA/TPA treatment.

| Analysis                      | Start of experiment [n] | Animals not measured [n] | Death due to other causes [n] | Death due to tumor size [n] | End of experiment [n] | Animals measured [n] |
|-------------------------------|-------------------------|--------------------------|-------------------------------|-----------------------------|-----------------------|----------------------|
| Tumor burden                  | 40                      | 4                        | 4                             | 1                           | 35                    | 36                   |
| Survival                      | 40                      | 0                        | 4                             | 1                           | 35                    | 40                   |
| Tumor-free survival           | 40                      | 0                        | 4                             | 1                           | 35                    | 40                   |
| Tumors/mouse                  | 40                      | 4                        | 4                             | 1                           | 35                    | 36                   |
| Tumor weight                  | 40                      | 4                        | 4                             | 1                           | 35                    | 36                   |
| Tumor size/mouse              | 40                      | 4                        | 4                             | 1                           | 35                    | 36                   |
| Tumor size distribution       | 40                      | 18                       | 4                             | 1                           | 35                    | 22                   |
| Tumor morphology distribution | 40                      | 37                       | 4                             | 1                           | 35                    | 3                    |
| Nuchal fold thickness         | 40                      | 4                        | 4                             | 1                           | 35                    | 36                   |

|                              |    |    |   |   |    |   |
|------------------------------|----|----|---|---|----|---|
| $\Delta$ epidermal thickness | 40 | 32 | 4 | 1 | 35 | 8 |
|------------------------------|----|----|---|---|----|---|

**Table 2.6** Number of *Ccr10*-deficient mice used for the listed analyses after 40 weeks of DMBA/TPA treatment.

### 2.3.3 Minimal Erythema Dose

A test was performed to determine the minimal erythema dose (MED). The MED is the minimal dose of irradiation after which an erythema developed. The MED at d-1 was used to calculate irradiation time for the mice in the UVB-irradiation experiment. The light test was performed using the following protocol: One day before irradiation was performed, 7 male mice from each group (WT and *Ccr10*-deficient mice) were shaved with an electric razor (Isis GT420, Aesculap Suhl GmbH, Suhl, Germany) and afterwards depilated with topical hair removal cream for sensitive skin (Veet, Slough, UK). Before the start of the experiment, the emission of UVB light was measured and the respective time periods of irradiation necessary in order to emit a specific UVB dose were calculated, using a UV-meter (Waldmann, Villingen-Schwenningen, Germany). Next, the mice were anaesthetized with ketamine 10% and rompun 2.5% dissolved in NaCl solution provided by the Institute of Animal Care of the Heinrich-Heine-University (ZETT, Düsseldorf, Germany). Half of the shaved areal of each mouse was protected against UV irradiation by using tape impermeable to radiation (Leukosilk, BSN medical, Hannover, Germany). Then the mice were exposed to ultraviolet irradiation corresponding to the distinct UV dose in an irradiation chamber (Saalman GmbH, Herford, Germany) with Philips UVB Broadband TL lamps (Philips, Amsterdam, Netherlands).

| UV dose [mJ/cm <sup>2</sup> ] | Duration of irradiation [min] |
|-------------------------------|-------------------------------|
| 30                            | 1.06                          |
| 40                            | 1.29                          |
| 50                            | 1.51                          |
| 60                            | 2.13                          |
| 70                            | 2.35                          |
| 80                            | 2.58                          |
| 100                           | 3.42                          |

**Table 2.7** Respective time periods of irradiation.



Right after irradiation and before the mice recovered from anesthesia, the tape was removed. The UV exposed area of the back of the mice was compared to the protected area of the back 24h after irradiation to determine the MED.

### 2.3.4 UVB-irradiation of mice

Groups of 10 WT and 10 *Ccr10*-deficient mice were included for an early time point, ending the experiment after 12 weeks of UVB-irradiation. Additionally, 40 WT mice and 40 *Ccr10*-deficient mice were included in the experiment for a late time point, ending the UVB-irradiation after 60 weeks. The dorsal area of the mice was trimmed at the start of the experiment and every second week with an electric razor (Isis GT420, Aesculap Suhl GmbH, Suhl, Germany) and every fifth week in conjunction with topical hair removal cream for sensitive skin (Veet, Slough, UK) to make sure that the tissue would not be damaged. Mice were irradiated with 50 mJ/cm<sup>2</sup> UVB (1.25 MED) three times a week on non-consecutive days for 12 or 60 weeks. Mice were irradiated as described in chapter 2.3.3. Philips UVB Broadband TL lamps (Philips, Amsterdam, Netherlands) emit in a range from 290-320 nm and peak at 302 nm according to manufacturers' specifications (<http://www.lighting.philips.com/main/prof/lamps/special-lamps/medical-lamps/medical-therapy-uvb-broad-band/uvb-broadband-tl>). To ensure the emitted dose of dorsal UVB-irradiation, the emission was measured and calculated as follows every time before exposure of the mice using a UV-meter (Waldmann, Villingen-Schwenningen, Germany):

$$\text{Energy} \left( \frac{\text{mJ}}{\text{cm}^2} \right) = \text{Intensity} \left( \frac{\text{mW}}{\text{cm}^2} \right) \times \text{Time (sec)}$$

$$\frac{\text{Energy} \left( \frac{\text{mJ}}{\text{cm}^2} \right)}{\text{Intensity} \left( \frac{\text{mW}}{\text{cm}^2} \right)} = \frac{\text{Time (sec)}}{60} = \text{duration of irradiation}$$

For the late time point after 60 weeks UVB-irradiation, the mice were observed for another 10 weeks without irradiation. The mice were observed daily and pictures of the mice were taken weekly (Canon EOS 1100 D, Tokyo, Japan). Additionally, developing tumors were counted and measured on a weekly basis. Furthermore, lesions with a minimum diameter of 1 mm were measured by using a caliper (Fine

Science Tools, Heidelberg, Germany). After 12 or 70 weeks or due to a tumor burden over 1 cm in diameter per tumor, mice were photographed (Canon EOS 1100 D, Tokyo, Japan) and sacrificed by CO<sub>2</sub> exposure, as described in section 2.3.1. After measuring the nuchal fold thickness with a dial caliper gage (Oditest 00T6, Kroeplin GmbH, Schlüchtern, Germany), tumors were excised and measured manually with a caliper (Fine Science Tools, Heidelberg, Germany) and weighed. Measurements of tumor volume were carried out as described for DMBA/TPA-treated mice. The spleen, the lymph nodes (inguinal, axillary and mandibular) and eyes were collected and a 5 mm skin biopsy of the back and the abdominal region was also performed with a skin biopsy punch (pfm medical ag, Cologne, Germany).

### 2.3.5 Detailed listing of animal numbers used in UVB experiments

For the early time point after 12 weeks of UVB-irradiation, 10 WT mice and 10 *Ccr10*-deficient mice were used in the experiment. All mice reached the end of experiment after 12 weeks of UVB-irradiation in both groups.

| Group                       | Start of experiment [n] | Death due to other causes [n] | Death due to tumor size [n] | End of experiment [n] |
|-----------------------------|-------------------------|-------------------------------|-----------------------------|-----------------------|
| WT                          | 10                      | 0                             | 0                           | 10                    |
| <i>Ccr10</i> <sup>-/-</sup> | 10                      | 0                             | 0                           | 10                    |

**Table 2.8** Number of total mice used for the 12-week early time point analysis after UVB-irradiation.

After 12 weeks of UVB-irradiation, early morphological changes of the skin were analyzed by measuring the changes in the epidermal thickness as a marker for cutaneous inflammation. In this analysis, all mice were included, which survived the end of the experiment (n = 10 WT and n = 10 *Ccr10*-deficient mice).

| Analysis              | Start of experiment [n] | Animals not measured [n] | Death due to other causes [n] | Death due to tumor size [n] | End of experiment [n] | Measured animals [n] |
|-----------------------|-------------------------|--------------------------|-------------------------------|-----------------------------|-----------------------|----------------------|
| Δ epidermal thickness | 10                      | 0                        | 0                             | 0                           | 10                    | 10                   |

**Table 2.9** Number of WT mice used in the analysis of epidermal thickness after 12 weeks of UVB-irradiation.

| Analysis                     | Start of experiment [n] | Animals not measured [n] | Death due to other causes [n] | Death due to tumor size [n] | End of experiment [n] | Measured animals [n] |
|------------------------------|-------------------------|--------------------------|-------------------------------|-----------------------------|-----------------------|----------------------|
| $\Delta$ epidermal thickness | 10                      | 0                        | 0                             | 0                           | 10                    | 10                   |

**Table 2.10** Number of *Ccr10*-deficient used in the analysis of epidermal thickness after 12 weeks of UVB-irradiation.

For the late time point after 70 weeks (60 weeks of chronic UVB-irradiation followed by additional 10 weeks of observation without UVB-irradiation), 40 WT mice and 40 *Ccr10*-deficient mice were used in the experiment to analyze tumor development. In both groups, most of the mice had to be sacrificed before the end of experiment after 70 weeks due to a tumor diameter over 1 cm per tumor (WT n = 27 and *Ccr10*-deficient n = 31). Additionally, five WT and seven *Ccr10*-deficient mice developed a cardiac degeneration and had to be sacrificed or died due to this cause. Sick mice were examined by the veterinarian at the ZETT of the Heinrich-Heine-University Düsseldorf. Therefore, only eight WT mice and two *Ccr10*-deficient mice reached the end of the experiment after 70 weeks.

| Group                       | Start of experiment [n] | Death due to other causes [n] | Death due to tumor size [n] | End of experiment [n] |
|-----------------------------|-------------------------|-------------------------------|-----------------------------|-----------------------|
| WT                          | 40                      | 5                             | 27                          | 8                     |
| <i>Ccr10</i> <sup>-/-</sup> | 40                      | 7                             | 31                          | 2                     |

**Table 2.11** Number of animals surviving to the late time point at week 70, following chronic UVB-irradiation for 60 weeks.

All mice sacrificed due to a tumor diameter over 1 cm and all mice surviving to the end of the experiment after 70 weeks were included into the analysis of the tumor burden (WT mice n = 35 and *Ccr10*-deficient mice n = 33). 40 WT mice and 40 *Ccr10*-deficient mice were included into the evaluation of overall and tumor-free survival. Five WT mice and seven *Ccr10*-deficient mice were censored in the analyses because of cardiac degeneration. Censored mice (WT n = 5 and *Ccr10*-deficient mice n = 7) are shown by a vertical line in the figures (Fig. 3.5 C and D). All mice sacrificed due to their tumor size and all mice surviving to the end of the experiment after 70 weeks were included (WT mice n = 35 and *Ccr10*-deficient mice n = 33) in the evaluation of tumors, tumor weight and tumor volume per mouse. For the evaluation of tumor size distribution, only mice, which developed tumors, were

included in the analysis. This included mice sacrificed based on their tumor size (WT mice  $n = 27$  and *Ccr10*-deficient mice  $n = 31$ ) and those, which developed tumors, smaller than 1 cm until the endpoint of the experiment after 70 weeks (WT mice  $n = 8$  and *Ccr10*-deficient mice  $n = 2$ ). Summarizing, 35 WT mice and 33 *Ccr10*-deficient mice were analyzed in the tumor size distribution. The difference between the numbers of tumors in both groups was the reason for the calculation of the data as a percentage. For the investigation of tumor morphology, only mice with intermediate and large tumors ( $> 50 \text{ mm}^3$ ) were included in the analysis (WT mice  $n = 31$  and *Ccr10*-deficient mice  $n = 32$ ). Mice with tumors  $< 50 \text{ mm}^3$  or mice, which died of cardiac degeneration, were excluded from the evaluation. In this analysis, data were shown as a percentage due to the difference in the tumor number. For the measurement of the nuchal fold thickness and changes in epidermal thickness, all mice surviving to the end of the experiment and all mice sacrificed earlier due to a tumor size  $> 1 \text{ cm}$  were included in the analyses (WT mice  $n = 35$  and *Ccr10*-deficient mice  $n = 33$ ). Furthermore, the nuchal fold thickness was measured in control mice (WT mice  $n = 4$  and *Ccr10*-deficient mice  $n = 4$ ) and for the calculation of changes in epidermal thickness the epidermal thickness in control mice (WT mice  $n = 5$  and *Ccr10*-deficient mice  $n = 5$ ), was measured.

| Analysis                      | Start of experiment [n] | Animals not measured [n] | Death due to other causes [n] | Death due to tumor size [n] | End of experiment [n] | Measured animals [n] |
|-------------------------------|-------------------------|--------------------------|-------------------------------|-----------------------------|-----------------------|----------------------|
| Tumor burden                  | 40                      | 5                        | 5                             | 27                          | 8                     | 35                   |
| Survival                      | 40                      | 0                        | 5                             | 27                          | 8                     | 40                   |
| Tumor-free survival           | 40                      | 0                        | 5                             | 27                          | 8                     | 40                   |
| Tumors/mouse                  | 40                      | 5                        | 5                             | 27                          | 8                     | 35                   |
| Tumor weight                  | 40                      | 5                        | 5                             | 27                          | 8                     | 35                   |
| Tumor size/mouse              | 40                      | 5                        | 5                             | 27                          | 8                     | 35                   |
| Tumor size distribution       | 40                      | 5                        | 5                             | 27                          | 8                     | 35                   |
| Tumor morphology distribution | 40                      | 9                        | 5                             | 27                          | 8                     | 31                   |
| Nuchal fold thickness         | 40                      | 5                        | 5                             | 27                          | 8                     | 35                   |
| $\Delta$ epidermal thickness  | 40                      | 5                        | 5                             | 27                          | 8                     | 35                   |

**Table 2.12** Number of WT mice used for the listed analyses after 70 weeks following 60 weeks of chronic UVB-irradiation.

| Analysis                      | Start of experiment [n] | Animals not measured [n] | Death due to other causes [n] | Death due to tumor size [n] | End of experiment [n] | Measured animals [n] |
|-------------------------------|-------------------------|--------------------------|-------------------------------|-----------------------------|-----------------------|----------------------|
| Tumor burden                  | 40                      | 7                        | 7                             | 31                          | 2                     | 33                   |
| Survival                      | 40                      | 0                        | 7                             | 31                          | 2                     | 40                   |
| Tumor-free survival           | 40                      | 0                        | 7                             | 31                          | 2                     | 40                   |
| Tumors/mouse                  | 40                      | 7                        | 7                             | 31                          | 2                     | 33                   |
| Tumor weight                  | 40                      | 7                        | 7                             | 31                          | 2                     | 33                   |
| Tumor size/mouse              | 40                      | 7                        | 7                             | 31                          | 2                     | 33                   |
| Tumor size distribution       | 40                      | 7                        | 7                             | 31                          | 2                     | 33                   |
| Tumor morphology distribution | 40                      | 8                        | 7                             | 31                          | 2                     | 32                   |
| Nuchal fold thickness         | 40                      | 7                        | 7                             | 31                          | 2                     | 33                   |
| $\Delta$ epidermal thickness  | 40                      | 7                        | 7                             | 31                          | 2                     | 33                   |

**Table 2.13** Number of *Ccr10*-deficient mice used for the listed analyses after 70 weeks following 60 weeks of chronic UVB-irradiation.

### 2.3.6 Measurement of epidermal thickness

For analysis of tumor development at early and late stages, mice were sacrificed after 12 weeks and either after 40 weeks for the DMBA/TPA-group or 70 weeks for the UVB-group. After 12 weeks, the treated dorsal skin was collected and sliced into several parts. The tissue slices were fixed in 4% formalin (Sigma-Aldrich, St. Louis, USA) and embedded in paraffin. Paraffin sections were cut at a thickness of 5  $\mu$ m. All paraffin sections were stained with haematoxylin/eosin using a tissue stainer with the following protocol, performing each step for 30 sec:

|                                   |
|-----------------------------------|
| Xylene                            |
| Xylene                            |
| 99% isopropyl                     |
| 96% isopropyl                     |
| 70% isopropyl                     |
| Tap water                         |
| Haematoxylin                      |
| Haematoxylin                      |
| Haematoxylin                      |
| Haematoxylin                      |
| Tap water                         |
| Hydrogen chloride (HCL) – alcohol |
| Tap water                         |
| Scott's tap water substitute      |
| Tap water                         |
| dH <sub>2</sub> O                 |
| Eosin                             |
| 96% isopropyl                     |
| 96% isopropyl                     |
| 99% isopropyl                     |
| 99% isopropyl                     |
| Xylene                            |
| Xylene                            |

For the late time points (40 and 70 weeks for DMBA/TPA and UVB, respectively) a 5 mm skin biopsy of the dorsal skin was performed with a skin biopsy punch (pfm medical ag, Cologne, Germany) and immediately embedded in Tissue-Tek®-O.C.T. compound (Sakura, Zoeterwoude, Netherlands). Frozen tissue sections were cut at a thickness of 12 µm using a cryostat (-35°C) (Leica CM3050 S, Leica Biosystems, Wetzlar, Germany). All frozen tissue sections were stained with haematoxylin/eosin using a tissue stainer with the following protocol, performing each step for 30 sec:

|                                   |
|-----------------------------------|
| Haematoxylin                      |
| Haematoxylin                      |
| Tap water                         |
| Hydrogen chloride (HCL) – alcohol |
| Tap water                         |
| Scott's tap water substitute      |
| Tap water                         |
| dH <sub>2</sub> O                 |
| Eosin                             |
| 96% isopropyl                     |
| 96% isopropyl                     |
| 99% isopropyl                     |
| 99% isopropyl                     |
| Xylene                            |
| Xylene                            |

Skin, dermal and epidermal thickness was measured by microscopic examination (Axioskop 40, Carl Zeiss, Germany, Axiovision 4.6.1 Software, Zeiss Microimaging, Oberkochen, Germany) of skin tissue sections. The  $\Delta$  epidermal thickness was determined in the following way: The mean of the epidermal thickness of untreated control animals of WT and of *Ccr10*-deficient background was calculated. Next, this mean value was used to normalize between treated and untreated animals by subtraction of this value from the measured epidermal thickness of treated mice at the 12-week time point and the 40-week time point for the DMBA/TPA-group or at the 12-week time point and the 70-week time point for the UVB-group giving a  $\Delta$  epidermal thickness value for each mouse.

### 2.3.7 Total DNA Isolation of murine tail tips

Total DNA extraction from murine tail tips was realized by using the DNeasy<sup>®</sup> Blood & Tissue Kit (Qiagen, Hilden, Germany) according to the manufacturer's instructions. For lysis of the murine tail tip, 180  $\mu$ l of ATL buffer and 20  $\mu$ l of proteinase K was added to the tail tip. Samples were vortexed and then lysed overnight at 56°C in a thermomixer 5437 (Eppendorf, Hamburg, Germany) until the tissue was completely lysed. After overnight incubation the sample was vortexed again and 200  $\mu$ l of each AL buffer and (96 – 100%) ethanol was added to purify the DNA. The solution was

again mixed by vortexing. The mixture was transferred into a DNeasy Mini spin column and subsequently centrifuged (8000 rpm for 1 min at RT) (Centrifuge 5415R, Eppendorf, Hamburg, Germany). During centrifugation, DNA of the mouse-tail tip bound to the DNeasy membrane. Contaminants were removed by washing the membrane with 500 µl AW1 buffer and a centrifugation step (8000 rpm for 1 min at RT) (Centrifuge 5415R, Eppendorf, Hamburg, Germany). Subsequently, a washing step was performed with 500 µl AW2 buffer and centrifugation (14,000 rpm for 3 min at RT) (Centrifuge 5415R, Eppendorf, Hamburg, Germany), followed by an additional dry centrifugation step (14,000 rpm for 1 min at RT) (Centrifuge 5415R, Eppendorf, Hamburg, Germany) to remove residual ethanol. The DNeasy Mini spin column was placed into a new 1.5 ml tube and the bound DNA was eluted with 200 µl AE buffer directly loaded on the column membrane. After incubation for 1 min a final centrifugation step was performed to elute the DNA from the membrane (8000 rpm for 1 min at RT) (Centrifuge 5415R, Eppendorf, Hamburg, Germany).

### **2.3.8 Polymerase chain reaction (PCR)**

PCR was performed to enzymatically amplify specific DNA sequences using two oligonucleotide primers for verification of the genotype of mice used in the experiment. First, the DNA was initially denatured. Then a three step procedure was performed (denaturation, annealing of primers and extension), which characterizes the principle of PCR method. During the denaturation step genomic DNA was heated up to 95°C, which separated the DNA double-strands from each other. This was followed by an annealing step to anneal primers to the complementary single-stranded DNA at a reduced temperature, according to nucleotide composition of the primers. In the last step, extension was performed and temperature was set to optimal working conditions for the Taq polymerase (72°C) to synthesize the DNA. Cycles were repeated 28 times to allow exponential amplification of a specific DNA sequence. Finally, a last extension step was performed. The PCR program, which was used, is listed in the following table:



| Reaction steps       | Temperature [°C] | Time   | Cycles |
|----------------------|------------------|--------|--------|
| Initial denaturation | 95               | 5 min  |        |
| Denaturation         | 95               | 30 sec | 1 x    |
| Annealing            | 60               | 30 sec |        |
| Extension            | 72               | 30 sec |        |
| Denaturation         | 95               | 30 sec | 1 x    |
| Annealing            | 57               | 30 sec |        |
| Extension            | 72               | 30 sec |        |
| Denaturation         | 95               | 30 sec | 28 x   |
| Annealing            | 54               | 30 sec |        |
| Extension            | 72               | 30 sec |        |
| Final extension      | 72               | 5 min  |        |
| Cooling              | 8                | ∞      |        |

**Table 2.14** Touchdown PCR program for genotyping.

PCR reactions were performed in a peqSTAR 96x Thermocycler-Gradient (PEQLAB Biotechnologie GmbH, Erlangen, Germany). A gradient PCR was carried out to determine the optimal annealing temperature for the primer pair. The temperature gradient was selected at  $\pm 5^{\circ}\text{C}$  of the expected annealing temperature. The expected annealing temperature was determined by calculating the average of the annealing temperatures of the forward and reverse primer. The annealing of the primer was further optimized by using 3 mM magnesium chloride ( $\text{MgCl}_2$ ). Additionally, optimization of annealing specificity was carried out by using a touchdown PCR. This type of PCR was performed to reduce nonspecific background. Therefore, the annealing temperature of the previous cycles was  $6^{\circ}\text{C}$  or  $3^{\circ}\text{C}$  higher. In the following table, PCR reagents are listed:

| Reagents                          | PCR mix for one reaction [ $\mu$ l] |
|-----------------------------------|-------------------------------------|
| Buffer [10x] without $MgCl_2$     | 1                                   |
| dNTP mix [10 mM]                  | 1                                   |
| Forward primer [10 pmol/ $\mu$ l] | 0.5                                 |
| Reverse primer [10 pmol/ $\mu$ l] | 0.5                                 |
| dH <sub>2</sub> O                 | 5.24                                |
| $MgCl_2$ [3 mM]                   | 0.6                                 |
| BSA [10%]                         | 0.08                                |
| Taq DNA Polymerase [5 U/ $\mu$ l] | 0.08                                |
| Genomic DNA                       | 1                                   |
| <b>Final volume</b>               | 10                                  |

**Table 2.15** Reagents and concentrations for one PCR reaction.

| Gene          | Primer                         | Amplicon [bp] | Genotype           |
|---------------|--------------------------------|---------------|--------------------|
| Ccr10 forward | ACC CTT GTA GCC AGA GAT GG     | 1566          | Balb/c<br>wildtype |
| Ccr10 reverse | CTG CCA GTA GAT CGG CTG TA     |               |                    |
| NE020U        | AGA TGG ATT GCA CGC AGG TTC TC | 250           | Knockout           |
| NE0276L       | TTC GCC CAA TAG CAG CCA GTC    |               |                    |

**Table 2.16** PCR primer pairs for genotyping PCR.

### 2.3.9 Agarose gel electrophoresis

Agarose gel electrophoresis was performed to separate DNA fragments by their size. This method is based on separation of DNA fragments by taking advantage of an electric field. In the electric field, the negatively charged DNA fragments migrate to the anode and are separated by size because smaller molecules move faster through the agarose gel than larger molecules. For optimal separation and visualization of DNA fragments a 2% agarose gel (Sigma-Aldrich, St. Louis, USA) with 15  $\mu$ l RedSafe<sup>™</sup> [20,000x] (iNtRON Biotechnology, Korea) was used. After polymerization of the agarose gel, the gel was covered with 1x TAE running buffer. First, 2  $\mu$ l orange DNA loading dye [6x] (Thermo Fisher Scientific, Waltham, USA) was added to the PCR samples. Then, 9  $\mu$ l of the PCR sample loading buffer mix was applied to the agarose gel. A voltage of 220 V was applied to start the electrophoresis process. O'RangeRuler 100 bp DNA Ladder [0.05  $\mu$ g/ $\mu$ l] (Thermo Fisher Scientific, Waltham, USA) was used as DNA size standard to analyze different fragment lengths from 100

— 1500 bp. During separation of DNA fragments, RedSafe™ binds to the DNA and emits a green fluorescence at 537 nm by irradiation with UV light for visualization of DNA fragments. Sizes of the DNA fragments were then determined by comparison to the DNA size standard.

### **2.3.10 Statistical analysis**

Statistical analyses were carried out using the nonparametric Mann-Whitney U test. Kaplan-Meier curves were used for the demonstration of follow-up data and survival analyses. For the analyses of Kaplan-Meier curves the log-rank test was used. Experimental endpoints were set after 12 and 40 weeks in the DMBA/TPA-model and after 12 and 70 weeks in the UVB-model, in addition a tumor diameter over 1 cm was a termination criterion of the experiment. Fisher's exact test was used for the evaluation of tumor morphologies and tumor sizes. Significations of P-values were set as following: \*,  $P < 0.05$ ; \*\*,  $P < 0.01$ ; \*\*\*,  $P < 0.001$ .

### 3 Results

#### 3.1 Analysis of the role of CCR10 in cutaneous carcinogenesis in two model systems

The impact of CCR10 on cutaneous carcinogenesis was examined. Recent findings, by Pivarcsi *et al.* indicated that the activation of the EGFR/Ras signaling pathway resulted in the progressive loss of the skin-specific chemokine CCL27 during cutaneous carcinogenesis [43]. Furthermore, loss of CCL27 correlated with significantly better tumor growth and inhibition of a robust immune response against the tumor [43]. Therefore, the aim of the present study was to further elucidate the impact of CCL27-CCR10 interactions on carcinogenesis *in vivo* by taking advantage of a *Ccr10*-deficient mouse strain. Two distinct models of carcinogenesis induction were analyzed, one depending on a background of chronic inflammation (DMBA/TPA-model) and the other depending on the inhibition of the immune system (UVB-model). Given previous findings it was expected that more carcinogenesis would occur in the *Ccr10*-negative background due to a deficiency of the mice in their tumor immune surveillance system.

#### 3.2 Tumor progression in *Ccr10*-deficient mice is significantly reduced compared to WT controls after DMBA/TPA treatment

DMBA/TPA treatment causes activated *Hras* mutations followed by EGFR activation leading to inflammation and epidermal hyperplasia [99, 101, 105]. After tumor induction by DMBA/TPA, macroscopic analysis upon tumor harvest showed that Balb/c WT mice had markedly more and bigger flank and back tumors, while *Ccr10*-deficient mice had less and smaller tumors (Fig. 3.1 A). In mice initiated with DMBA (stage I) and promoted with TPA for 40 weeks (stage II), first lesions occur between the 9th and 15th week. In both groups the number of tumors per mouse increased with time. The WT group demonstrated an increased tumor burden of 0.5 tumors per mouse after 20 weeks up to 2.9 tumors per mouse after 40 weeks of treatment, compared to the *Ccr10*-deficient group, where the average number of tumors was 0.1 tumors per mouse after 20 weeks and 1.4 tumors per mouse after 40 weeks of treatment. After 25 weeks of DMBA/TPA treatment the tumor burden markedly increased in both groups. The final tumor yield after 40 weeks in the *Ccr10*-deficient group was significantly lower with a reduction of 52% compared to the WT. These

results indicate that *Ccr10*-deficient mice had a low risk for tumor formation when compared to Balb/c WT mice. The decreased rate of tumor formation, induced by the loss of *Ccr10*, suggests a partial protection against chemically induced skin carcinogenesis in *Ccr10*-deficient mice (Fig. 3.1 B). The DMBA/TPA treatment also had an effect on mouse survival rates. Up until week 22, survival rates of Balb/c WT mice and *Ccr10*-deficient mice were identical. After week 22, survival rates started to diverge. *Ccr10*-deficient mice demonstrated an increased survival (97%) compared to the WT group (85%) after 40 weeks (Fig. 3.1 C). The tumor onset for both groups was at week 9 but after week 15 the tumor incidence was persistently lower in the *Ccr10*-deficient group (Fig. 3.1 D). As demonstrated by the results depicted in Figure 3.1 D, loss of *Ccr10* results in a significantly decreased skin tumorigenesis compared to the WT control. After 40 weeks of DMBA/TPA treatment, 40% of *Ccr10*-deficient mice remained tumor-free, whereas only 15% of WT mice were observed to be tumor-free at this time point. *Ccr10*-deficient mice show an increased tumor-free survival of 25% (Fig. 3.1 D). Taken together, contrary to the initial hypothesis, *Ccr10*-deficiency was correlated with a decreased number of initiated tumors, a lower tumor burden and improved tumor-free survival in the inflammation driven two-stage DMBA/TPA carcinogenesis model.

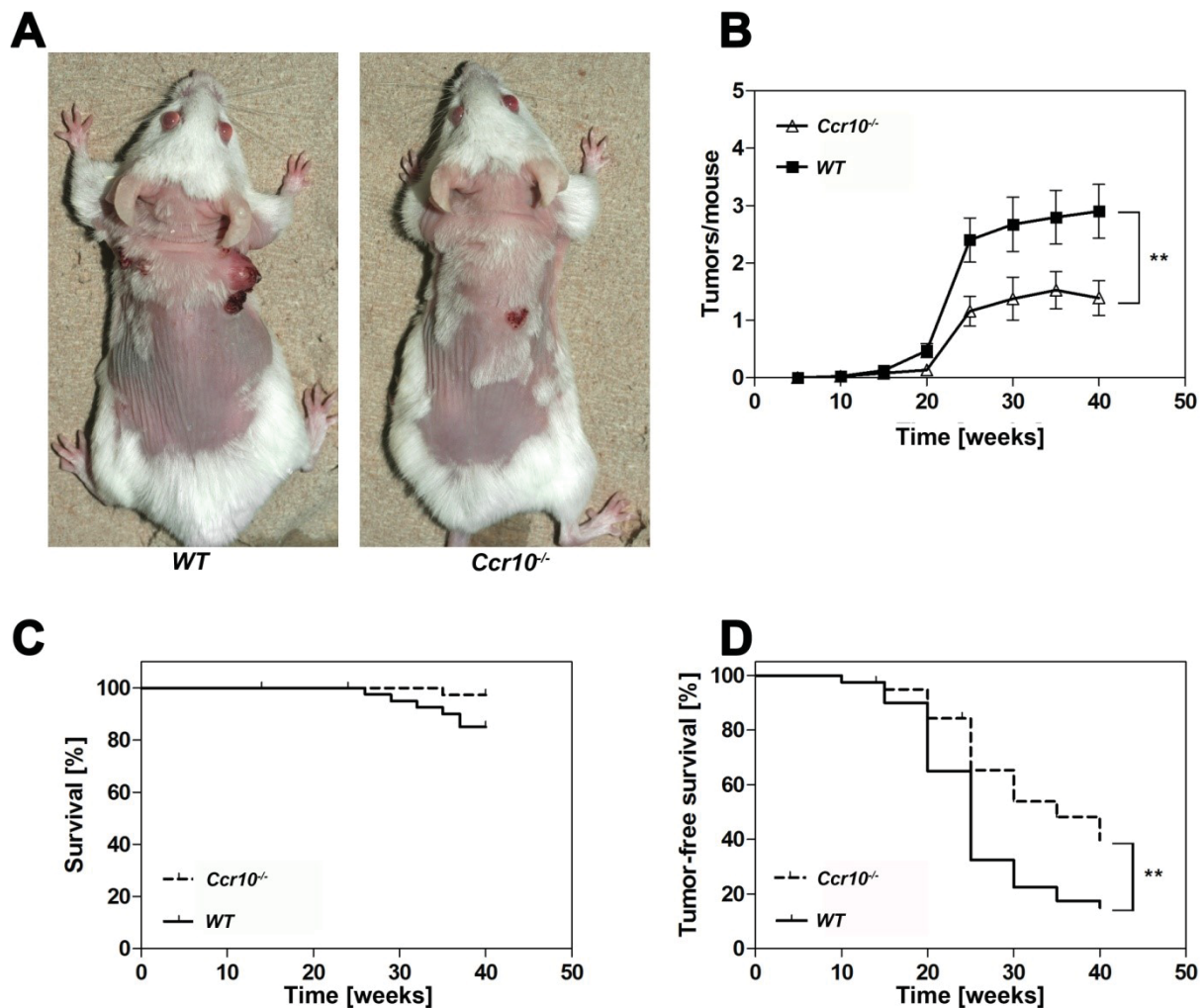


**Figure 3.1** Tumor progression in Balb/c-*Ccr10*-deficient (*Ccr10*<sup>-/-</sup>) mice is significantly reduced when compared to Balb/c wildtype (WT) controls after DMBA/TPA treatment. **(A)** Macroscopic analysis of skin tumors in WT and *Ccr10*-deficient mice 40 weeks after DMBA/TPA treatment. Representative images are shown. **(B)** Tumor burden is shown as average tumor numbers per mouse. Data obtained after 40 weeks of DMBA/TPA treatment: WT mice (n = 40; 2.9 ± 0.469 tumors per mouse); *Ccr10*-deficient mice (n = 36; 1.4 ± 0.299 tumors per mouse) mean ± SEM.; \*\*, P < 0.01 (Mann-Whitney U test). **(C)** Kaplan Meier curve demonstrating increased survival in *Ccr10*-deficient mice treated with DMBA/TPA. WT mice (n = 40); *Ccr10*-deficient mice (n = 40); P < 0.07 n.s. (log rank test). **(D)** Kaplan Meier curve of tumor-free survival. Delayed tumor appearance in *Ccr10*-deficient mice treated with DMBA/TPA. WT mice (n = 40); *Ccr10*-deficient mice (n = 40); \*\*, P = 0.0034 (log rank test).

### 3.3 Absence of CCR10 signaling decreases cutaneous carcinogenesis in an ‘inflammation’-dependent (DMBA/TPA) tumor model

As demonstrated in Figure 3.2 A, *Ccr10*-deficient mice have a significantly reduced number of tumors per mouse after 40 weeks. Contrary to previous findings by Pivarcsi *et al.*, where the inhibition of CCL27 by neutralizing antibodies promotes tumor growth in a syngeneic melanoma model [43], in this study *Ccr10*-deficient mice

developed significantly less and smaller tumors compared to WT controls. These mice developed a median number of 1 tumor per mouse, while WT mice developed a median number of 2 tumors per mouse. The number of tumors in *Ccr10*-deficient mice was decreased by 50% (Fig. 3.2 A). The effect of decreased tumor numbers in the *Ccr10*-deficient group corresponded with a decreased tumor weight and volume as shown in Figure 3.2 B and C. *Ccr10*-deficient mice seemed to be more efficient in reducing the tumor development and progression in a DMBA/TPA inflammation-induced tumor-model than WT mice. WT mice developed tumors with a median tumor weight of 0.09 g, while *Ccr10*-deficient mice developed tumors with tumor weights of a median of 0.02 g. Therefore, tumors in *Ccr10*-deficient mice had only in median 78% of the weight of tumors in WT mice (Fig. 3.2 B). Similarly, determination of the tumor volume of DMBA/TPA-induced tumors showed that the tumor volume in WT mice was greater compared to *Ccr10*-deficient mice. WT mice presented tumors with a median tumor volume of 34.37 mm<sup>3</sup> and *Ccr10*-deficient mice presented tumors with a median tumor volume of 3.62 mm<sup>3</sup>. Compared to WT mice, *Ccr10*-deficient mice developed tumors with an 89% decrease in tumor volume (Fig. 3.2 C). In summary, the inhibitory effect on cutaneous carcinogenesis of *Ccr10*-deficiency resulted in significantly decreased average tumor numbers, tumor weight and volume per mouse.

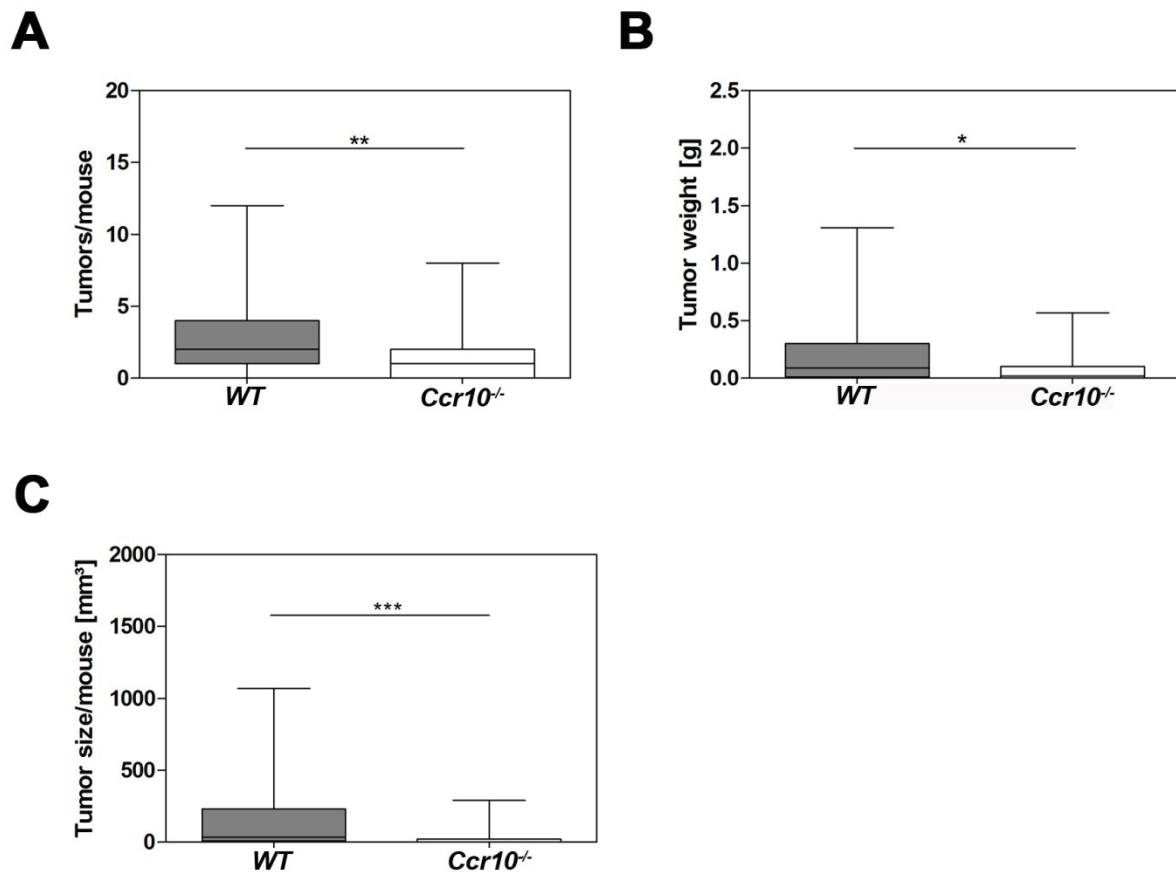


**Figure 3.2** Absence of CCR10 signaling decreases cutaneous carcinogenesis in an inflammation-dependent (DMBA/TPA) tumor model. **(A)** The box-plot shows the number of tumors per mouse. The horizontal bar in the box indicates the median number of tumors in each genotype. Balb/c wildtype (WT) mice (n = 40; 0 min to 12 max tumors per mouse); Balb/c-*Ccr10*-deficient mice (n = 36; 0 min to 8 max tumors per mouse); Whiskers: min to max; \*\*, P = 0.0059 (Mann-Whitney U test). **(B)** The box-plot shows the weight of tumors dissected 40 weeks after beginning of treatment. The horizontal bar in the box indicates the median weight in each genotype. WT mice (n = 39; 0 g min to 1.31 g max tumor weight); *Ccr10*-deficient mice (n = 36; 0 g min to 0.57 g max tumor weight); Whiskers: min to max; \*, P = 0.0181 (Mann-Whitney U test). **(C)** The box-plot shows tumor growth, evaluated by measuring the tumor volume after removal of the tumor. The horizontal bar in the box indicates the median tumor volume in each genotype. WT mice (n = 40; 0 mm<sup>3</sup> min to 1071 mm<sup>3</sup> max tumor volume); *Ccr10*-deficient mice (n = 36; 0 mm<sup>3</sup> min to 290.1 mm<sup>3</sup> max tumor volume); Whiskers: min to max; \*\*\*, P = 0.0004 (Mann-Whitney U test).

### 3.4 *Ccr10*-deficiency induces different tumor morphologies compared to WT controls

Reference material was obtained from all tumors, but was not available for follow-up analyses. In a random sampling, microscopic examination of histological slices of intermediate and large tumors of both groups and all of those tumors presented an epithelial differentiation corresponding to those of a developed SCC (Fig. 3.3 B and D). This is in accordance with the literature, saying that a small number of papillomas



progress into SCCs [98, 104]. Analysis of DMBA/TPA-induced tumors indicated two morphologically different phenotypes (Fig. 3.3 A and C). Tumors developed either with a central exulceration (Fig. 3.3 A) or with a papilliform and hyperkeratotic shape (Fig. 3.3 C). The tumors with a central exulceration had a round shape and were very large (Fig. 3.3 A), while the other tumor phenotype was characterized by a papilliform and hyperkeratotic shape (Fig. 3.3 C). Microscopic analysis of a random sampling of intermediate and large tumors showed a cell-rich tumor microenvironment with a diffuse infiltration of immune cells in tumors with a central exulceration, while in contrast, papilliform hyperkeratotic tumors showed a hyperparakeratosis and underneath it a papillomatous enlarged epithelium. The epithelium of these tumors presented with atypical keratinocytes, which exhibit an increased amount of mitosis. A clear invasion into the corium was not observed. The Infiltrate in the environment is lymphohistiocytic, but further analysis of the infiltrate was not possible. The analysed tumors were validated as microinvasive (Fig. 3.3 D). Tumors with a central exulceration were characterized as SCCs (Fig. 3.3 B). All morphological phenotyping was kindly performed by PD Dr. med. Julia Reifemberger, dermatohistopathologist in the department of dermatology at the university hospital Düsseldorf. The relative number of small, intermediate and large tumors was also analyzed. The cutoff value to evaluate tumor sizes was set at biologically relevant values. Most developed tumors were small and show tumor volumes up to 40 mm<sup>3</sup> (first cutoff). The mean tumor volume was calculated around 150 mm<sup>3</sup>, therefore this value was chosen for the second cutoff for intermediate tumors. Bigger tumors with a volume > 150 mm<sup>3</sup> were rated as large (third cutoff). After DMBA/TPA treatment for 40 weeks, the formation of a high number of small tumors was observed, whereupon the relative number of small tumors in the *Ccr10*-deficient group (92%) was higher compared to the WT group (79%). The relative number of intermediate and large tumors was decreased in the *Ccr10*-deficient group (intermediate tumors 4% and large tumors 4%) compared to WT mice (intermediate tumors 12% and large tumors 9%) (Fig. 3.3 E). When limiting the analysis of tumor morphology to tumors of only large and intermediate size, there was a significant difference in the type of tumor morphology depending on the observed group. The WT group presented only with papilliform and hyperkeratotic tumors (100%), which were markedly less, observed in the *Ccr10*-deficient group (33%). In contrast, the relative number of tumors, which developed

with a central exulceration, was only found in the *Ccr10*-deficient group and the predominantly tumor phenotype in these mice (67%) (Fig. 3.3 F).

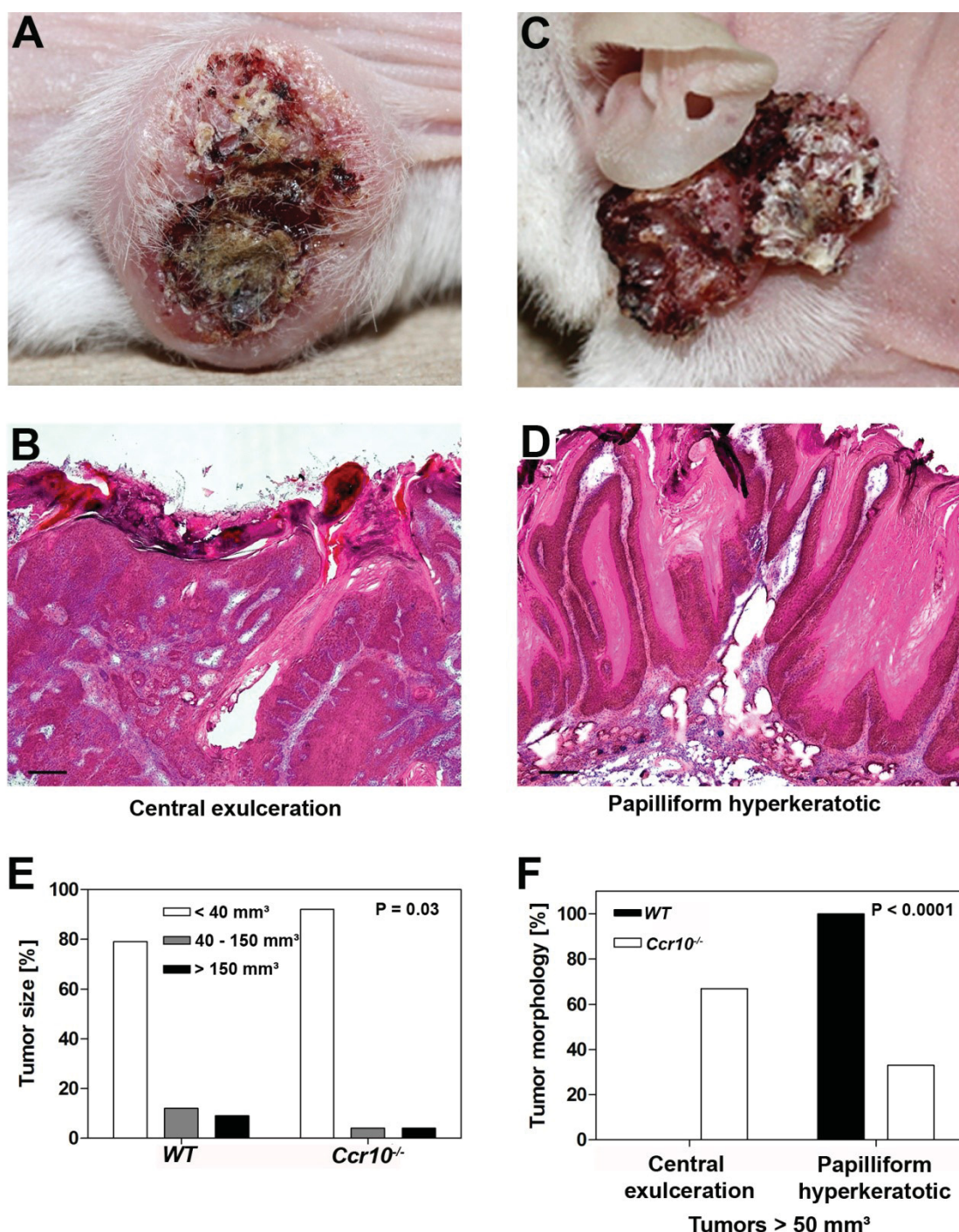


**Figure 3.3** DMBA/TPA administration induces morphologically different tumors in Balb/c wildtype (WT) and Balb/c-*Ccr10*-deficient mice. **(A)** Macroscopic analysis of a tumor with a central exulceration. A representative image of a skin tumor with central exulceration is depicted. WT tumors (n=14) and *Ccr10*-deficient tumors (n=3) **(B)** Microscopic analysis of a tumor with a central exulceration (n = 2). Haematoxylin & eosin staining of a DMBA/TPA-induced tumor (40x magnification; scale bar 200  $\mu$ m). **(C)** Macroscopic analysis of a papilliform and hyperkeratotic tumor 40 weeks after DMBA/TPA treatment. A representative

image of a papilliform and hyperkeratotic skin tumor is shown. **(D)** Microscopic analysis of a papilliform and hyperkeratotic tumor (n = 2). Haematoxylin & eosin staining of a DMBA/TPA-induced papilliform and hyperkeratotic skin tumor (40x magnification; scale bar 200  $\mu$ m). **(E)** Tumor size distribution in percentage terms showing the relative number of small (< 40 mm<sup>3</sup>), intermediate (40-150 mm<sup>3</sup>) and large tumors (> 150 mm<sup>3</sup>) determined for each genotype (all measured as tumor volume). WT mice (n = 34); *Ccr10*-deficient mice (n = 22); WT tumors (n = 116); *Ccr10*-deficient tumors (n = 50); \*, P = 0.03 (Fisher's exact test). **(F)** Tumor morphology distribution in percentage, showing the tumor morphology of the relative number of tumors (> 50 mm<sup>3</sup>) determined for each genotype. All tumors presented with either a central exulceration or a papilliform and hyperkeratotic morphology. WT mice (n = 9); *Ccr10*-deficient mice (n = 3); WT tumors (n = 14); *Ccr10*-deficient tumors (n = 3); \*\*\*, P < 0.0001 (Fisher's exact test).

### 3.5 *Ccr10*-deficient mice do not exhibit reduced nuchal fold thickness to DMBA/TPA administration

To determine a potential underlying mechanism for the inhibition of tumor development in *Ccr10*-deficient mice after DMBA/TPA administration, the inflammatory response of the mice was analyzed. Previous studies showed that CCL27-CCR10 interaction is important in the development of cutaneous inflammation in a murine atopy-like skin inflammation model [67]. In particular, the recruitment of T cells into the skin was impaired and resulted in decreased skin thickness and decreased acanthosis [67]. Moreover, Pivarcsi *et al.* have shown that administration of a neutralizing antibody against murine CCL27 leads to significantly decreased recruitment of CD4 and CD8 lymphocytes, decreased IFN- $\gamma$  release, and increased tumor growth in a murine melanoma model *in vivo* [43]. Therefore, it was ascertained whether the loss of *Ccr10* would alter the inflammation-induced thickening of the skin. Figure 3.4 A shows a markedly increased skin thickness of the epidermal and dermal compartment accompanied by an increased immune response in the WT and *Ccr10*-deficient group after DMBA/TPA treatment compared to control mice. Surprisingly, there was not a difference in DMBA/TPA-induced skin thickening between the WT and the *Ccr10*-deficient mice (Fig. 3.4 A). Nuchal fold thickness was measured as a marker for inflammation-induced skin thickening. A larger thickness denotes a stronger induction of an inflammatory response. Additionally, the treatment with DMBA/TPA resulted in a significant increase in nuchal fold thickness in both *Ccr10*-deficient and WT mice after 40 weeks. In WT control mice, which were never treated with DMBA/TPA, the mean of the measured nuchal fold thickness was 0.745 mm and was markedly increased in WT mice treated with DMBA/TPA for 40 weeks with a mean nuchal fold thickness of 0.978 mm. The nuchal fold thickness in WT mice was increased by 31% as a result of DMBA/TPA treatment for 40 weeks (Fig. 3.4 B).

Similarly, in *Ccr10*-deficient control mice the mean nuchal fold thickness was measured at 0.770 mm and was significantly increased in DMBA/TPA-treated mice, which presented with a mean nuchal fold thickness of 0.959 mm. In *Ccr10*-deficient mice the nuchal fold thickness was increased by 25%, following 40 weeks of DMBA/TPA treatment (Fig. 3.4 B). No significant difference between *Ccr10*-deficient mice and WT mice was observed. Furthermore, changes in epidermal thickness were measured after 12 and 40 weeks of DMBA/TPA treatment. An increase of acanthosis was seen after 12 weeks of DMBA/TPA treatment in both WT and *Ccr10*-deficient mice (Fig. 3.4 C). WT mice presented with an enhanced mean epidermal thickness of 12.15  $\mu\text{m}$  compared to *Ccr10*-deficient mice, in which the epidermal thickness increased to a mean of 20.59 after 12 weeks of DMBA/TPA treatment. Determination of epidermal thickness changes after 40 weeks of DMBA/TPA treatment exhibit only a mean increase of 5.41  $\mu\text{m}$  in the WT group and a mean increase of 9.43  $\mu\text{m}$  in the *Ccr10*-deficient group compared to control mice. No significant difference between *Ccr10*-deficient and WT mice was observed at week 12 or at week 40 of DMBA/TPA treatment.



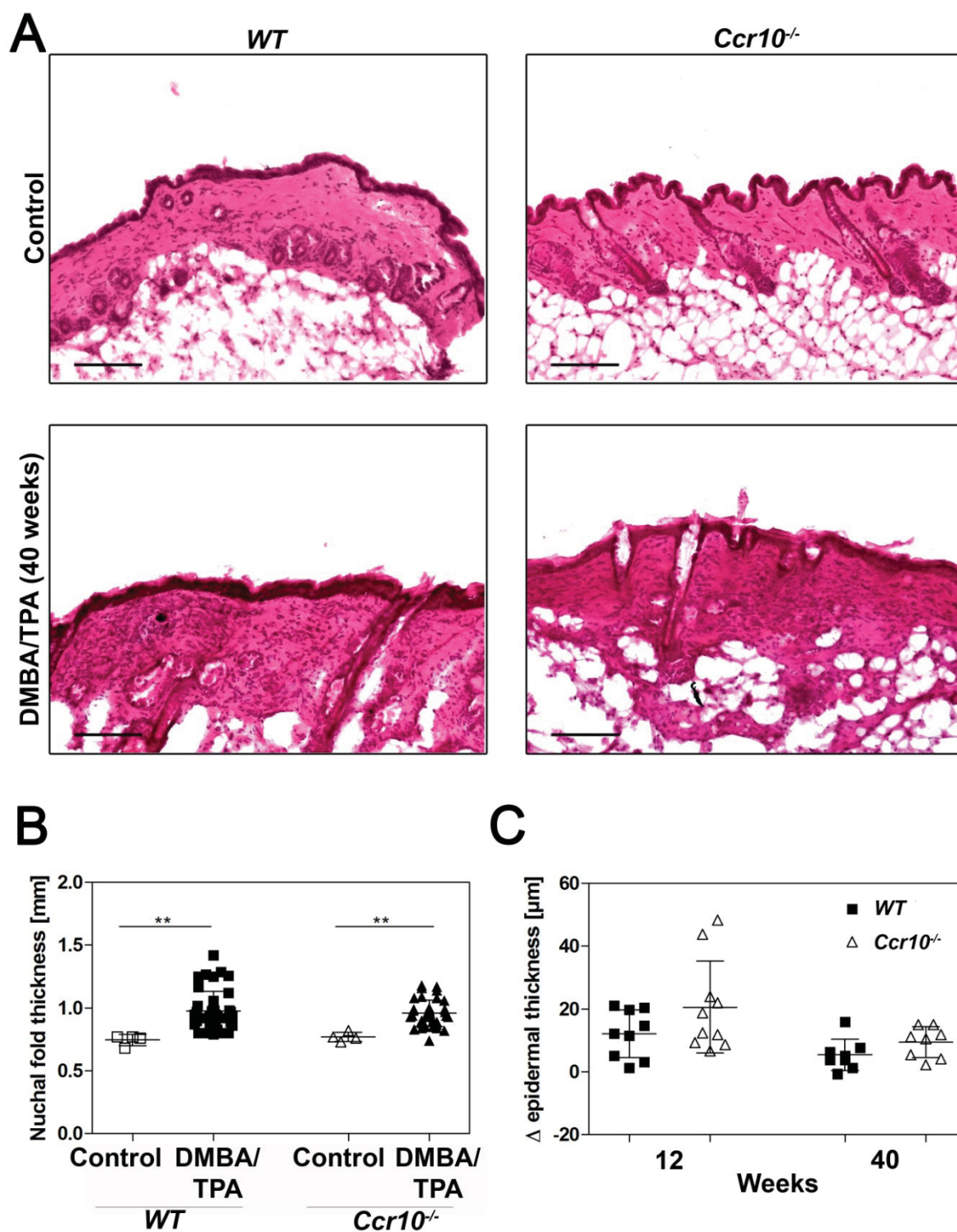


**Figure 3.4** DMBA/TPA treatment induces an inflammatory response in the skin of Balb/c wildtype (WT) and Balb/c-*Ccr10*-deficient mice. **(A)** Microscopic analysis of DMBA/TPA-treated mouse skin. Haematoxylin & eosin staining of untreated skin and 40 weeks (cryo sections) after treatment (100x magnification, scale bar 200 μm). Representative images are shown. **(B)** At week 40, nuchal skin fold thickness was measured in untreated WT (n = 4; nuchal fold thickness 0.745 mm ± 0.044 mm) and *Ccr10*-deficient mice (n = 4; nuchal fold thickness 0.770 mm ± 0.037 mm) as well as DMBA/TPA-treated WT (n = 40; nuchal fold thickness 0.978 mm ± 0.157 mm) and *Ccr10*-deficient mice (n = 36; nuchal fold thickness 0.959 mm ± 0.106 mm); mean ± SD; Untreated WT mice versus treated WT mice \*\*, P < 0.0012 and untreated Balb/c-*Ccr10*-deficient mice versus treated Balb/c-*Ccr10*-deficient mice

<sup>\*\*</sup>,  $P < 0.0021$  (Mann-Whitney U test). No significant difference between *Ccr10*-deficient and WT mice was observed. **(C)** Changes in epidermal thickness ( $\Delta$  epidermal thickness) were measured after 12 and 40 weeks following DMBA/TPA treatment. 12 week DMBA/TPA-treated WT mice ( $n = 9$ ; epidermal thickness  $12.15 \mu\text{m} \pm 7.61 \mu\text{m}$ ); 12 week DMBA/TPA-treated *Ccr10*-deficient mice ( $n = 10$ ; epidermal thickness  $20.59 \mu\text{m} \pm 14.64 \mu\text{m}$ ); 40 week DMBA/TPA-treated WT mice ( $n = 8$ ; epidermal thickness  $5.41 \mu\text{m} \pm 5.007 \mu\text{m}$ ); 40 week DMBA/TPA-treated *Ccr10*-deficient mice ( $n = 8$ ; epidermal thickness  $9.43 \mu\text{m} \pm 4.90 \mu\text{m}$ ); mean  $\pm$  SD;  $P = \text{n.s.}$  (Mann-Whitney U test).

### 3.6 Chronic UVB-irradiation causes a decreased overall survival in *Ccr10*-deficient mice

Chronic UV-exposure has been determined as the major risk factor for cutaneous carcinogenesis [140]. The aim of this part of the study is the analysis of the effect of CCR10-signaling during UVB carcinogenesis by taking advantage of a *Ccr10*-deficient mouse strain and an “immunosuppression”-dependent UVB-irradiation cutaneous carcinogenesis model. First the MED was determined in seven male WT and *Ccr10*-deficient mice as described in the Material and Methods section. The skin of the mice was macroscopically examined and the MED was determined to be  $40 \text{ mJ/cm}^2$ . Following this, 40 female WT and *Ccr10*-deficient mice were irradiated for 60 weeks and sacrificed after 70 weeks at the end of the experiment as outlined in the Material and Methods section. Macroscopic inspection of UVB exposed mice show that in the *Ccr10*-deficient group large tumors developed, while the WT group presented predominantly with tumors of small sizes (Fig. 3.5 A). The tumor number per mouse increased in both groups between week 40 and week 55. At the end of the experiment by week 70, a mean number of tumors per mouse reached a plateau at 3.5 in the *Ccr10*-deficient group and a mean of 4.0 tumors per mouse for the WT group, showing no significant difference between both groups (Fig. 3.5 B). Surprisingly, analyzing the overall survival at the end of the experiment by week 70, a significantly lower survival rate was found for *Ccr10*-deficient mice (6%) compared to WT controls (25%). The overall survival of *Ccr10*-deficient mice is decreased by 19% compared to the WT group (Fig. 3.5 C). Interestingly, photocarcinogenesis resulted in 100% tumor incidence within 60 weeks regardless of group. Development of macroscopic tumors did not occur before week 15. Between week 15 and 40 tumor incidences rose, until 50% of mice had tumors at week 40. After 40 weeks the groups presented with a marked increase in the tumor number per mouse, which is negatively correlated with tumor-free survival (Fig. 3.5 B and D), and after 60 weeks of treatment all animals developed UVB-induced tumors. This result shows no

significant differences in the tumor-free survival between WT mice and *Ccr10*-deficient mice (Fig. 3.5 D). Indicating that the decreased overall survival of *Ccr10*-deficient mice is not a result of increased tumor numbers per mouse or tumor-free survival in *Ccr10*-deficient mice compared to WT mice.

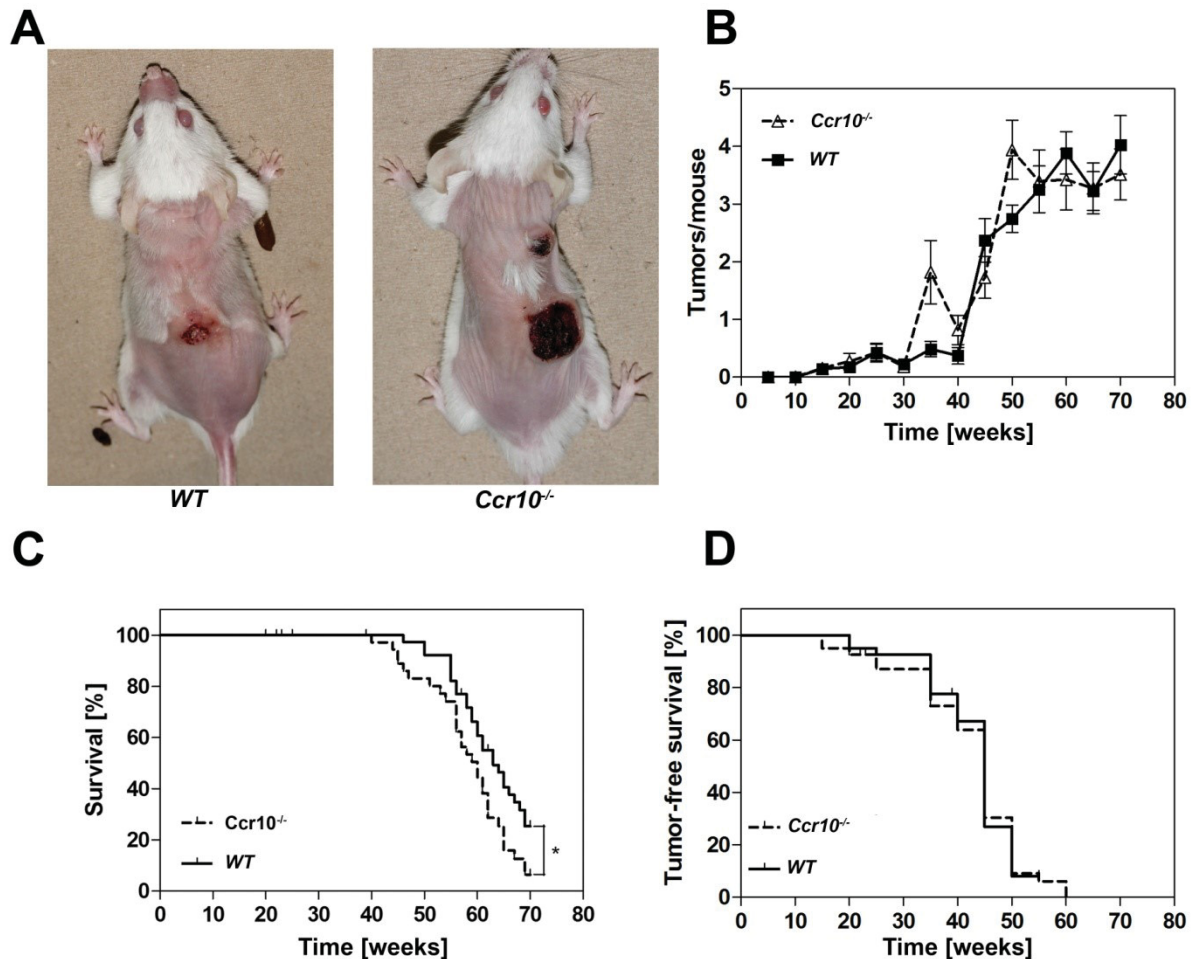


**Figure 3.5** *Ccr10* contribution to mouse skin tumor formation after chronic UVB-irradiation. **(A)** Macroscopic analysis of skin tumors in Balb/c wildtype and Balb/c-*Ccr10*-deficient mice after 60 weeks following chronic UVB-irradiation. Representative images are shown. **(B)** Number of tumors is shown as the average of tumors per mouse. Data were obtained after 70 weeks after the skin was subjected to chronic UVB-irradiation for 60 weeks: WT mice (n = 35;  $4.0 \pm 0.506$  SEM tumors per mouse); *Ccr10*-deficient mice (n = 33;  $3.5 \pm 0.422$  SEM tumors per mouse); mean  $\pm$  SEM; P = n.s. (Mann-Whitney U test). **(C)** Kaplan Meier curve showing decreased survival in *Ccr10*-deficient mice treated with UVB. WT mice (n = 40); *Ccr10*-deficient mice (n = 40); \*, P = 0.0158 (log rank test). **(D)** Kaplan Meier curve of tumor-free survival. All mice develop tumors when they are irradiated with UVB after 60 weeks of treatment. WT mice (n = 40); *Ccr10*-deficient mice (n = 40); P = n.s. (log rank test).

### 3.7 UVB-irradiation increases tumor burden in the absence of CCR10 signaling

To determine the reason for the significantly decreased overall survival of *Ccr10*-deficient mice, tumor numbers, weight and volume were analyzed. Interestingly, significantly enhanced tumor size and volume after chronic UVB-exposure in the *Ccr10*-deficient group was observed (Fig. 3.6 A-C). WT mice presented with a median tumor number of 3 tumors per mouse, similarly *Ccr10*-deficient mice developed a median tumor number of 3 tumors per mouse (Fig. 3.6 A). After 70 weeks, a significantly enhanced median tumor weight of 0.48 g in the *Ccr10*-deficient group compared to a median tumor weight of 0.35 g in the WT group was observed. This is a significant increase in tumor weight by 37% in *Ccr10*-deficient mice compared to WT mice (Fig. 3.6 B). Furthermore, determination of tumor volume per mouse showed a median tumor volume of 234 mm<sup>3</sup> in the WT group, while *Ccr10*-deficient mice were found with a significantly increased tumor volume presenting with a median of 367.3 mm<sup>3</sup>. The median tumor volume per mouse was increased by 57% in the knock-out group compared to the WT group as shown in Figure 3.6 C.

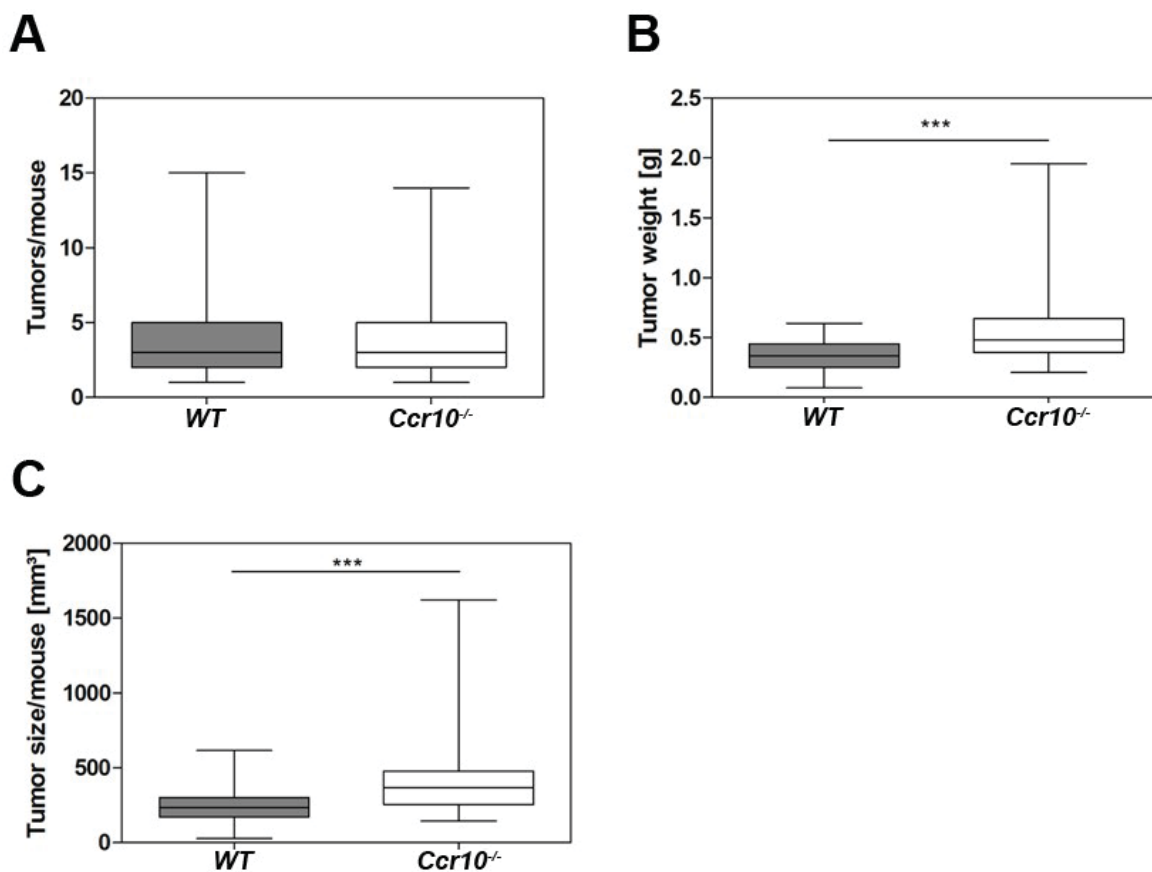




**Figure 3.6** Chronic UVB-irradiation increases tumor burden in the absence of CCR10 signaling. **(A)** The box-plots show the number of tumors per mouse. The horizontal bar in the box indicates the median number of tumors in each genotype. Balb/c wildtype (WT) mice (n = 35; 1 min to 15 max tumors per mouse); Balb/c-*Ccr10*-deficient mice (n = 33; 1 min to 14 max tumors per mouse); Whiskers: min to max; P = n.s. (Mann-Whitney U test). **(B)** Box-plot showing the weight of tumors at the end of the experiment at week 70. The horizontal bar indicates the median weight in each genotype. WT mice (n = 35; 0.08 g min to 0.62 g max tumor weight); *Ccr10*-deficient mice (n = 33; 0.21 g min to 1.95 g max tumor weight); Whiskers: min to max; \*\*\*, P = 0.0002 (Mann-Whitney U test). **(C)** The box-plot reports tumor growth, evaluated by measuring tumor volume after explantation of the tumor. The horizontal bar indicates the median tumor volume in each genotype. WT mice (n = 35; 26.71 mm<sup>3</sup> min to 625.5 mm<sup>3</sup> max tumor volume); *Ccr10*-deficient mice (n = 33; 145.4 mm<sup>3</sup> min to 1622 mm<sup>3</sup> max tumor volume); Whiskers: min to max; \*\*\*, P = 0.0003 (Mann-Whitney U test).

### 3.8 Loss of *Ccr10* results in morphologically different tumors compared to WT mice in a photocarcinogenesis model

Reference material was obtained from all tumors, but was not available for follow-up analyses. In a random sampling, microscopic examination of histological slices of intermediate and large tumors of both groups and all of those tumors presented an epithelial differentiation corresponding to those of a SCC. According to the literature, one of the main causes for SCC development is UVB-irradiation [19, 23]. Observation of UVB-induced tumors revealed two morphologically distinct phenotypes (Fig. 3.7 A and C). One type was characterized as tumors with central exulceration. These tumors showed a round shape and high tumor weights (Fig. 3.7 A). Upon microscopic analysis of a random sampling of intermediate and large tumors, tumors with a central exulceration presented a cell-rich tumor microenvironment with a diffuse infiltration of immune cells, while flat, erosive and scaly tumors presented with reactive enlarged epithelial and containing horn beads. Tumors with a central exulceration were characterized as moderately – lowly differentiated SCC (Fig. 3.7 B), while flat, erosive and scaly tumors were characterized as highly – moderately differentiated SCC (Fig. 3.7 C and D). All morphological phenotyping was kindly performed by PD Dr. med. Julia Reifemberger, dermato-histopathologist in the department of dermatology at the university hospital Düsseldorf. The cutoff for the statistical analysis of small, intermediate and large tumors was set to biological relevant values. Most of the tumors were small and presented with a size of < 50mm<sup>3</sup> (first cutoff). The cutoff for intermediate tumors was applied based on the upper 95% CI of the tumor size in the *Ccr10*-deficient group (500 mm<sup>3</sup>). All tumors above this tumor size (> 500 mm<sup>3</sup>) were characterized as large (third cutoff). The evaluation of small, intermediate and large tumors showed that numbers of small tumors in the

*Ccr10*-deficient group was lower (66%) and the number of large tumors was higher (4%) when compared to WT mice, which presented with 74% small tumors and only one percent of large tumors. Furthermore, the number of intermediate tumors was decreased in WT (25%) and increased *Ccr10*-deficient mice (30%); overall there was no significant difference in tumor numbers between the *Ccr10*-deficient and the WT mice (Fig. 3.7 E). Next, tumor morphology distribution analysis of intermediate and large tumors was performed. Interestingly, tumors with a central exulceration were significantly higher in number (89%) compared to flat, erosive and scaly tumors (11%) in *Ccr10*-deficient mice, while WT mice developed more flat, erosive and scaly tumors (37%) than *Ccr10*-deficient mice (11%) (Fig. 3.7 F). Collectively, *Ccr10*-deficient mice developed a significantly increased number of tumors with a central exulceration (89%) (Fig. 3.7 E), characterized by an enhanced tumor weight (Fig. 3.6 B) and volume (Fig. 3.6 C); indicating that *Ccr10*-deficiency promotes tumor growth in an immune-suppressed UVB-induced carcinogenesis model.

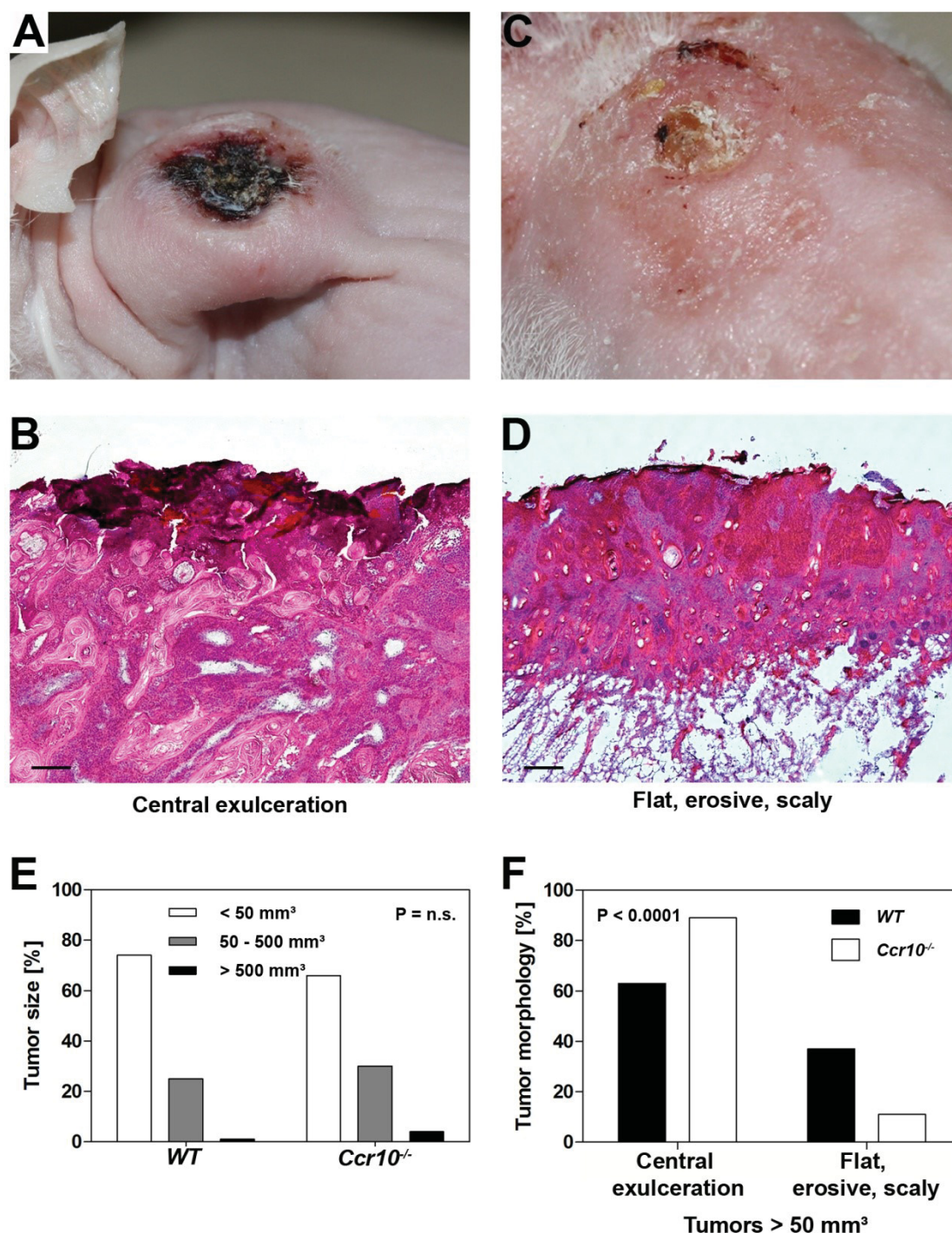


**Figure 3.7** Chronic UVB-irradiation induces morphologically different tumors in Balb/c wildtype (WT) and Balb/c-*Ccr10*-deficient mice. **(A)** Macroscopic analysis of a tumor after 70 weeks with a central exulceration after the skin was subjected to chronic UVB treatment for 60 weeks. A typical image of a skin tumor with a central exulceration is reported. **(B)** Microscopic analysis of a tumor with a central exulceration (n = 2). Haematoxylin & eosin staining of a UVB-induced tumor (40x magnification; scale bars 200  $\mu$ m). **(C)** Macroscopic analysis of a flat, erosive and scaly tumor at the end of the experiment at week 70 after UVB treatment for 60 weeks. A typical image of a flat, erosive and scaly skin tumor is reported. **(D)** Microscopic analysis of a flat, erosive and scaly tumor (n = 2). Haematoxylin & eosin staining of a UVB-induced flat, erosive and scaly skin tumor (40x magnification; scale bar 200  $\mu$ m). **(E)** Tumor size distribution in percentage terms showing the relative number of small (< 50

mm<sup>3</sup>), intermediate (50-500 mm<sup>3</sup>) and large tumors (> 500 mm<sup>3</sup>) determined for each genotype (all measured as tumor volume). WT mice (n = 35); *Ccr10*-deficient mice (n = 33); WT tumors (n = 141); *Ccr10*-deficient tumors (n = 116); P = n.s. (Fisher's exact test). **(F)** Tumor morphology distribution in percentage, showing the tumor morphology of the relative number of intermediate (50-500 mm<sup>3</sup>) and large tumors (> 500 mm<sup>3</sup>) determined for each genotype (all tumors presented with either a central exulceration or a flat, erosive and scaly morphology). WT mice (n = 31); *Ccr10*-deficient mice (n = 32); WT tumors (n = 34); *Ccr10*-deficient tumors (n = 41); \*\*\*, P < 0.0001 (Fisher's exact test).

### 3.9 Decreased epidermal thickness in *Ccr10*-deficient mice is associated with an increased tumor burden

Due to the fact that the development of acanthosis is a physiological light protection mechanism of the skin [2], the morphological changes of the skin were determined. Before treatment, *Ccr10*-deficient and WT mice did not show any difference in skin morphology, epidermal and dermal thickness or in the amount of infiltrating cells as seen in microscopic analysis of H&E-stained skin sections (Fig. 3.8 A). After 12 weeks of treatment a slight increase in the thickness of the skin and acanthosis was observed in both groups, but not in the dermal compartment (Fig 3.8 C), which was accompanied by an increased amount of infiltrating cells in the WT group (data not shown). The mean  $\Delta$  epidermal thickness in WT mice had a value of 16.72  $\mu$ m compared to a mean  $\Delta$  epidermal thickness of 5.13  $\mu$ m in *Ccr10*-deficient mice. This corresponds to an epidermal thickness in the *Ccr10*-deficient group, which is 69% thinner, when compared to the WT group (Fig. 3.8 C). At the end of the experiment at week 70, chronic UVB-exposure resulted in a significant increase of nuchal fold thickness in WT mice accompanied by a strong induction of acanthosis, which was not observed in the same manner in *Ccr10*-deficient mice (Fig. 3.8 A-C). The mean nuchal fold thickness measured in WT controls increased to a mean nuchal fold thickness of 0.89 mm in UVB-treated WT mice. This was an increase of 17% following UVB-irradiation. In contrast, the nuchal fold thickness of *Ccr10*-deficient mice did only slightly increase after UVB-exposure and the mean nuchal fold thickness of the *Ccr10*-deficient controls was measured at 0.84 mm and increased slightly to a mean nuchal fold thickness of 0.90 mm after UVB-irradiation in the treated group (Fig. 3.8 B). This corresponds to an increase of 7% in treated *Ccr10*-deficient mice compared to the control. The acanthosis in the *Ccr10*-deficient mice was significantly less after 12 weeks and did not increase after 70 weeks of UVB-irradiation compared to the WT. Analyses of  $\Delta$  epidermal thickness at the end of the experiment after 70 weeks revealed a mean increase of 24.34  $\mu$ m in WT mice and a



mean increase of 5.23  $\mu\text{m}$  in *Ccr10*-deficient mice. The observed acanthosis in the *Ccr10*-deficient group was only 22% of the thickness observed in WT animals at the end of the experiment at week 70 after UVB-irradiation for 60 weeks (Fig. 3.8 C).

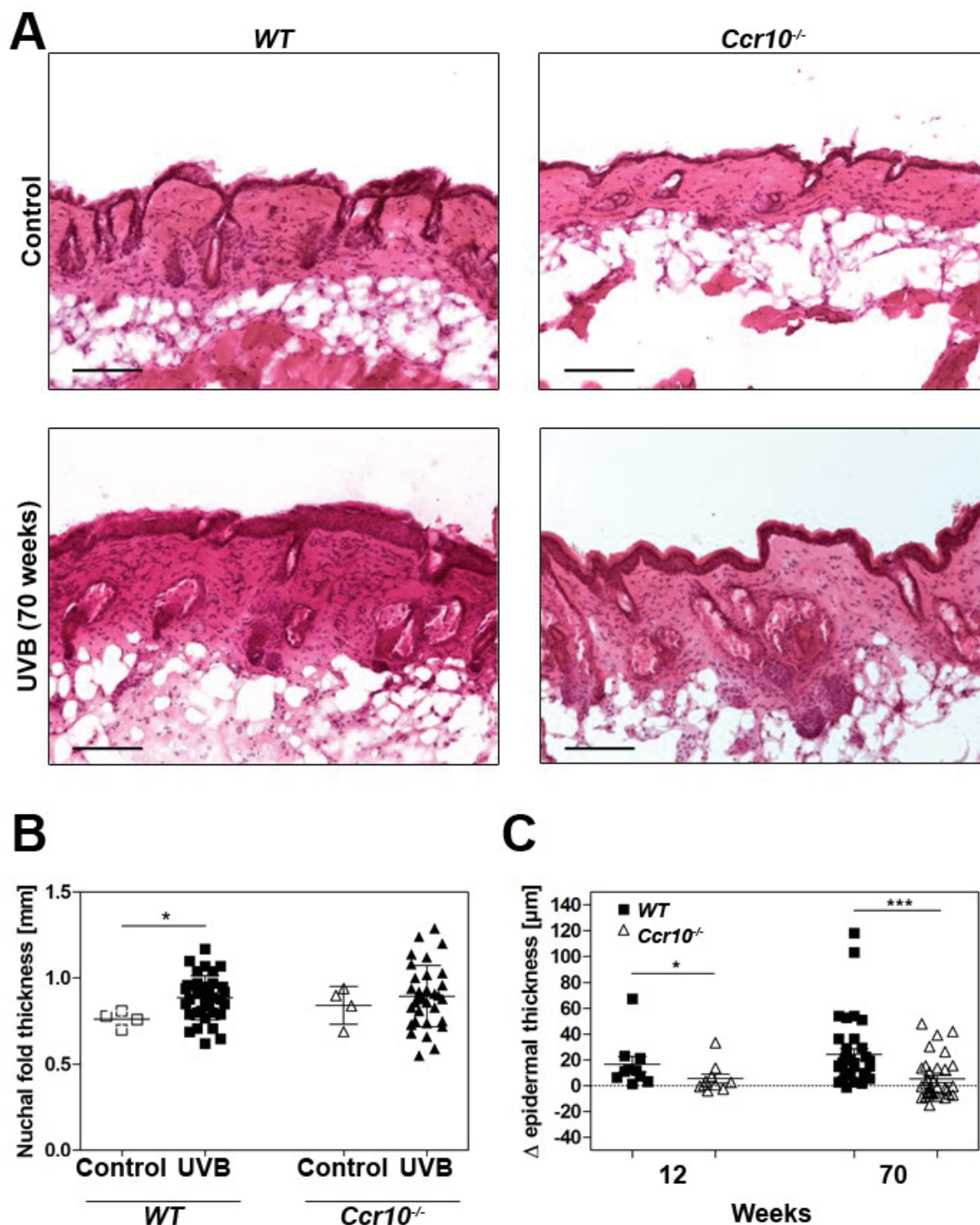


**Figure 3.8** Chronic UVB-irradiation causes skin thickening in Balb/c wildtype (WT) but not in *Ccr10*-deficient mice. **(A)** Microscopic analysis of UVB-treated mouse skin. Haematoxylin & eosin staining of untreated skin and of skin at the end of experiment after 70 weeks following chronic UVB-irradiation for 60 weeks (cryo sections; 100x magnification). **(B)**

Nuchal fold thickness was measured at the end of the experiment at week 70 following chronic UVB-irradiation for 60 weeks in untreated WT mice ( $n = 4$ ;  $0.76 \text{ mm} \pm 0.04646 \text{ mm}$  nuchal fold thickness); *Ccr10*-deficient mice ( $n = 4$ ;  $0.84 \text{ mm} \pm 0.1097 \text{ mm}$  nuchal fold thickness); 60 week chronically UVB-irradiated WT mice ( $n = 35$ ;  $0.89 \text{ mm} \pm 0.1286 \text{ mm}$  nuchal fold thickness); 60 week chronically UVB-irradiated *Ccr10*-deficient mice ( $n = 33$ ;  $0.90 \text{ mm} \pm 0.1787 \text{ mm}$  nuchal fold thickness); mean  $\pm$  SD; \*,  $P = 0.0371$  (Mann-Whitney U test).

**(C)** Changes in epidermal thickness ( $\Delta$  epidermal thickness) were measured after 12 and 70 weeks following chronic UVB-irradiation for 60 weeks. 12 week UVB-irradiated WT mice ( $n = 10$ ;  $16.72 \text{ } \mu\text{m} \pm 19.13 \text{ } \mu\text{m}$   $\Delta$  epidermal thickness); 12 week UVB-irradiated *Ccr10*-deficient mice ( $n = 10$ ;  $5.13 \text{ } \mu\text{m} \pm 10.99 \text{ } \mu\text{m}$   $\Delta$  epidermal thickness); \*,  $P = 0.0312$ . 70 week UVB-irradiated WT mice ( $n = 35$ ;  $24.34 \text{ } \mu\text{m} \pm 26.55 \text{ } \mu\text{m}$   $\Delta$  epidermal thickness); 70 week UVB-irradiated *Ccr10*-deficient mice ( $n = 33$ ;  $5.23 \text{ } \mu\text{m} \pm 16.12 \text{ } \mu\text{m}$   $\Delta$  epidermal thickness); mean  $\pm$  SD; \*,  $P = 0.0312$ ; \*\*\*,  $P < 0.0001$  (Mann-Whitney U test).

## 4 Discussion

The aim of this work was to elucidate the role of CCL27/CCR10 interactions in skin carcinogenesis by taking advantage of two different murine *in vivo*-models of cutaneous carcinogenesis.

The findings of the present study show that the role of CCR10 signaling during cutaneous carcinogenesis is context dependent. In the inflammation-driven DMBA/TPA skin carcinogenesis model, CCR10 promotes tumor development and progression, while under conditions of immune suppression, generated using chronic UVB-irradiation, CCR10 signaling is beneficial via the reduction of tumor growth accompanied by an increased overall survival (Figure 4.1 B+C).

There are at least two different avenues leading to cutaneous carcinogenesis. First, chronic inflammation supports squamous cell carcinoma development in patients suffering from chronic wounds, like non-healing post-burn scar ulcers [141], epidermolysis bullosa [142] and non-healing vascular, diabetic, and pressure ulcers [143], in which only a part of the ulcer transforms into a malignant state and the remaining part is characterized by non-healing inflamed tissue [142]. Another example of chronic inflammation turning into cutaneous carcinogenesis is seen in patients suffering from lichen ruber planus [144, 145], characterized by a markedly increased chemokine-driven inflammatory infiltrate [146].

In contrast to inflammation-induced carcinogenesis, the primary cause for the formation of non-melanoma skin cancer is an UV- or drug-induced immunosuppression [19, 26, 27]. An important effect of UV-induced carcinogenesis is the UV-dependent local and systemic suppression of immune surveillance [147]. Solar keratosis and cutaneous SCCs develop in skin areas of chronic UV-irradiation [148, 149]. The solar keratosis is a precancerous lesion of the skin, which develops into an invasive SCC in 5-10% of patients [149]. The tumor incidence of SCCs of the skin in immune-suppressed solid organ transplant recipients (OTRs) is much higher compared to the general population [149, 150]. 30% of OTRs suffering from solar keratosis develop an invasive SCC [149]. The risk for OTRs to develop a solar keratosis is increased by 250-fold and additionally, they have a 100-fold increased risk for developing an invasive SCC [149]. Interestingly, tumor development in OTRs depends on the duration and the dose-intensity of immunosuppressive therapy [147]. Patients infected with human immunodeficiency virus (HIV) can develop aggressively

growing SCC much earlier in their life (on average at the age of 44 years) [151]. This contrasts with the incidence in a HIV-negative population, which according to a Belgium study published in 2016 that showed incidence rates for the development of SCC increasing with age with an average age for the development of SCCs at 76 years including men and women [152]. Tumors in HIV-infected patients have a high potential for local recurrence and metastatic spread [151]. HIV suppresses the host immunity by elimination of CD4<sup>+</sup> T cells, which in turn is responsible for the enhanced development of cutaneous tumors [147].

Chronic lymphocytic leukemia (CLL) is a malignancy characterized by immune defects and the development of aggressive skin cancers in patients suffering from the disease is increased [147]. Patients, which are immuno-compromised due to HIV infection, solid organ transplantation or CLL, have an increased risk to develop anal SCC [153].

Experimentally, these different avenues of cutaneous carcinogenesis can be mimicked in the murine DMBA/TPA- or in the chronic UVB-model. The DMBA/TPA-model is based on the initiation-promotion protocol, characterized by one initiating topical application of DMBA causing an activated *Hras* gene mutation followed by the promotion stage, in which TPA induces a chronic inflammation in the skin [99]. Therefore, this model is mimicking the diseases and chronic wounds in which chronic inflammation leads to cutaneous carcinogenesis. Liu *et al.* reported recently that DMBA/TPA-induced carcinogenesis induction and promotion was significantly reduced by an additional treatment of the dorsal murine skin with the immunosuppressant methanol in a dose-dependent manner [154]. Furthermore, another study using (+)-catechin emulsified gel showed that a reduction of the inflammatory response decreased tumor development [155].

In contrast, DMBA/TPA tumor development was increased by treatment of the skin with the immunosuppressant tacrolimus [112]. This effect is accompanied by reduced levels of CD4<sup>+</sup>/CD8<sup>+</sup> T cells in lymph nodes [112]. Other studies, concentrating on the type of the induced inflammatory response, demonstrated that a modulation of the inflammatory infiltrate to a Th1 response, including recruitment of INF- $\gamma$ -producing CD8<sup>+</sup> T cells, reduces DMBA/TPA-induced skin carcinogenesis [117, 119]. These studies show that inflammation or a distinct type of inflammatory response is crucial for DMBA/TPA-induced cutaneous carcinogenesis. In contrast to the DMBA/TPA



inflammation-driven skin carcinogenesis model, UVB-irradiation is associated with immune suppression and therefore is responsible for tumor progression and cutaneous carcinogenesis [120]. Fortner and Kripke showed that UV-induced tumors grow progressively in UV-irradiated mice, whereas they regressed in mice never exposed to UVB light [120]. They suggested that a reduction of cytotoxic lymphocytes is responsible for this kind of tumor growth behavior due to UVB-irradiation [120]. Other studies suggested an important change of T cell subpopulations after irradiation to a Th2-dependent immune response, characterized by increased recruitment of CD4<sup>+</sup> Tregs and macrophages, and a suppression of CD8<sup>+</sup> effector T cells [122, 123]. Further studies validated the role for CD8<sup>+</sup> T cells in the reduction of cutaneous carcinogenesis [124, 125]. Especially, the study of Nasti *et al.* showed the opposing effects of different T cell subsets and their role during cutaneous carcinogenesis, where CD8<sup>+</sup> T cells are important for a reduction of carcinogenesis, while CD4<sup>+</sup> T cells promote tumor development and progression [125]. Tumors arising due to immune suppression are highly immunogenic, because they developed under conditions, where they never needed to evade the effects of the immune system on tumor promotion or reduction.

Previous findings on the role of CCL27/CCR10 signaling in cutaneous biology demonstrated that CCL27 is specifically expressed in the skin and recruits CLA<sup>+</sup> skin homing T cells to sites of chemokine expression [61, 67, 78] (Figure 4.1 A). *In vivo* models of atopy-like dermatitis demonstrated an increased expression of CCL27 in the skin accompanied by a markedly increased inflammatory response dominated by lymphocytes, while inhibition of CCL27/CCR10 signaling suppressed cutaneous inflammation and inflammation-induced skin thickening [67]. Pivarcsi *et al.* observed a progressive loss of CCL27 expression during cutaneous carcinogenesis in tumor cells, caused by an activation of the EGFR signaling pathway [43]. Furthermore, in an *in vivo* tumor mouse model anti-CCL27 antibodies promote tumor growth by decreasing the recruitment of CD4<sup>+</sup> and CD8<sup>+</sup> T cells [43].

In contrast, patients treated with EGFRIs presented with an up-regulation of CCL27 expression and an increased inflammatory response in the skin, characterized by clustering macrophages, intraepidermal LCs, CD4<sup>+</sup> and CD8<sup>+</sup> T cells, thereby indicating a strong correlation between CCL27 expression and the EGFR signaling pathway [81]. In addition, these results show the importance of CCL27/CCR10

interactions for the development of a robust immune response in the skin. Therefore, it was expected that an increased cutaneous carcinogenesis would be observed in this work's experiments due to *Ccr10*-deficiency supporting tumor immune escape in both models of cutaneous carcinogenesis induction.

In the UVB model, the results supported our prediction that loss of CCL27/CCR10 interactions supports tumor growth. Findings of the present study show an increased tumor growth in *Ccr10*-deficient mice in the "immunosuppression"-dependent chronic UVB-model of cutaneous carcinogenesis (Figure 4.1 C). Although both groups of mice developed the same amount of tumors at the end of the experiment and the loss of *Ccr10* does not have a strong impact on tumor induction, because tumor multiplicity and the percentage of tumor-free survival were not different in both groups at the end of the experiment, survival was severely impacted by loss of CCL27/CCR10 signaling. In particular, shorter survival was associated with the loss of *Ccr10*, indicating an effect of CCL27/CCR10 signaling for a better disease outcome and reduced tumor progression in the UVB-model.

A significantly increased tumor growth was found in *Ccr10*-deficient mice, though tumor numbers per mouse were equal in both groups. This implies that CCR10 has no effect on tumor induction, but may play an important role in tumor suppression in an immune-impaired carcinogenesis model, suggesting that CCR10 might be beneficial in reducing tumor growth in higher staged patients. These findings are in line with observations of Pivarcsi *et al.* showing that anti-CCL27 treatment increases tumor growth in a CCR10-negative melanoma model [43]. Pivarcsi *et al.* used an "immunogenic" CCR10-negative melanoma cell line (B16F10) to study the role of CCL27/CCR10 interactions in cutaneous immune surveillance [43]. Neutralization of CCL27/CCR10 signaling markedly decreased the recruitment of INF- $\gamma$ -expressing T cells into the tumor microenvironment [43]. Furthermore, tumor progression was associated with an upregulation of matrix metalloproteinase and cyclooxygenase 2 expression [43]. This is in accordance with other studies, which showed an important role for CCL27/CCR10 interactions for the recruitment of T cells into the skin during immune surveillance [61, 78]. An inhibition of these interactions *in vivo* by a mCCL27 antibody leads to markedly reduced recruitment of lymphocytes, but not eosinophils,

into the skin accompanied by a significantly reduced skin thickness under inflammatory conditions [67].

A recent study by Fu *et al.* showed the importance of CCL27/CCR10 interactions for the recruitment of CD8<sup>+</sup> resident T cells under homeostatic conditions [72]. Moreover, they reported a function for CD8<sup>+</sup> resident T cells in the regulation of CD4<sup>+</sup> T cell homeostasis [72]. Another group showed in their work that CCL27/CCR10 interactions are important for the recruitment of CCR10<sup>+</sup> innate lymphoid cells (ILCs) into the skin, where they are responsible for the maintenance of skin-resident T cells [71] (Figure 4.1 A).

For the present study these results indicate that in contrast to WT mice, *Ccr10*-deficient mice lacking CCL27/CCR10 interactions are impaired in their immune surveillance, which might be the cause for unrestricted tumor growth and decreased survival in the case of a suppressed immune system. In the work of Pivarcsi *et al.*, it was shown that during cutaneous carcinogenesis the EGFR/Ras signaling pathway is activated *in vivo* [43]. *In vitro* experiments elucidated that CCL27 mRNA and protein expression is negatively correlated with the level of Ras activity [43]. Furthermore, the EGFR is essential for tissue homeostasis and promotes tumor development [81]. EGFR signaling pathway activation in keratinocytes is important for the skin inflammatory response, host barrier function and immune surveillance [81], but high activation of EGFR signaling can result in tumor development and progression [156]. One of the effects of an overabundance of EGFR/Ras signaling is that the expression of CCL27 is inhibited [43]. This was associated with tumors of epithelial origin [43]. An overexpression of EGFR/Ras signaling followed by CCL27 inhibition during skin carcinogenesis leads to tumor immune escape as well as tumor growth and progression [43] (Figure 4.1 C). Cancer patients treated with EGFR inhibitors present with increased expression of CCL27 followed by a strong inflammatory response in the skin, which correlates with the patient's treatment response [81]. In addition, mice deficient in epidermal EGFR are found with a comparable skin phenotype, which is characterized by a strong chemokine-driven inflammatory response in the skin [81].

In this study, the loss of CCL27 will arise gradually over time due to increasing levels of activation of the EGFR/Ras signaling pathway during carcinogenesis. Therefore, in *Ccr10*-deficient mice, where no CCL27/CCR10 signaling is possible, enhanced tumor growth and progression will be observed compared to wildtype mice due to reduced immune surveillance. Under UVB-treatment wildtype mice, which bear a functional

immune system with reduced but still functional CCL27/CCR10 signaling, would be able to recognize and eliminate transformed cells and as a consequence present with reduced tumor growth and progression compared to *Ccr10*-deficient mice (Figure 4.1 C).

It has been shown that after UVB-induced tissue damage, CCL27 is highly expressed in the basal epidermis followed by a strong release of CCL27 into the papillary dermis of patients with dermatitis solaris and UV-induced cutaneous lupus erythematosus (LE), suggesting an increased recruitment of CCR10<sup>+</sup> skin-homing leukocytes into the UV-irradiated skin [157]. Meanwhile, patients with advanced or chronic UV-induced cutaneous LE are found with reduced CCL27 expression [157].

Interestingly, in this study, CCR10 has no impact on tumor induction in an immune-suppressed environment, but it has an important role in the reduction tumor progression of established tumors. Consequent on the studies mentioned above the recruitment of CD8<sup>+</sup> T cells should be inhibited in *Ccr10*-deficient mice. Especially, the study of Nasti *et al.* showed that these cells are very important for the reduction of tumor progression [125].

Norris *et al.* demonstrated in their work that patients suffering from xeroderma pigmentosum have an increased risk of tumor induction by an impaired immune surveillance of NK cells [158]. In an *in vivo* model analyzing the role of NK cells after UVB-irradiation, mice-lacking NK cells develop more tumors than mice with a high amount of NK cells [159]. These two studies are implicating a role for NK cells in reducing UV-induced tumor induction [158, 159]. PCR analysis by Gao *et al.* shows that NK cells markedly express *Ccr10* [160]. They were the first group, who suggests NK cell recruitment by CCL27/CCR10 interaction [160]. A recent study reported that drugs against multiple sclerosis (glatiramer acetate, dimethyl fumarate, and monomethyl fumarate) increase CCR10 cell surface expression on NK cells [161]. In addition, the study shows that these drugs increase tumor cell destruction by NK cells [161]. In the current study, NK cells might be unaffected by CCL27/CCR10 signaling and as a result; this may lead to the same numbers of tumors in both groups.

Additionally, chronic UVB-irradiation reduces *Ccl27* and *INF-γ* expression in the skin, resulting in decreased recruitment of Th and CTL protective immune cells into the tumor microenvironment and an increased recruitment of immune-suppressive Treg cells, which, together with enhanced vascular endothelial growth factor (VEGF) expression, leads to increased angiogenesis and promotion of tumor growth [162].

Not all cells are transformed and the healthy neighboring cells still have the ability to express reduced levels of CCL27. This could lead to Balb/c wildtype mice having the ability to moderately recruit anti-tumor immune cells via a low CCL27 expression, whereas *Ccr10*-deficient mice lack this ability. This might explain the reduced tumor growth in Balb/c wildtype mice, while enhanced Treg infiltration due to UVB-irradiation without cells able to respond to a baseline CCL27 expression might cause a further suppression of beneficial immune responses in *Ccr10*-deficient mice (Figure 4.1 A).

The tumor growth analysis showed that *Ccr10*-deficient mice developed a higher percentage of intermediate and large tumors, when compared to wildtype mice, even though the result was not significant. After analyzing the tumor morphology of intermediate and large tumors of *Ccr10*-deficient mice these showed mostly a central exulceration, indicating an increased proliferative capacity of tumor cells. In contrast, Balb/c wildtype mice developed significantly more flat, erosive and scaly tumors, demonstrating that CCL27/CCR10 interaction protected against UVB-induced tumor growth, while the absence of CCL27/CCR10 interaction leads to the development of large tumors with a central exulceration.

CCL27 is predominantly produced by keratinocytes in the basal layer of the epidermal compartment and is displayed on the outer membrane of dermal endothelia cells [67]. In addition, the production of vitamin D3 in the skin is strongly induced by UVB-irradiation [163]. The study by Schlumpf *et al.* showed that in the presence of vitamin D3, T cells were activated and expressed CCR10, which recruits T cells into the epidermis, where CCL27 is expressed [163]. In contrast to normal skin, the skin of patients with cutaneous lupus erythematosus (LE) showed an increased expression of CCL27 in the basal layer of the epidermal compartment establishing a chemokine gradient into the papillary dermis, resulting in the activation and migration of T cells and INF- $\alpha$ -producing pDCs as an early response due to UVB-irradiation [157]. CCL27 expression is markedly reduced in advanced or chronic discoid LE suggesting that increased CCL27 expression due to UVB-irradiation is an early response which decreases during disease progression and continuing UVB-irradiation [157]. Moreover, UVB-irradiation decreases Th17 immune responses when applied three times weekly for eight weeks [164].

For the present study, this indicates that UVB-irradiation might markedly reduce the expression of CCL27 over time, but may increase vitamin D3 production in the skin of the mice leading to a higher number of CCR10<sup>+</sup> immune cells in Balb/c wildtype. Therefore, Balb/c wildtype mice expressing *Ccr10* might have an increased ability to recruit CCR10<sup>+</sup>-expressing T cells and pDCs to the skin during the start of the experiment compared to *Ccr10*-deficient mice which are lacking this ability. Consequently, this might lead to the elimination of transformed cells and result in reduced tumor growth and increased survival of Balb/c wildtype mice (Figure 4.1 C). Speculating from the study of Xia *et al.*, *Ccr10*-deficient mice, in contrast to Balb/c wildtype mice, might exhibit a shifted immune response towards Th17 cells and may have the ability to clear out transformed cells at the start of the experiment, but due to long-term treatment and no *Ccr10* expression, these mice might be impaired in the process of tumor cell clearance, thereby resulting in markedly increased tumor progression and decreased survival [73].

The last part of the present study focused on the analysis of morphologically changes of the skin due to UVB-irradiation. Interestingly, the nuchal fold thickness of Balb/c wildtype mice is significantly increased, while *Ccr10*-deficient mice show only a slight thickening of the skin. Further analysis uncovered that *Ccr10*-deficient mice are impaired in developing acanthosis, compared to Balb/c wildtype mice (Figure 4.1 C). The development of acanthosis is a physiological protection mechanism of the skin against UV-irradiation [2]. An impairment of this protection mechanism suggests a higher sensitivity to UVB-induced tumor progression of *Ccr10*-deficient mice.

Recently, Hessner *et al.* showed that S100A10 calcium-binding proteins are able to bind directly to CCR10 [165]. S100A10 interacts with annexin A2, forming a heterotetrameric complex [165]. This complex binds via S100A10 directly to the C-terminal tail of CCR10 located within the 326 to 339 amino acid residues [165]. CCR10 occurs as a dimer and builds a heterotetrameric complex with two annexin A2 molecules [166]. S100A10 is permanently activated and loses its ability to bind calcium, which is very unique among this protein family [166]. Together with S100A10, S100A8 and S100A9 are localized in a gene cluster on the human chromosome 1q21 [167, 168]. The S100 gene cluster consists of three subgroups [168]. The first subgroup containing the genes S100A2 and S100A6, the second subgroup containing the genes A100A8, S100A9 and S100A12 and the third



subgroup consists of the genes S100A10 and S100A11 [168]. The latter gene cluster is also called the epidermal differentiation complex (EDC) [169]. Corresponding to the S100 gene cluster on the human chromosome 1q21 the genes S100A10, S100A8 and S100A9 are syntenically clustered on mouse chromosome 3 [170]. A recently published paper dealing with the expression of S100 genes in correlation with melanoma showed a strong expression of S100A10, S100A8 and S100A9 genes in primary melanoma but more interestingly, the paper showed a strong positive correlation of these genes with each other by using correlation analysis [171].  $\gamma\delta$ T cells migrate according to their CCR10 expression into the epidermal compartment [72]. In the human tumor microenvironment of a neuroblastoma cell line  $\gamma\delta$ T cells secrete growth factors like EGF and PDGF [172]. In astrocytes, EGF is responsible for the induction of FGF-2 protein and mRNA [173]. It has also been shown that an EGF family member regulates FGF-2 expression in pulmonary fibroblasts [174]. In turn, FGF-2 is able to induce the expression of S100A8 mRNA in a 3T3 fibroblast cell line [175]. In combinational treatment with heparin the effect increased by two-fold [175]. S100A9 forms a heterodimer with S100A8 called calprotectin [176]. Lee *et al.* reported that S100A9 and S100A8 can function as homo- or heterodimers [177]. In 2008, a study demonstrated that advanced glycation end-products (AGE) function as a ligand of calprotectin [178]. In this study, *Rage*-deficient mice treated with DMBA/TPA had impaired development of epidermal hyperplasia [178], reminiscent of the phenotype shown by UVB-treated *Ccr10*-deficient mice in the current study. Additionally, hyperproliferation of the epidermal compartment in psoriasis was associated with a marked upregulation of S100A8 and S100A9 [179]. A strong expression of CCL27 and CCR10 in psoriatic skin was also published [67]. An important observation in UV-irradiated skin and UV-induced SCCs is the highly increased expression of S100A9 calcium-binding proteins, which are barely detectable in normal skin, but present with increased expression in psoriasis [180, 181]. The expression of S100A9 calcium-binding proteins is increased in the epidermis under UV-induced and inflammatory conditions and was observed to recruit various immune cells to sites of tissue damage [177, 180, 181]. Several studies linked epidermal hyperproliferation to S100A8/S100A9 overexpression [179, 181-183]. The mechanism to achieve a hyperproliferative state of the epidermal compartment seems to be very complex. Iotzova-Weiss *et al.* published recently a study in which they indicate that S100A8/S100A9 signaling mediates the

development of acanthosis via Rage [183]. Interestingly, they speculated that in OTRs this mechanism might contribute to increased SCC formation [183]. In turn, S100A8/S100A9 mediated cell proliferation seems to depend on cytokine induction [182]. S100A8/S100A9 complex and/or S100A8 and S100A9 themselves function as a chemoattractant for the recruitment of immune cells [177]. Recruited immune cells may crosstalk with keratinocytes resulting in the production of cytokines which leads to a positive feedback loop and enhanced secretion of S100A8 and S100A9 and, in addition, to keratinocyte hyperproliferation [177, 182]. This suggests a high impact of S100A9 calcium-binding proteins in mediating and reacting to keratinocyte hyperproliferation [181] and a thickening of the skin.

When epidermal thickening was analyzed in the current study, it was observed that it developed over time in Balb/c wildtype mice. There was no difference in epidermal thickening between wildtype and *Ccr10*-deficient mice in the beginning of the experiment and therefore may not have had an impact on tumor induction. Instead a correlation between acanthosis and tumor progression was observed, as *Ccr10*-deficient mice showed increased tumor growth followed by decreased survival, while lacking the increased thickness of the epidermis observed in wildtype mice (Figure 4.1 C).

There is evidence that *Ccr10*-deficient mice have an inhibition of epidermal hyperproliferation. The reason for this could be a lack of CCR10<sup>+</sup> γδT cell recruitment via CCL27 and the missing induction of S100A8. The effect of this impairment might become more crucial during tumor progression, because the development of acanthosis increases over time.

The proinflammatory activities of S100A8/S100A9 calcium-binding proteins in combination with CCR10 in Balb/c wildtype mice might be important for the hyperproliferation of keratinocytes, promoting the development of acanthosis, which protects against UVB-irradiation, resulting in reduced tumor growth in Balb/c wildtype mice.

In contrast, *Ccr10*-deficient mice might have an impaired epidermal hyperproliferation due to the lack of CCR10<sup>+</sup> γδT cell recruitment via CCL27 and the missing induction of S100A8, which would explain the inhibition of acanthosis leading to inadequate protection against UVB-irradiation and the insufficient protection against UV-induced carcinogenesis. A possible connection of CCR10<sup>+</sup> γδT cell recruitment and S100A8



induction has not been demonstrated to date and further analysis is needed to validate this hypothesis. A recently published paper examining chemokine ligand-receptor interactions in cutaneous wound healing offers another possible explanation for acanthosis development [75]. The authors were able to show that CCL27 expression in concert with CCR10-expressing wound-infiltrating fibroblasts and endothelial cells increase wound repair [75]. It might be possible that in the UVB-model due to UVB-induced tissue damage CCL27/CCR10 interactions lead to the recruitment of structural cells to increase tissue repair. Bünemann *et al.* also suggest a role for infiltrating CD3<sup>+</sup> CCR10<sup>+</sup> lymphocytes, which by promote endothelial cell proliferation and recruitment [75]. The reported mechanisms for cutaneous wound healing could be responsible for the development of acanthosis in wildtype mice in the UVB-model, while *Ccr10*-deficient mice lacking these mechanisms due to the loss of CCR10 might be impaired in acanthosis development.

In contrast to the findings in an “immunosuppression”-dependent UVB-model, the present study demonstrates that the formation of tumors was decreased in *Ccr10*-deficient mice in an “inflammation”-dependent DMBA/TPA-model of cutaneous carcinogenesis (Figure 4.1 B). Findings by Murakami *et al.* using CCR10-expressing melanoma cells demonstrate that direct stimulation of CCR10 on melanoma cells via its ligand promotes melanoma cell survival [184]. This resistance to Fas-mediated apoptosis in the presence of CCL27/CCR10 signaling [184], might also play a role under circumstances of the present study. Not all cells are affected by DMBA/TPA treatment, which results in Ras activation and loss of CCL27 expression, therefore some keratinocytes might still express CCL27, and thereby recruit CCR10<sup>+</sup> T cells into the skin of WT mice, which might have an effect of resistance to Fas-mediated apoptosis. It is reported that EGF-induced EGFR activation leads to Akt activation which inhibits Fas-mediated apoptosis [185]. Murakami *et al.* observed that CCR10-B16 melanoma cells show a strong enrichment of Akt phosphorylation after CCL27/CCR10 interaction [184]. In addition, they showed that without CCL27/CCR10 interactions, INF- $\gamma$  is able to increase Fas expression, which mediates apoptosis in B16 cells [184]. If this would be the case in the present study speculating from the work of Murakami *et al.* that for Akt mediated Fas-inhibition, CCR10 is required. Kaplan-Meier survival analysis showed that the loss of *Ccr10* has a tendency to increase the survival of mice by reducing tumor development. Additionally, results of

the present study showed that tumor-free survival was significantly increased in *Ccr10*-deficient mice, indicating an important role for CCR10 during tumor induction in an inflammation-dependent carcinogenesis model. This was in accordance with a study by Kai *et al.* which investigated CCL27 and CCR10 expression in cutaneous SCC and reported that CCL27/CCR10 signaling seems to be favorable for tumor cell survival and proliferation [186]. The discrepancy of this observation with the results by Pivarcsi *et al.* might be due to a different patient cohort [43, 186]. The group of Martinez-Rodriguez *et al.* observed that a high CCL27 expression in patients suffering from cutaneous malignant melanoma was correlated with increased survival [187]. In the study of Martinez-Rodriguez *et al.* the immunological environment in skin is completely different from the present study. Patients suffering from the malignant melanoma subtype which showed CCL27 expression in this study develop in body areas with chronic UV-exposure and do not present with chronic-inflammation in the skin [187], whereas in the present study carcinogenesis is based on chronic-inflammation in the skin. This might be the reason that the present study showed contrary results when analyzing overall-survival. Interestingly, DMBA/TPA-treated *Cd4*-deficient mice developed significantly less tumors and the tumor incidence was also significantly reduced compared to DMBA/TPA-treated WT mice [119]. Indicating for the present study that *Cd4*-deficient and *Ccr10*-deficient mice were observed with the same reaction to DMBA/TPA-induced cutaneous carcinogenesis. Suggesting that CD4<sup>+</sup> T cells play a main role in CCL27/CCR10 signaling for the promotion of DMBA/TPA-induced cutaneous carcinogenesis.

When analyzing mice for tumor numbers, *Ccr10*-deficient mice developed significantly less tumors per mouse compared to the wildtype mice. Moreover, tumor growth (weight and volume) was significantly reduced in *Ccr10*-deficient mice (Figure 4.1 B). In contrast, earlier studies showed that CCL27/CCR10 interactions reduce tumor growth and are beneficial for tumor survival [43, 188]. In these studies, tumor cells were injected into the flank of the mice and the injected tumor cells were generated from different tumor entities (melanoma and ovarian cancer). Further experiments with an *ex vivo* transfection of a murine CCL27 expressing vector into CT26 colon carcinoma cells and B16BL6 melanoma cells showed only a slight reduction of tumor growth in CT26 colon carcinoma [189] and no effect in B16BL6 melanoma. Additionally, the works of Okada *et al.* and Pivarcsi *et al.* showed a

reduced tumor growth due to CCL27/CCR10 signaling in melanoma *in vivo* [43, 190]. Moreover, other experiments with intratumoral injection of a CCL27 expressing vector *in vivo* indicate no impact of CCL27/CCR10 interactions for tumor growth inhibition in OV-HM murine ovarian carcinoma and Meth-A murine fibrosarcoma [160, 191]. Only a combined intratumoral injection of IL12 and CCL27 (in a ratio 1:1 or 9:1 but not 1:9 for OV-HM tumors) was able to significantly reduce tumor growth in OV-HM and Meth-A [160, 191]. These results indicate that CCL27/CCR10 signaling *in vivo* alone is not sufficient for an effect, e.g. other factors, besides CCL27 signaling, must be present to achieve tumor growth reduction. In all of these cases above, large numbers of already malignant tumor cells were introduced into non-inflamed, homeostatic skin, whereas the model used in this work, establishes first a chronic inflammation and only during the process of inflammation malignant transformation does occur. This fundamental difference might be the root cause for the diverging observations. Other important aspects are the influence of the carcinogenic induction and the state of the immune system. Similar to the observations in the present study, it was reported that CCL27/CCR10 signaling resulted in tumor progression via the inhibition of Fas-triggered apoptosis, while inhibition of CCL27 signaling utilizing neutralizing antibodies markedly decreased tumor growth in murine melanoma cells transduced with *Ccr10* [184]. Huang *et al.* connected significantly increased tumor growth of colorectal cancer with IL-22 expression [192]. Furthermore, they identified an increased migration of Th22 cells within the tumor microenvironment expressing higher levels of CCL27 [192]. In addition, IL-22 is responsible for anti-apoptotic effects via STAT3 signaling [192]. This indicates that, as a result of chronic inflammation, CCL27/CCR10 interactions might lead to enhanced tumor growth by avoiding apoptosis via an accumulation of Th22 CCR4<sup>+</sup>CCR6<sup>+</sup>CCR10<sup>+</sup> cells producing IL-22 in the tumor microenvironment in Balb/c wildtype mice (Figure 4.1 B). In contrast, the loss of *Ccr10* might enable tumor cell elimination by apoptosis which causes reduced tumor progression in *Ccr10*-deficient mice (Figure 4.1 B).

Macroscopic evaluation of intermediate and large tumors, which developed in this study, by a dermato-histopathologist characterized the tumors as squamous cell carcinoma. Reference material was obtained from all developed tumors but is not available for further histopathological analyses. Histopathological analysis of a random sampling of developed tumors confirmed the macroscopic evaluation and

showed an epithelial differentiation in the notion of a developed SCC. The observation of developed lesions and tumors was in accordance with the literature, which largely reports that, following DMBA/TPA treatment, squamous papillomas predominantly develop and in the course of tumor progression a small number of papillomas progress into SCCs [98, 103, 193]. The development of BCC could be excluded because only mice with an aberrant hedgehog signaling develop BCCs [194, 195]. When analyzing the tumor morphology of DMBA/TPA-treated mice, *Ccr10*-deficient mice showed reduced tumor formation and growth, as demonstrated by a percentage analysis which compared tumor size per group of deficient and wildtype mice. A CCR10-positive immune system seems to be an important factor in tumor growth, which is absent in *Ccr10*-deficient mice (Figure 4.1 B). The investigation of intermediate and large tumors showed an impairment in the ability to develop hyperkeratotic tumors in *Ccr10*-deficient mice. Robinson *et al.* suggest that S100A10, annexin I, and S100A11 function as “envelope organizer proteins” [196]. Interestingly, *Arnt*-deficient mice present with problems in epidermal barrier function resulting in a short lifespan [197]. The Aryl hydrocarbon Receptor Nuclear Translocator (*Arnt*) belongs to the Per-Arnt-Sim (PAS) protein family, which plays a role in several biological functions like the maintenance of epidermal barrier function [197, 198]. The *Arnt*-deficient mice develop parakeratosis with a strong cornification of keratinocytes and additionally, showed a thick corny layer and tightly packed corneocytes [197]. A microarray analysis of *Arnt*-deficient epidermis showed significantly increased expression of genes linked to the EDC, among them S100A10 [197]. Geng *et al.* confirmed an important role for these genes in the development of the cornified envelope at late epidermal differentiation [197]. The main role for S100A10 together with annexin A II seems to be the regulation of several proteins by affecting their cell surface expression [199]. A recent study showed that S100A10 is able to bind to CCR10 which results in a decreased CCR10 cell surface presentation [165]. An altered expression of S100A10 was previously found in SCCs [200-202]. Ito *et al.* demonstrated an important role for S100A10 in papillary carcinoma [201]. They suggest that the S100A10 and annexin II complex promotes tumor initiation and/or tumor progression [201]. Interestingly, a recent study found that oncogenic Ras positively regulates the expression of S100A10 [203]. It is known that DMBA-treatment causes an activated *Hras* gene mutation [99-101]. This suggests that

DMBA-induced *Hras* activation, as present in this study's experiment, might lead to S100A10 overexpression.

SCCs are also associated with keratin 6 and 16 expression [180, 204, 205]. IL-22 is able to induce the expression of keratin 6 and 16, which is usually associated with the wound healing process of the epidermis, but also shows an increased expression in the epidermal compartment of patients suffering from systemic sclerosis [150]. Experimentally, the DMBA/TPA-model is mimicking the chronic inflammation-induced development of squamous cell carcinoma in patients suffering e.g. from chronic wounds. Kai *et al.* reported that an overexpression of CCR10 and CCL27 in advanced SCC is predominantly related to hyperkeratotic lesions of altered keratinocytes [186]. Speculating from the studies above, morphological changes in tumor development of *Ccr10*-deficient mice, as observed in the recent study, may be a consequence of an impaired S100A10/CCR10 interaction, which might have an important role for papillary hyperkeratotic tumor development.

Finally, when analyzing the morphologic changes of the DMBA/TPA-treated skin, surprisingly, *Ccr10*-deficient and Balb/c wildtype mice demonstrated similar inflammation-induced thickening of the nuchal fold and the epidermal compartment. This result indicates that CCR10 is not solely responsible for the proliferative response to DMBA/TPA treatment. In a chronic atopic dermatitis mouse model the inhibition of CCL27/CCR10 interactions leads to markedly reduced ovalbumin-induced skin inflammation characterized by reduced inflammation-induced skin and epidermal thickening, accompanied by decreased recruitment of lymphocytes to sites of inflammation [67]. Winkler *et al.* observed in their study that chemokine receptor *Cxcr3*-deficiency leads to decreased epidermal proliferation in response to DMBA/TPA treatment and associated that with significant decreased recruitment of CD4<sup>+</sup> and CD8<sup>+</sup> T cells [116]. They suggest that CD4<sup>+</sup> and CD8<sup>+</sup> T cells were responsible for the induction of DMBA/TPA-induced epidermal proliferation [116]. Additionally, *Ccr10*-deficient mice had significantly reduced tumor development and progression, leading to increased tumor-free survival, which seems not to be dependent on differences of skin morphology changes during inflammation in the *Ccr10*-deficient mice, as was expected at the start of the experiment. Therefore, the crucial advantage of *Ccr10*-deficient mice in inhibiting skin carcinogenesis might be based on changes of the immune response type. It is well known that CCR10 is

important in recruitment of CD4<sup>+</sup> and CD8<sup>+</sup> T cells into the skin during homeostatic and inflammatory conditions [66, 73]. CCL27 expression vector injection into OV-HM tumors increased predominantly the recruitment of CD4<sup>+</sup> T cells, while only small numbers of CD8<sup>+</sup> T cells were recruited. In contrast in Meth-A tumors, CCL27 vector injection had the opposite effect [191]. In these tumors, the recruitment of CD8<sup>+</sup> T cells was favored through CCL27/CCR10 signaling instead of the CD4<sup>+</sup> T cell subset [191]. This suggests a tumor specific effect for CCL27/CCR10-mediated T cell subset recruitment [191]. In accordance with the recent study, *Cd4*-deficient mice showed increased tumor-free survival and developed significantly less tumors compared to WT mice [119]. This is evidence for an important role of CD4<sup>+</sup> T cells in CCR10-mediated tumor promotion. A recent report by Xia *et al.* suggests that CCR10 has a leading role in balancing the recruitment and function of resident Treg and effector T cells (Th17 cells), which in turn are responsible for skin homeostasis [73]. The study shows that Th17 effector T cells cause prolonged immune reactions, while regulatory T cells have the important role to counterbalance Th17 overactive immune responses by suppressing the function of Th17 cells in heterozygous *Ccr10* knockout mice [73]. *Ccr10*-deficient mice are impaired in T cell memory responses and have less regulatory T cells in their skin, which leads to overactive immune responses compared to heterozygous *Ccr10* knockout mice [73]. This indicates a role for CCR10 in regulating Treg and effector T cell responses under homeostatic conditions [73]. Furthermore, *Ccr10*-deficiency has much more impact on the CD8<sup>+</sup> T cell subset than on CD4<sup>+</sup> cells [73]. These results were supported by another study from Fu *et al.* which reports that CD8<sup>+</sup> T cells are required for the maintenance and the survival of Treg in the skin under homeostatic conditions [72]. Interestingly, CCR10<sup>+</sup> innate lymphoid cells (ILC) are important for the maintenance of Treg in the skin and in turn a balanced recruitment and function of Treg and effector T cells is important for the recruitment of CCR10<sup>+</sup> ILCs to the skin [71] (Figure 4.1 A). It could be speculated that due to these dysregulations in *Ccr10*-deficient mice and the DMBA/TPA treatment, transformed cells can be cleared more effectively due to immune response shifts from Treg to Th17 cells. In Balb/c wildtype mice, the immune response may be shifted towards Treg to turn down an overactive immune response due to the immune suppressive effect of Treg cells (Figure 4.1 B). Facciabene *et al.* reported that a CCR10-related migration of Treg cells into sites of tumor formation promotes immunotolerance and angiogenesis of the tumor, through impairment of effector T



cell function and secretion of vascular endothelial growth factor A (VEGFA), which increases tumor angiogenesis, and is related to tumor growth *in vivo* [206]. This might be the cause of the enhanced tumor induction and growth in Balb/c wildtype mice, which might be orchestrated by a larger population of Treg cells. Interestingly, INF- $\gamma$ -producing Th17 cells are also negatively regulated by CCR10-expressing Th22 cells, which play an essential role in psoriasis and atopic dermatitis [69, 150, 207]. Therefore, in addition to the possible larger population of Treg cells, Th22 cells might play an important role in creating a tumor-promoting environment, which might be responsible for tumor formation and progression in wildtype mice. Importantly, the DMBA/TPA treatment will also induce the expression of other chemokines, e.g. Ccl20, which will also be responsible for creating a tumor-promoting microenvironment. Duhon *et al.* reported that the induction of Th22 cells is mediated by plasmacytoid dendritic cells (pDCs) [69]. pDCs express CCR6 and CCR10 chemokine receptors, which promote pDC recruitment to sites of inflamed epithelia [68]. It is also known that pDCs migrate to imiquimod-treated skin tumors in mice, which possibly promotes local inflammation [68]. In conclusion, there is evidence that the loss of CCR10 signaling may shift the immune response to INF- $\gamma$ -expressing Th17/Th1 cells, resulting in robust tumor immune response and clearance of transformed cells (Figure 4.1 B). This leads to significantly reduced tumor formation and progression, resulting in significantly enhanced tumor-free survival (Figure 4.1 B). Whereas in Balb/c wildtype mice, due to DMBA/TPA treatment, an inflammatory, tumor promoting environment is established, which may shift the immune response towards an increased recruitment of Treg-, Th22-cells and pDCs. As a result, this may lead to significantly increased tumor formation and progression with markedly reduced tumor-free survival (Figure 4.1 B).

Taken together, the two different carcinogenesis models show opposing effects of *Ccr10*-deficiency. In the DMBA/TPA-model, which depends on local skin inflammation, the results suggest that the loss of CCR10 signaling modulates the inflammatory response towards tumor cell clearance, resulting in lower tumor formation and progression, while the inflammation-independent UVB carcinogenesis model showed a disadvantage of *Ccr10*-deficiency, resulting in increased tumor growth and decreased survival. This could be the result of an impaired acanthosis development in combination with increased tumor immune escape in *Ccr10*-deficient

mice (Figure 4.1 C). The mechanism of carcinogenesis induction appears to be instrumental in deciding the effect of CCR10 on carcinogenesis. It is well known that inflammation is a hallmark of cancer, and CCR10-neutralization might offer an advantage to patients due to an abrogation of an orchestrated immune response, which favors tumor growth. However, considering the usual mechanism of SCC induction in a real patient's scenario, which depends on UVB-exposure of the skin, CCL27 expression, and therefore induction of the anti-tumor response observed in the UVB-mouse-model, might be a more worthwhile therapeutic strategy to follow. One important insight of this study is that the effect of CCR10 depends on the mechanism of carcinogenesis induction. Further analysis will elucidate the alterations in the immune response and the expression of genes important for the observed morphological changes. In conclusion, CCR10 plays an important role in skin carcinogenesis, but its impact depends on the individual circumstances. Therefore, it might be a dangerous therapeutic strategy to either completely inhibit or induce a strong expression of CCL27. A robust therapeutic strategy should take the context of skin carcinogenesis formation into account. Based on the recent study, inhibition of CCL27 in chronic inflammation and in contrast, an enhancement of CCL27 expression in an immune suppressive context might be worthwhile avenues for a supportive therapy. Further studies elucidating the role of this interesting chemokine receptor in carcinogenesis seem to be worthwhile.



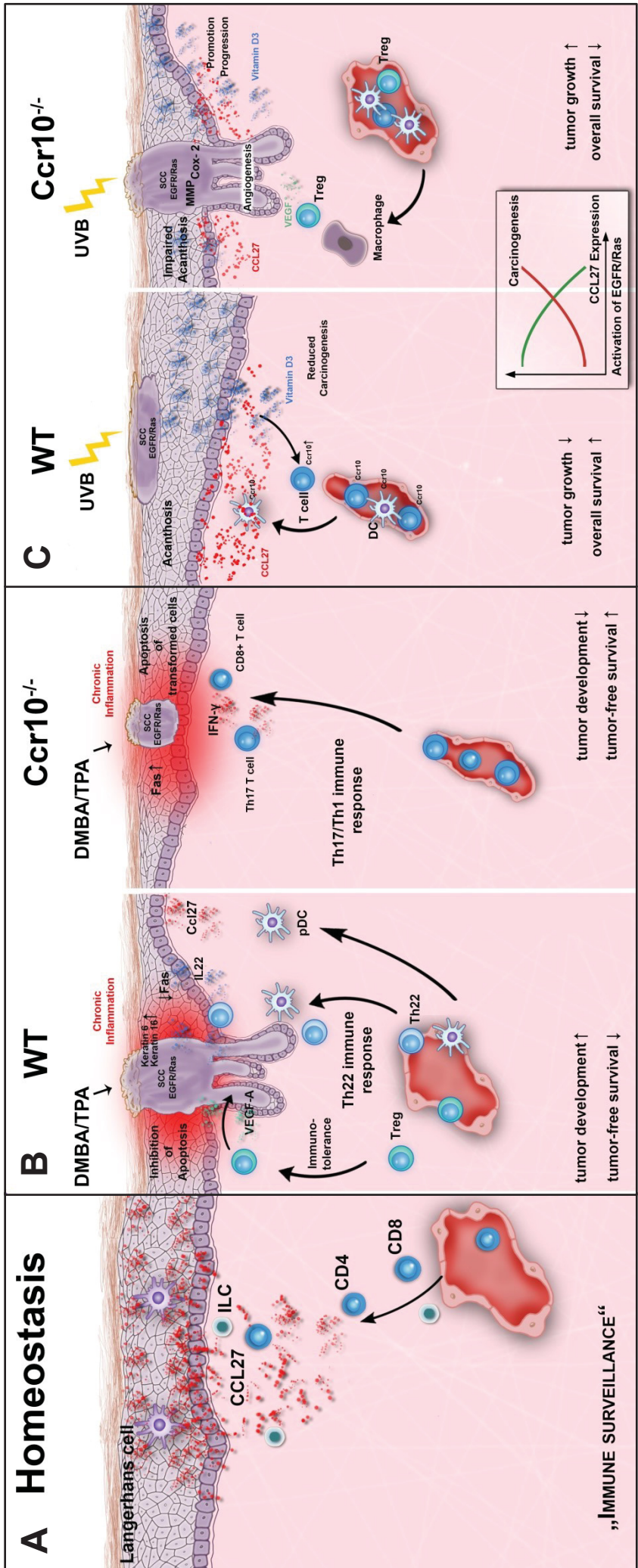


**Figure 4.1** Schematic view of CCR10 signaling during skin homeostasis and cutaneous carcinogenesis. **(A)** During skin homeostasis in human skin CCL27/CCR10 signaling recruits immune cells along a gradient of the chemokine CCL27 into the skin, where they are able to detect transformed cells and eliminate them [61, 67, 71, 72, 78]. **(B)** During local skin inflammation-induced carcinogenesis in Balb/c mice (DMBA/TPA-model) the loss of CCR10 signaling might modulate the inflammatory response towards tumor cell clearance, resulting in less tumor development and increased tumor-free survival. **(C)** In contrast, during UVB-induced carcinogenesis the loss of CCR10 results in increased tumor growth and decreased survival by a possible impairment of acanthosis in combination with increased tumor immune escape in Balb/c mice. **(B-C)** Hence, the two different carcinogenesis models present contrasting effects of CCR10 absence.

## 5 References

1. Sterry, W., *Kurzlehrbuch Dermatologie*. 2011.
2. Terhorst, D., *Basics Dermatologie*. 4th ed. 2015, Munich, Germany: Urban & Fischer/ Elsevier GmbH.
3. Holick, M.F., *Sunlight and vitamin D for bone health and prevention of autoimmune diseases, cancers, and cardiovascular disease*. Am J Clin Nutr, 2004. **80**(6 Suppl): p. 1678S-88S.
4. Faller, A., *Der Körper des Menschen*. 13th ed. 1999, Stuttgart, Germany: Thieme.
5. Liu, Y.J., *Dendritic cell subsets and lineages, and their functions in innate and adaptive immunity*. Cell, 2001. **106**(3): p. 259-62.
6. Boyman, O., et al., *Activation of dendritic antigen-presenting cells expressing common heat shock protein receptor CD91 during induction of psoriasis*. Br J Dermatol, 2005. **152**(6): p. 1211-8.
7. Lowes, M.A., A.M. Bowcock, and J.G. Krueger, *Pathogenesis and therapy of psoriasis*. Nature, 2007. **445**(7130): p. 866-73.
8. Fuchs, E., *Scratching the surface of skin development*. Nature, 2007. **445**(7130): p. 834-42.
9. Segre, J.A., *Epidermal barrier formation and recovery in skin disorders*. J Clin Invest, 2006. **116**(5): p. 1150-8.
10. Oaklander, A.L. and S.M. Siegel, *Cutaneous innervation: form and function*. J Am Acad Dermatol, 2005. **53**(6): p. 1027-37.
11. Presland, R.B. and B.A. Dale, *Epithelial structural proteins of the skin and oral cavity: function in health and disease*. Crit Rev Oral Biol Med, 2000. **11**(4): p. 383-408.
12. Fuchs, E. and H. Green, *Changes in keratin gene expression during terminal differentiation of the keratinocyte*. Cell, 1980. **19**(4): p. 1033-42.
13. Arda, O., N. Goksugur, and Y. Tuzun, *Basic histological structure and functions of facial skin*. Clin Dermatol, 2014. **32**(1): p. 3-13.
14. Stern, R., A.A. Asari, and K.N. Sugahara, *Hyaluronan fragments: an information-rich system*. Eur J Cell Biol, 2006. **85**(8): p. 699-715.
15. Fraser, J.R., T.C. Laurent, and U.B. Laurent, *Hyaluronan: its nature, distribution, functions and turnover*. J Intern Med, 1997. **242**(1): p. 27-33.

16. Laurent, T.C. and J.R. Fraser, *Hyaluronan*. FASEB J, 1992. **6**(7): p. 2397-404.
17. Menon, G.K., *New insights into skin structure: scratching the surface*. Adv Drug Deliv Rev, 2002. **54 Suppl 1**: p. S3-17.
18. Janes, S.M., S. Lowell, and C. Hutter, *Epidermal stem cells*. J Pathol, 2002. **197**(4): p. 479-91.
19. Xiang, F., et al., *Incidence of nonmelanoma skin cancer in relation to ambient UV radiation in white populations, 1978-2012: empirical relationships*. JAMA Dermatol, 2014. **150**(10): p. 1063-71.
20. Kraywinkel, K., U. Wolf, and A. Katalinic *Hautkrebs – Epidemiologie und Früherkennung*. 2012.
21. Nordrhein-Westfalen, E.-N.-E.K., *Jahresbericht 2014 mit Datenreport 2012*. 2014.
22. Brantsch, K.D., et al., *Analysis of risk factors determining prognosis of cutaneous squamous-cell carcinoma: a prospective study*. Lancet Oncol, 2008. **9**(8): p. 713-20.
23. Strickland, P.T., et al., *Quantitative carcinogenesis in man: solar ultraviolet B dose dependence of skin cancer in Maryland watermen*. J Natl Cancer Inst, 1989. **81**(24): p. 1910-3.
24. Albert, M.R. and M.A. Weinstock, *Keratinocyte carcinoma*. CA Cancer J Clin, 2003. **53**(5): p. 292-302.
25. Markey, A.C., *Etiology and pathogenesis of squamous cell carcinoma*. Clin Dermatol, 1995. **13**(6): p. 537-43.
26. Breuninger, H., et al., *Brief S2k guidelines--Cutaneous squamous cell carcinoma*. J Dtsch Dermatol Ges, 2013. **11 Suppl 3**: p. 37-45, 39-47.
27. Silverberg, M.J., et al., *HIV infection status, immunodeficiency, and the incidence of non-melanoma skin cancer*. J Natl Cancer Inst, 2013. **105**(5): p. 350-60.
28. Armstrong, B.K. and A. Kricker, *The epidemiology of UV induced skin cancer*. J Photochem Photobiol B, 2001. **63**(1-3): p. 8-18.
29. Staples, M.P., et al., *Non-melanoma skin cancer in Australia: the 2002 national survey and trends since 1985*. Med J Aust, 2006. **184**(1): p. 6-10.
30. Fabbrocini, G., et al., *Epidemiology of skin cancer: role of some environmental factors*. Cancers (Basel), 2010. **2**(4): p. 1980-9.

31. Lucas, R.M., et al., *The consequences for human health of stratospheric ozone depletion in association with other environmental factors*. Photochem Photobiol Sci, 2015. **14**(1): p. 53-87.
32. Brewster, D.H., et al., *Recent trends in incidence of nonmelanoma skin cancers in the East of Scotland, 1992-2003*. Br J Dermatol, 2007. **156**(6): p. 1295-300.
33. Green, A., et al., *Skin cancer in a subtropical Australian population: incidence and lack of association with occupation. The Nambour Study Group*. Am J Epidemiol, 1996. **144**(11): p. 1034-40.
34. Owens, D.M., *p53, chemokines, and squamous cell carcinoma*. J Clin Invest, 2007. **117**(7): p. 1752-5.
35. Weinberg, A.S., C.A. Ogle, and E.K. Shim, *Metastatic cutaneous squamous cell carcinoma: an update*. Dermatol Surg, 2007. **33**(8): p. 885-99.
36. Sato, H., et al., *Gene expression in skin tumors induced in hairless mice by chronic exposure to ultraviolet B irradiation*. Photochem Photobiol, 1997. **65**(5): p. 908-14.
37. Bolshakov, S., et al., *p53 mutations in human aggressive and nonaggressive basal and squamous cell carcinomas*. Clin Cancer Res, 2003. **9**(1): p. 228-34.
38. Melnikova, V.O., et al., *Mutant p53 is constitutively phosphorylated at Serine 15 in UV-induced mouse skin tumors: involvement of ERK1/2 MAP kinase*. Oncogene, 2003. **22**(38): p. 5958-66.
39. Lindelof, B., et al., *Incidence of skin cancer in 5356 patients following organ transplantation*. Br J Dermatol, 2000. **143**(3): p. 513-9.
40. Carucci, J.A., *Cutaneous oncology in organ transplant recipients: meeting the challenge of squamous cell carcinoma*. J Invest Dermatol, 2004. **123**(5): p. 809-16.
41. Cooper, J.Z. and M.D. Brown, *Special concern about squamous cell carcinoma of the scalp in organ transplant recipients*. Arch Dermatol, 2006. **142**(6): p. 755-8.
42. Smoller, B.R. and R.A. Warnke, *Cutaneous infiltrate of chronic lymphocytic leukemia and relationship to primary cutaneous epithelial neoplasms*. J Cutan Pathol, 1998. **25**(3): p. 160-4.
43. Pivarcsi, A., et al., *Tumor immune escape by the loss of homeostatic chemokine expression*. Proc Natl Acad Sci U S A, 2007. **104**(48): p. 19055-60.



- 
44. Mueller, M.M., *Inflammation in epithelial skin tumours: old stories and new ideas*. Eur J Cancer, 2006. **42**(6): p. 735-44.
  45. Pettersen, J.S., et al., *Tumor-associated macrophages in the cutaneous SCC microenvironment are heterogeneously activated*. J Invest Dermatol, 2011. **131**(6): p. 1322-30.
  46. Rossi, D. and A. Zlotnik, *The biology of chemokines and their receptors*. Annu Rev Immunol, 2000. **18**: p. 217-42.
  47. Zlotnik, A. and O. Yoshie, *Chemokines: a new classification system and their role in immunity*. Immunity, 2000. **12**(2): p. 121-7.
  48. Zlotnik, A., O. Yoshie, and H. Nomiyama, *The chemokine and chemokine receptor superfamilies and their molecular evolution*. Genome Biol, 2006. **7**(12): p. 243.
  49. Karin, N. and G. Wildbaum, *The Role of Chemokines in Shaping the Balance Between CD4(+) T Cell Subsets and Its Therapeutic Implications in Autoimmune and Cancer Diseases*. Front Immunol, 2015. **6**: p. 609.
  50. Zlotnik, A. and O. Yoshie, *The chemokine superfamily revisited*. Immunity, 2012. **36**(5): p. 705-16.
  51. Homey, B. and A. Zlotnik, *Chemokines in allergy*. Curr Opin Immunol, 1999. **11**(6): p. 626-34.
  52. McCully, M.L. and B. Moser, *The human cutaneous chemokine system*. Front Immunol, 2011. **2**: p. 33.
  53. Ma, Q., et al., *Impaired B-lymphopoiesis, myelopoiesis, and derailed cerebellar neuron migration in CXCR4- and SDF-1-deficient mice*. Proc Natl Acad Sci U S A, 1998. **95**(16): p. 9448-53.
  54. Muller, A., et al., *Involvement of chemokine receptors in breast cancer metastasis*. Nature, 2001. **410**(6824): p. 50-6.
  55. Bachelierie, F., et al., *International Union of Basic and Clinical Pharmacology. [corrected]. LXXXIX. Update on the extended family of chemokine receptors and introducing a new nomenclature for atypical chemokine receptors*. Pharmacol Rev, 2014. **66**(1): p. 1-79.
  56. Tachibana, K., et al., *The chemokine receptor CXCR4 is essential for vascularization of the gastrointestinal tract*. Nature, 1998. **393**(6685): p. 591-4.

- 
57. Peled, A., et al., *Dependence of human stem cell engraftment and repopulation of NOD/SCID mice on CXCR4*. Science, 1999. **283**(5403): p. 845-8.
  58. Nagasawa, T., et al., *Defects of B-cell lymphopoiesis and bone-marrow myelopoiesis in mice lacking the CXC chemokine PBSF/SDF-1*. Nature, 1996. **382**(6592): p. 635-8.
  59. Haynes, N.M., et al., *Role of CXCR5 and CCR7 in follicular Th cell positioning and appearance of a programmed cell death gene-1high germinal center-associated subpopulation*. J Immunol, 2007. **179**(8): p. 5099-108.
  60. Su, Y. and A. Richmond, *Chemokine Regulation of Neutrophil Infiltration of Skin Wounds*. Adv Wound Care (New Rochelle), 2015. **4**(11): p. 631-640.
  61. Homey, B., et al., *Cutting edge: the orphan chemokine receptor G protein-coupled receptor-2 (GPR-2, CCR10) binds the skin-associated chemokine CCL27 (CTACK/ALP/ILC)*. J Immunol, 2000. **164**(7): p. 3465-70.
  62. Marchese A., D.j.M., Nguyen T., Heiber M., Cheng R., Heng H.H., Tsui L.C., Shi X., George S.R., and O'Dowd B.F., *Cloning of humn genes encoding noval G protein-coupled receptors*. Genomics, 1994: p. 609-618.
  63. Homey, B., A. Muller, and A. Zlotnik, *Chemokines: agents for the immunotherapy of cancer?* Nat Rev Immunol, 2002. **2**(3): p. 175-84.
  64. Kunkel, E.J., et al., *CCR10 expression is a common feature of circulating and mucosal epithelial tissue IgA Ab-secreting cells*. J Clin Invest, 2003. **111**(7): p. 1001-10.
  65. Wang, W., et al., *Identification of a novel chemokine (CCL28), which binds CCR10 (GPR2)*. J Biol Chem, 2000. **275**(29): p. 22313-23.
  66. Hudak, S., et al., *Immune surveillance and effector functions of CCR10(+) skin homing T cells*. J Immunol, 2002. **169**(3): p. 1189-96.
  67. Homey, B., et al., *CCL27-CCR10 interactions regulate T cell-mediated skin inflammation*. Nat Med, 2002. **8**(2): p. 157-65.
  68. Sisirak, V., et al., *CCR6/CCR10-mediated plasmacytoid dendritic cell recruitment to inflamed epithelia after instruction in lymphoid tissues*. Blood, 2011. **118**(19): p. 5130-40.
  69. Duhen, T., et al., *Production of interleukin 22 but not interleukin 17 by a subset of human skin-homing memory T cells*. Nat Immunol, 2009. **10**(8): p. 857-63.

- 
70. Trifari, S., et al., *Identification of a human helper T cell population that has abundant production of interleukin 22 and is distinct from T(H)-17, T(H)1 and T(H)2 cells*. Nat Immunol, 2009. **10**(8): p. 864-71.
  71. Yang, J., et al., *Selective programming of CCR10(+) innate lymphoid cells in skin-draining lymph nodes for cutaneous homeostatic regulation*. Nat Immunol, 2016. **17**(1): p. 48-56.
  72. Fu, Y., J. Yang, and N. Xiong, *Cutting Edge: Skin CCR10+ CD8+ T Cells Support Resident Regulatory T Cells through the B7.2/Receptor Axis To Regulate Local Immune Homeostasis and Response*. J Immunol, 2016. **196**(12): p. 4859-64.
  73. Xia, M., et al., *CCR10 regulates balanced maintenance and function of resident regulatory and effector T cells to promote immune homeostasis in the skin*. J Allergy Clin Immunol, 2014. **134**(3): p. 634-644 e10.
  74. Morteau, O., et al., *An indispensable role for the chemokine receptor CCR10 in IgA antibody-secreting cell accumulation*. J Immunol, 2008. **181**(9): p. 6309-15.
  75. Bunemann, E., et al., *Chemokine ligand-receptor interactions critically regulate cutaneous wound healing*. Eur J Med Res, 2018. **23**(1): p. 4.
  76. Karnezis, T., et al., *CCL27/CCL28-CCR10 Chemokine Signaling Mediates Migration of Lymphatic Endothelial Cells*. Cancer Res, 2019. **79**(7): p. 1558-1572.
  77. Graham, G.J., *D6 and the atypical chemokine receptor family: novel regulators of immune and inflammatory processes*. Eur J Immunol, 2009. **39**(2): p. 342-51.
  78. Morales, J., et al., *CTACK, a skin-associated chemokine that preferentially attracts skin-homing memory T cells*. Proc Natl Acad Sci U S A, 1999. **96**(25): p. 14470-5.
  79. Baselga, J., *Why the epidermal growth factor receptor? The rationale for cancer therapy*. Oncologist, 2002. **7 Suppl 4**: p. 2-8.
  80. Eilers, R.E., Jr., et al., *Dermatologic infections in cancer patients treated with epidermal growth factor receptor inhibitor therapy*. J Natl Cancer Inst, 2010. **102**(1): p. 47-53.
  81. Lichtenberger, B.M., et al., *Epidermal EGFR controls cutaneous host defense and prevents inflammation*. Sci Transl Med, 2013. **5**(199): p. 199ra111.



82. Wang, J.M., et al., *Chemokines and their role in tumor growth and metastasis*. J Immunol Methods, 1998. **220**(1-2): p. 1-17.
83. Lazennec, G. and A. Richmond, *Chemokines and chemokine receptors: new insights into cancer-related inflammation*. Trends Mol Med, 2010. **16**(3): p. 133-44.
84. Hanahan, D. and R.A. Weinberg, *The hallmarks of cancer*. Cell, 2000. **100**(1): p. 57-70.
85. Hanahan, D. and R.A. Weinberg, *Hallmarks of cancer: the next generation*. Cell, 2011. **144**(5): p. 646-74.
86. Pietras, K. and A. Ostman, *Hallmarks of cancer: interactions with the tumor stroma*. Exp Cell Res, 2010. **316**(8): p. 1324-31.
87. Emtage, P.C., et al., *Adenoviral vectors expressing lymphotactin and interleukin 2 or lymphotactin and interleukin 12 synergize to facilitate tumor regression in murine breast cancer models*. Hum Gene Ther, 1999. **10**(5): p. 697-709.
88. Vicari, A.P., et al., *Antitumor effects of the mouse chemokine 6Ckine/SLC through angiostatic and immunological mechanisms*. J Immunol, 2000. **165**(4): p. 1992-2000.
89. Braun, S.E., et al., *The CC chemokine CK beta-11/MIP-3 beta/ELC/Exodus 3 mediates tumor rejection of murine breast cancer cells through NK cells*. J Immunol, 2000. **164**(8): p. 4025-31.
90. Balkwill, F., *Cancer and the chemokine network*. Nat Rev Cancer, 2004. **4**(7): p. 540-50.
91. Arenberg, D.A., et al., *The role of CXC chemokines in the regulation of angiogenesis in non-small cell lung cancer*. J Leukoc Biol, 1997. **62**(5): p. 554-62.
92. Coussens, L.M. and Z. Werb, *Inflammation and cancer*. Nature, 2002. **420**(6917): p. 860-7.
93. Strieter, R.M., *Chemokines: not just leukocyte chemoattractants in the promotion of cancer*. Nat Immunol, 2001. **2**(4): p. 285-6.
94. Belperio, J.A., et al., *CXC chemokines in angiogenesis*. J Leukoc Biol, 2000. **68**(1): p. 1-8.

- 
95. Arenberg, D.A., et al., *Epithelial-neutrophil activating peptide (ENA-78) is an important angiogenic factor in non-small cell lung cancer*. J Clin Invest, 1998. **102**(3): p. 465-72.
  96. Liotta, L.A., *An attractive force in metastasis*. Nature, 2001. **410**(6824): p. 24-5.
  97. Amersi, F.F., et al., *Activation of CCR9/CCL25 in cutaneous melanoma mediates preferential metastasis to the small intestine*. Clin Cancer Res, 2008. **14**(3): p. 638-45.
  98. DiGiovanni, J., *Multistage carcinogenesis in mouse skin*. Pharmacol Ther, 1992. **54**(1): p. 63-128.
  99. Slaga, T.J., *Overview of tumor promotion in animals*. Environ Health Perspect, 1983. **50**: p. 3-14.
  100. Hennings, H., et al., *Malignant conversion and metastasis of mouse skin tumors: a comparison of SENCAR and CD-1 mice*. Environ Health Perspect, 1986. **68**: p. 69-74.
  101. Bizub, D., A.W. Wood, and A.M. Skalka, *Mutagenesis of the Ha-ras oncogene in mouse skin tumors induced by polycyclic aromatic hydrocarbons*. Proc Natl Acad Sci U S A, 1986. **83**(16): p. 6048-52.
  102. Roop, D.R., et al., *An activated Harvey ras oncogene produces benign tumours on mouse epidermal tissue*. Nature, 1986. **323**(6091): p. 822-4.
  103. Yuspa, S.H., *The pathogenesis of squamous cell cancer: lessons learned from studies of skin carcinogenesis--thirty-third G. H. A. Clowes Memorial Award Lecture*. Cancer Res, 1994. **54**(5): p. 1178-89.
  104. Rundhaug, J.E., et al., *Changes in protein expression during multistage mouse skin carcinogenesis*. Mol Carcinog, 1997. **20**(1): p. 125-36.
  105. Xian, W., et al., *Activation of the epidermal growth factor receptor by skin tumor promoters and in skin tumors from SENCAR mice*. Cell Growth Differ, 1995. **6**(11): p. 1447-55.
  106. Kiguchi, K., et al., *Altered expression of epidermal growth factor receptor ligands in tumor promoter-treated mouse epidermis and in primary mouse skin tumors induced by an initiation-promotion protocol*. Mol Carcinog, 1998. **22**(2): p. 73-83.
  107. Glick, A.B., et al., *Targeted deletion of the TGF-beta 1 gene causes rapid progression to squamous cell carcinoma*. Genes Dev, 1994. **8**(20): p. 2429-40.

- 
108. Van Waes, C., et al., *The A9 antigen associated with aggressive human squamous carcinoma is structurally and functionally similar to the newly defined integrin alpha 6 beta 4*. Cancer Res, 1991. **51**(9): p. 2395-402.
  109. Allen, M. and J. Louise Jones, *Jekyll and Hyde: the role of the microenvironment on the progression of cancer*. J Pathol, 2011. **223**(2): p. 162-76.
  110. Whiteside, T.L., *The tumor microenvironment and its role in promoting tumor growth*. Oncogene, 2008. **27**(45): p. 5904-12.
  111. Lewis, J.G. and D.O. Adams, *Inflammation, oxidative DNA damage, and carcinogenesis*. Environ Health Perspect, 1987. **76**: p. 19-27.
  112. Rahman, S., et al., *Nordihydroguaiaretic acid attenuates skin tumorigenesis in Swiss albino mice with the condition of topical co-administration of an immunosuppressant*. Chem Biol Interact, 2015. **233**: p. 106-14.
  113. Niwa, Y., T. Terashima, and H. Sumi, *Topical application of the immunosuppressant tacrolimus accelerates carcinogenesis in mouse skin*. Br J Dermatol, 2003. **149**(5): p. 960-7.
  114. Cipolat, S., et al., *Epidermal barrier defects link atopic dermatitis with altered skin cancer susceptibility*. Elife, 2014. **3**: p. e01888.
  115. Benavides, F., et al., *Protective role of cathepsin L in mouse skin carcinogenesis*. Mol Carcinog, 2012. **51**(4): p. 352-61.
  116. Winkler, A.E., et al., *CXCR3 enhances a T-cell-dependent epidermal proliferative response and promotes skin tumorigenesis*. Cancer Res, 2011. **71**(17): p. 5707-16.
  117. Schioppa, T., et al., *B regulatory cells and the tumor-promoting actions of TNF-alpha during squamous carcinogenesis*. Proc Natl Acad Sci U S A, 2011. **108**(26): p. 10662-7.
  118. Xiao, M., et al., *IFNgamma promotes papilloma development by up-regulating Th17-associated inflammation*. Cancer Res, 2009. **69**(5): p. 2010-7.
  119. Yusuf, N., et al., *Antagonistic roles of CD4+ and CD8+ T-cells in 7,12-dimethylbenz(a)anthracene cutaneous carcinogenesis*. Cancer Res, 2008. **68**(10): p. 3924-30.
  120. Fortner, G.W. and M.L. Kripke, *In vitro reactivity of splenic lymphocytes from normal and UV-irradiated mice against syngeneic UV-induced tumors*. J Immunol, 1977. **118**(4): p. 1483-7.

- 
121. Katiyar, S.K., *Dietary proanthocyanidins inhibit UV radiation-induced skin tumor development through functional activation of the immune system*. Mol Nutr Food Res, 2016. **60**(6): p. 1374-82.
  122. Spellman, C.W. and R.A. Daynes, *Immunoregulation by ultraviolet light-III. Enhancement of suppressor cell activity in older animals*. Exp Gerontol, 1978. **13**(3-4): p. 141-6.
  123. Schade, N., C. Esser, and J. Krutmann, *Ultraviolet B radiation-induced immunosuppression: molecular mechanisms and cellular alterations*. Photochem Photobiol Sci, 2005. **4**(9): p. 699-708.
  124. Loeser, S., et al., *Spontaneous tumor rejection by cbl-b-deficient CD8+ T cells*. J Exp Med, 2007. **204**(4): p. 879-91.
  125. Nasti, T.H., et al., *Differential roles of T-cell subsets in regulation of ultraviolet radiation induced cutaneous photocarcinogenesis*. Photochem Photobiol, 2011. **87**(2): p. 387-98.
  126. Wang, H., et al., *Therapeutic and immune effects of 5-aminolevulinic acid photodynamic therapy on UVB-induced squamous cell carcinomas in hairless mice*. Exp Dermatol, 2013. **22**(5): p. 362-3.
  127. Hatton, J.L., et al., *Depletion of CD4+ cells exacerbates the cutaneous response to acute and chronic UVB exposure*. J Invest Dermatol, 2007. **127**(6): p. 1507-15.
  128. Hart, P.H., M.A. Grimaldeston, and J.J. Finlay-Jones, *Sunlight, immunosuppression and skin cancer: role of histamine and mast cells*. Clin Exp Pharmacol Physiol, 2001. **28**(1-2): p. 1-8.
  129. Kripke, M.L., et al., *Pyrimidine dimers in DNA initiate systemic immunosuppression in UV-irradiated mice*. Proc Natl Acad Sci U S A, 1992. **89**(16): p. 7516-20.
  130. Ullrich, S.E. and D.A. Schmitt, *The role of cytokines in UV-induced systemic immune suppression*. J Dermatol Sci, 2000. **23 Suppl 1**: p. S10-2.
  131. Ullrich, S.E., *The role of epidermal cytokines in the generation of cutaneous immune reactions and ultraviolet radiation-induced immune suppression*. Photochem Photobiol, 1995. **62**(3): p. 389-401.
  132. Kanjilal, S., et al., *High frequency of p53 mutations in ultraviolet radiation-induced murine skin tumors: evidence for strand bias and tumor heterogeneity*. Cancer Res, 1993. **53**(13): p. 2961-4.

- 
133. Masaki, H., T. Atsumi, and H. Sakurai, *Detection of hydrogen peroxide and hydroxyl radicals in murine skin fibroblasts under UVB irradiation*. Biochem Biophys Res Commun, 1995. **206**(2): p. 474-9.
  134. Moodycliffe, A.M., I. Kimber, and M. Norval, *The effect of ultraviolet B irradiation and urocanic acid isomers on dendritic cell migration*. Immunology, 1992. **77**(3): p. 394-9.
  135. Ziegler, A., et al., *Mutation hotspots due to sunlight in the p53 gene of nonmelanoma skin cancers*. Proc Natl Acad Sci U S A, 1993. **90**(9): p. 4216-20.
  136. Brash, D.E., et al., *A role for sunlight in skin cancer: UV-induced p53 mutations in squamous cell carcinoma*. Proc Natl Acad Sci U S A, 1991. **88**(22): p. 10124-8.
  137. English, D.R., et al., *Case-control study of sun exposure and squamous cell carcinoma of the skin*. Int J Cancer, 1998. **77**(3): p. 347-53.
  138. Green, A., et al., *Daily sunscreen application and betacarotene supplementation in prevention of basal-cell and squamous-cell carcinomas of the skin: a randomised controlled trial*. Lancet, 1999. **354**(9180): p. 723-9.
  139. Downward, J., *Targeting RAS signalling pathways in cancer therapy*. Nat Rev Cancer, 2003. **3**(1): p. 11-22.
  140. Kraywinkel, K.W., U; Katalinic, A, *Hautkrebs - Epidemiologie und Früherkennung*. 2012.
  141. Das, K.K., et al., *Incidences of malignancy in chronic burn scar ulcers: experience from Bangladesh*. Burns, 2015. **41**(6): p. 1315-21.
  142. Mallipeddi, R., *Epidermolysis bullosa and cancer*. Clin Exp Dermatol, 2002. **27**(8): p. 616-23.
  143. Onesti, M.G., et al., *Ten years of experience in chronic ulcers and malignant transformation*. Int Wound J, 2015. **12**(4): p. 447-50.
  144. Taghavi Zenouz, A., et al., *Squamous cell carcinoma arising from an oral lichenoid lesion: a case report*. J Dent Res Dent Clin Dent Prospects, 2012. **6**(1): p. 29-32.
  145. Tong, L.X., et al., *Widely metastatic squamous cell carcinoma originating from malignant transformation of hypertrophic lichen planus in a 24-year-old woman: case report and review of the literature*. Pediatr Dermatol, 2015. **32**(3): p. e98-101.

- 
146. Meller, S., M. Gilliet, and B. Homey, *Chemokines in the pathogenesis of lichenoid tissue reactions*. J Invest Dermatol, 2009. **129**(2): p. 315-9.
  147. Connolly, K., et al., *Papillomavirus-associated squamous skin cancers following transplant immunosuppression: one Notch closer to control*. Cancer Treat Rev, 2014. **40**(2): p. 205-14.
  148. Harvey, I., et al., *Non-melanoma skin cancer and solar keratoses II analytical results of the South Wales Skin Cancer Study*. Br J Cancer, 1996. **74**(8): p. 1308-12.
  149. Majores, M. and E. Bierhoff, *[Actinic keratosis, Bowen's disease, keratoacanthoma and squamous cell carcinoma of the skin]*. Pathologe, 2015. **36**(1): p. 16-29.
  150. Fujita, H., *The role of IL-22 and Th22 cells in human skin diseases*. J Dermatol Sci, 2013. **72**(1): p. 3-8.
  151. Nguyen, P., et al., *Aggressive squamous cell carcinomas in persons infected with the human immunodeficiency virus*. Arch Dermatol, 2002. **138**(6): p. 758-63.
  152. Callens, J., et al., *Epidemiology of basal and squamous cell carcinoma in Belgium: the need for a uniform and compulsory registration*. J Eur Acad Dermatol Venereol, 2016. **30**(11): p. 1912-1918.
  153. Sunesen, K.G., et al., *Immunosuppressive disorders and risk of anal squamous cell carcinoma: a nationwide cohort study in Denmark, 1978-2005*. Int J Cancer, 2010. **127**(3): p. 675-84.
  154. Liu, Z., et al., *Chemopreventive efficacy of menthol on carcinogen-induced cutaneous carcinoma through inhibition of inflammation and oxidative stress in mice*. Food Chem Toxicol, 2015. **82**: p. 12-8.
  155. Monga, J., et al., *Topical (+)-catechin emulsified gel prevents DMBA/TPA-induced squamous cell carcinoma of the skin by modulating antioxidants and inflammatory biomarkers in BALB/c mice*. Food Funct, 2014. **5**(12): p. 3197-207.
  156. Sibilía, M., et al., *The epidermal growth factor receptor: from development to tumorigenesis*. Differentiation, 2007. **75**(9): p. 770-87.
  157. Meller, S., et al., *Ultraviolet radiation-induced injury, chemokines, and leukocyte recruitment: An amplification cycle triggering cutaneous lupus erythematosus*. Arthritis Rheum, 2005. **52**(5): p. 1504-16.



- 
158. Norris, P.G., et al., *Immune function, mutant frequency, and cancer risk in the DNA repair defective genodermatoses xeroderma pigmentosum, Cockayne's syndrome, and trichothiodystrophy*. J Invest Dermatol, 1990. **94**(1): p. 94-100.
  159. Ishigaki, Y., et al., *A comparison of UVB-carcinogenesis between nude mice and nude beige mice*. J Radiat Res, 1998. **39**(2): p. 119-27.
  160. Gao, J.Q., et al., *NK cells are migrated and indispensable in the anti-tumor activity induced by CCL27 gene therapy*. Cancer Immunol Immunother, 2009. **58**(2): p. 291-9.
  161. Maghazachi, A.A., K.L. Sand, and Z. Al-Jaderi, *Glatiramer Acetate, Dimethyl Fumarate, and Monomethyl Fumarate Upregulate the Expression of CCR10 on the Surface of Natural Killer Cells and Enhance Their Chemotaxis and Cytotoxicity*. Front Immunol, 2016. **7**: p. 437.
  162. Dhabhar, F.S., et al., *High-anxious individuals show increased chronic stress burden, decreased protective immunity, and increased cancer progression in a mouse model of squamous cell carcinoma*. PLoS One, 2012. **7**(4): p. e33069.
  163. Schlumpf, M., et al., *Fundamental questions to sun protection: A continuous education symposium on vitamin D, immune system and sun protection at the University of Zurich*. Dermatoendocrinol, 2010. **2**(1): p. 19-25.
  164. Eysteinsdottir, J.H., et al., *The role of Th17/Tc17 peripheral blood T cells in psoriasis and their positive therapeutic response*. Scand J Immunol, 2013. **78**(6): p. 529-37.
  165. Hessner, F., et al., *CC chemokine receptor 10 cell surface presentation in melanocytes is regulated by the novel interaction partner S100A10*. Sci Rep, 2016. **6**: p. 22649.
  166. Ozorowski, G., S. Milton, and H. Luecke, *Structure of a C-terminal AHNAK peptide in a 1:2:2 complex with S100A10 and an acetylated N-terminal peptide of annexin A2*. Acta Crystallogr D Biol Crystallogr, 2013. **69**(Pt 1): p. 92-104.
  167. Schafer, B.W., et al., *Isolation of a YAC clone covering a cluster of nine S100 genes on human chromosome 1q21: rationale for a new nomenclature of the S100 calcium-binding protein family*. Genomics, 1995. **25**(3): p. 638-43.
  168. Wicki, R., et al., *Characterization of the human S100A12 (calgranulin C, p6, CAAF1, CGRP) gene, a new member of the S100 gene cluster on chromosome 1q21*. Cell Calcium, 1996. **20**(6): p. 459-64.



- 
169. Mischke, D., et al., *Genes encoding structural proteins of epidermal cornification and S100 calcium-binding proteins form a gene complex ("epidermal differentiation complex") on human chromosome 1q21*. J Invest Dermatol, 1996. **106**(5): p. 989-92.
  170. Moseley W.S., S.M.F., *Definitio of mouse chromosome 1 and 3 gene linkage groups that are conserved on human chromosome 1: evidence that a conserved linkage group spans the centromere of human chroosome 1*. Genomics, 1989: p. 899-905.
  171. Xiong, T.F., F.Q. Pan, and D. Li, *Expression and clinical significance of S100 family genes in patients with melanoma*. Melanoma Res, 2019. **29**(1): p. 23-29.
  172. Schilbach, K., et al., *Immune response of human propagated gammadelta-T-cells to neuroblastoma recommend the Vdelta1+ subset for gammadelta-T-cell-based immunotherapy*. J Immunother, 2008. **31**(9): p. 896-905.
  173. Moffett, J., et al., *Transcriptional regulation of fibroblast growth factor-2 expression in human astrocytes: implications for cell plasticity*. Mol Biol Cell, 1998. **9**(8): p. 2269-85.
  174. Liu, J., et al., *Heparin-binding EGF-like growth factor regulates elastin and FGF-2 expression in pulmonary fibroblasts*. Am J Physiol Lung Cell Mol Physiol, 2003. **285**(5): p. L1106-15.
  175. Rahimi, F., et al., *FGF-2, IL-1beta and TGF-beta regulate fibroblast expression of S100A8*. FEBS J, 2005. **272**(11): p. 2811-27.
  176. Brophy, M.B., et al., *Contributions of the S100A9 C-terminal tail to high-affinity Mn(II) chelation by the host-defense protein human calprotectin*. J Am Chem Soc, 2013. **135**(47): p. 17804-17.
  177. Lee, Y., et al., *S100A8 and S100A9 are messengers in the crosstalk between epidermis and dermis modulating a psoriatic milieu in human skin*. Biochem Biophys Res Commun, 2012. **423**(4): p. 647-53.
  178. Gebhardt, C., et al., *RAGE signaling sustains inflammation and promotes tumor development*. J Exp Med, 2008. **205**(2): p. 275-85.
  179. Benoit, S., et al., *Elevated serum levels of calcium-binding S100 proteins A8 and A9 reflect disease activity and abnormal differentiation of keratinocytes in psoriasis*. Br J Dermatol, 2006. **155**(1): p. 62-6.

- 
180. Rundhaug, J.E., et al., *SAGE profiling of UV-induced mouse skin squamous cell carcinomas, comparison with acute UV irradiation effects*. Mol Carcinog, 2005. **42**(1): p. 40-52.
  181. Broome, A.M., D. Ryan, and R.L. Eckert, *S100 protein subcellular localization during epidermal differentiation and psoriasis*. J Histochem Cytochem, 2003. **51**(5): p. 675-85.
  182. Nukui, T., et al., *S100A8/A9, a key mediator for positive feedback growth stimulation of normal human keratinocytes*. J Cell Biochem, 2008. **104**(2): p. 453-64.
  183. Iotzova-Weiss, G., et al., *S100A8/A9 stimulates keratinocyte proliferation in the development of squamous cell carcinoma of the skin via the receptor for advanced glycation-end products*. PLoS One, 2015. **10**(3): p. e0120971.
  184. Murakami, T., et al., *Immune evasion by murine melanoma mediated through CC chemokine receptor-10*. J Exp Med, 2003. **198**(9): p. 1337-47.
  185. Gibson, S., et al., *Epidermal growth factor protects epithelial cells against Fas-induced apoptosis. Requirement for Akt activation*. J Biol Chem, 1999. **274**(25): p. 17612-8.
  186. Kai, H., et al., *CCR10 and CCL27 are overexpressed in cutaneous squamous cell carcinoma*. Pathol Res Pract, 2011. **207**(1): p. 43-8.
  187. Martinez-Rodriguez, M., A.K. Thompson, and C. Monteagudo, *High CCL27 immunoreactivity in 'supratumoral' epidermis correlates with better prognosis in patients with cutaneous malignant melanoma*. J Clin Pathol, 2016.
  188. Gao, J.Q., et al., *Antitumor effect by interleukin-11 receptor alpha-locus chemokine/CCL27, introduced into tumor cells through a recombinant adenovirus vector*. Cancer Res, 2003. **63**(15): p. 4420-5.
  189. Okada, N., et al., *Anti-tumor activity of chemokine is affected by both kinds of tumors and the activation state of the host's immune system: implications for chemokine-based cancer immunotherapy*. Biochem Biophys Res Commun, 2004. **317**(1): p. 68-76.
  190. Okada, N., et al., *Tumor suppressive efficacy through augmentation of tumor-infiltrating immune cells by intratumoral injection of chemokine-expressing adenoviral vector*. Cancer Gene Ther, 2006. **13**(4): p. 393-405.
  191. Gao, J.Q., et al., *Cotransduction of CCL27 gene can improve the efficacy and safety of IL-12 gene therapy for cancer*. Gene Ther, 2007. **14**(6): p. 491-502.

192. Huang, Y.H., et al., *Th22 cell accumulation is associated with colorectal cancer development*. World J Gastroenterol, 2015. **21**(14): p. 4216-24.
193. Rundhaug, J.E., et al., *Opposite effect of stable transfection of bioactive transforming growth factor-beta 1 (TGF beta 1) versus exogenous TGF beta 1 treatment on expression of 92-kDa type IV collagenase in mouse skin squamous cell carcinoma CH72 cells*. Mol Carcinog, 1997. **19**(2): p. 122-36.
194. Uhmman, A., et al., *DMBA/TPA treatment is necessary for BCC formation from patched deficient epidermal cells in Ptch(flox/flox)CD4Cre(+/-) mice*. J Invest Dermatol, 2014. **134**(10): p. 2620-9.
195. Brennan-Crispi, D.M., et al., *Crosstalk between Desmoglein 2 and Patched 1 accelerates chemical-induced skin tumorigenesis*. Oncotarget, 2015. **6**(11): p. 8593-605.
196. Robinson, N.A., et al., *S100A11, S100A10, annexin I, desmosomal proteins, small proline-rich proteins, plasminogen activator inhibitor-2, and involucrin are components of the cornified envelope of cultured human epidermal keratinocytes*. J Biol Chem, 1997. **272**(18): p. 12035-46.
197. Geng, S., et al., *Targeted ablation of Arnt in mouse epidermis results in profound defects in desquamation and epidermal barrier function*. J Cell Sci, 2006. **119**(Pt 23): p. 4901-12.
198. Reyes, H., S. Reisz-Porszasz, and O. Hankinson, *Identification of the Ah receptor nuclear translocator protein (Arnt) as a component of the DNA binding form of the Ah receptor*. Science, 1992. **256**(5060): p. 1193-5.
199. Rescher, U. and V. Gerke, *S100A10/p11: family, friends and functions*. Pflugers Arch, 2008. **455**(4): p. 575-82.
200. Domoto, T., et al., *Evaluation of S100A10, annexin II and B-FABP expression as markers for renal cell carcinoma*. Cancer Sci, 2007. **98**(1): p. 77-82.
201. Ito, Y., et al., *S100A10 expression in thyroid neoplasms originating from the follicular epithelium: contribution to the aggressive characteristic of anaplastic carcinoma*. Anticancer Res, 2007. **27**(4C): p. 2679-83.
202. Li, J., et al., *S100A expression in normal corneal-limbal epithelial cells and ocular surface squamous cell carcinoma tissue*. Mol Vis, 2011. **17**: p. 2263-71.
203. Madureira, P.A., et al., *Cell surface protease activation during RAS transformation: Critical role of the plasminogen receptor, S100A10*. Oncotarget, 2016.

204. Kopan, R. and E. Fuchs, *The use of retinoic acid to probe the relation between hyperproliferation-associated keratins and cell proliferation in normal and malignant epidermal cells*. J Cell Biol, 1989. **109**(1): p. 295-307.
205. Stoler, A., et al., *Use of monospecific antisera and cRNA probes to localize the major changes in keratin expression during normal and abnormal epidermal differentiation*. J Cell Biol, 1988. **107**(2): p. 427-46.
206. Facciabene, A., et al., *Tumour hypoxia promotes tolerance and angiogenesis via CCL28 and T(reg) cells*. Nature, 2011. **475**(7355): p. 226-30.
207. Karakawa, M., et al., *CCL27 is downregulated by interferon gamma via epidermal growth factor receptor in normal human epidermal keratinocytes*. J Cell Physiol, 2014. **229**(12): p. 1935-45.

## 6 List of figures

|            |  |    |
|------------|--|----|
| Figure 1.1 | Epidermal layers of human skin   | 7  |
| Figure 1.2 | Structure of the human skin  | 9  |
| Figure 1.3 | Normal mouse skin  | 10 |
| Figure 1.4 | The chemokine superfamily  | 15 |
| Figure 2.1 | Thermo Scientific O'GeneRuler 100 bp DNA Ladder  | 30 |
| Figure 3.1 | Tumor progression in Balb/c- <i>Ccr10</i> -deficient ( <i>Ccr10</i> <sup>-/-</sup> ) mice is significantly reduced when compared to Balb/c wildtype (WT) controls after DMBA/TPA treatment | 50 |
| Figure 3.2 | Absence of CCR10 signaling decreases cutaneous carcinogenesis in an inflammation-dependent (DMBA/TPA) tumor model  | 52 |
| Figure 3.3 | DMBA/TPA administration induces morphologically different tumors in Balb/c wildtype (WT) and Balb/c- <i>Ccr10</i> -deficient mice  | 54 |
| Figure 3.4 | DMBA/TPA administration induces an inflammatory response in the skin of Balb/c wildtype (WT) and Balb/c- <i>Ccr10</i> -deficient mice  | 57 |
| Figure 3.5 | <i>Ccr10</i> contribution to mouse skin tumor formation after chronic UVB-irradiation  | 59 |
| Figure 3.6 | Chronic UVB-irradiation increases tumor burden in the absence of CCR10 signaling   | 60 |
| Figure 3.7 | Chronic UVB-irradiation induces morphologically different tumors in Balb/c wildtype (WT) and Balb/c- <i>Ccr10</i> -deficient mice  | 63 |
| Figure 3.8 | Chronic UVB-irradiation causes a skin thickening in Balb/c wildtype mice (WT) but not in <i>Ccr10</i> -deficient mice  | 65 |
| Figure 4.1 | Schematic view of CCR10 signaling during skin homeostasis and cutaneous carcinogenesis   | 85 |

## 7 List of tables

|            |  |    |
|------------|--|----|
| Table 1.1  | Passive and active functions of the skin   | 3  |
| Table 2.1  | Number of total mice used for the 12-week early time point analysis after DMBA/TPA treatment                                     | 32 |
| Table 2.2  | Number of WT mice used in the analysis of epidermal thickness after 12 weeks of DMBA/TPA treatment                               | 33 |
| Table 2.3  | Number of <i>Ccr10</i> -deficient mice used in the analysis of epidermal thickness after 12 weeks of DMBA/TPA treatment          | 33 |
| Table 2.4  | Number of animals used for the late time point after 40 weeks of DMBA/TPA treatment  | 33 |
| Table 2.5  | Number of WT mice used for the listed analyses after 40 weeks of DMBA/TPA treatment  | 35 |
| Table 2.6  | Number of <i>Ccr10</i> -deficient mice used for the listed analyses after 40 weeks of DMBA/TPA treatment                         | 36 |
| Table 2.7  | Respective time periods of irradiation   | 36 |
| Table 2.8  | Number of total mice used for the 12-week early time point analysis after UVB-irradiation  | 38 |
| Table 2.9  | Number of WT mice used in the analysis of epidermal thickness after 12 weeks of UVB-irradiation                                  | 38 |
| Table 2.10 | Number of <i>Ccr10</i> -deficient mice used in the analysis of epidermal thickness after 12 weeks of UVB-irradiation             | 39 |
| Table 2.11 | Number of animals surviving to the late time point at week 70, following chronic UVB-irradiation for 60 weeks                    | 39 |
| Table 2.12 | Number of WT mice used for the listed analyses after 70 weeks following 60 weeks of chronic UVB-irradiation                      | 41 |
| Table 2.13 | Number of <i>Ccr10</i> -deficient mice used for the listed analyses after 70 weeks following 60 weeks of chronic UVB-irradiation | 41 |
| Table 2.14 | Touchdown PCR program for genotyping   | 45 |
| Table 2.15 | Reagents and concentrations for one PCR reaction   | 46 |
| Table 2.16 | PCR primer pairs for genotyping PCR  | 46 |

## 8 Vita

### Personal Information

|                |                  |
|----------------|------------------|
| Name           | Stephanie Müller |
| Date of birth  | 09/16/1983       |
| Place of birth | Essen, Germany   |

### Education

|           |  |
|-----------|--|
| 2018-     | Teacher, Gesamtschule Xanten-Sonsbeck, comprehensive school, Xanten, Germany                           |
| 2016-2018 | Teacher training, Gesamtschule Xanten-Sonsbeck, comprehensive school, Xanten, Germany                  |
| 2014-2016 | Doctoral student, Heinrich-Heine University Düsseldorf, Düsseldorf, Germany                            |
| 2011-2014 | Doctoral Scholar, Department of Dermatology, University Hospital Düsseldorf, Düsseldorf, Germany       |
| 2010-2011 | Doctoral Scholar, Clinic of Gastroenterology and Hepatology, Essen University Hospital, Essen, Germany |
| 2003-2009 | Diploma in Biology (Human Genetics, Faculty of Medicine) Ruhr University Bochum, Bochum, Germany       |
| 2000-2003 | Grashof Gymnasium, Academic High School, Essen, Germany  |
| 1994-2000 | Albert-Einstein-Realschule, Middle School, Essen, Germany  |

### Research Activities

|           |   |
|-----------|---|
| 2008-2009 | Diploma, Thesis Research on “Genetische Variabilität der angeborenen Immunabwehr und ihre Bedeutung in der Pathogenese der ANCA-assoziierten Vaskulitiden”<br>Ruhr University Bochum, Bochum, Germany |
|-----------|---|



## 9 Publications

### 9.1 Scientific articles

January 2010                      Stefan Wieczorek, Julia U. Holle, **Stephanie Müller**, Harald Fricke, Wolfgang L. Gross, Jörg T. Epplen, "A functionally relevant IRF5 haplotype is associated with reduced risk to Wegener's granulomatosis." J Mol Med 2010

May 2014                         CA. Husmann, JU. Holle, F. Moosig, **S. Mueller**, B. Wilde, JW. Cohen Tervaert, L. Harper, G. Assmann, WL. Gross, JT. Epplen, S. Wieczorek, "Genetics of toll like receptor 9 in ANCA associated vasculitides." Ann Rheum Dis. 2014

### 9.2 Poster

March 2014                      **Stephanie Müller**, Andreas Hippe, Juliane Noffke, Andreas Kislal, Erich Bünemann and Bernhard Homey  
"Skin carcinogenesis is reduced in immune deprived *Ccr10*-deficient mice"  
*Düsseldorf School of Oncology 'DSO-Retreat', Düsseldorf, Germany*

September 2014                **Stephanie Müller**, Andreas Hippe, Juliane Noffke, Andreas Kislal, Erich Bünemann and Bernhard Homey  
"Skin carcinogenesis is modulated in immune deprived *Ccr10*-deficient mice"  
*European Society for Dermatological Research 'The ESDR 2014', Copenhagen, Denmark*

## 10 Acknowledgements

An important chapter of my life is drawing to an end and a new chapter begins, therefore I would like to thank everyone, who accompanied and supported me, thank you so much!

First of all, I would like to express my sincere gratitude to my supervisor Prof. Dr. Bernhard Homey for giving me the opportunity to write my dissertation at the department of dermatology and for providing this deeply interesting research subject. I appreciate his scientific guidance, the helpful suggestions and the interesting discussions. I would particularly like to thank Prof. Dr. Johannes Hegemann for co-advising this work.

Additionally, I would like to offer special thanks to Dr. Andreas Hippe for the cooperation and supervision of my thesis. Finishing this dissertation would not have been possible without his patient guidance, advice and interesting discussions.

I want to thank all members of the laboratory for their competent and friendly help during my thesis. At this point, I would like to thank everybody for the pleasant working atmosphere and the valuable conversations.

I owe the most to my parents and my partner, Brian, who always encouraged and constantly supported me. You were always there for me whenever I needed you. Thank you for your loving support.

Finally, I would like to express my warm thanks to my dear friend Leonie. Now, it has been 15 years since we met each other and you still stand by my side by giving good advice and continuous encouragement. Thank you!

Last but not least, I want to thank Juliane Noffke, Heike Friedrich, Flora Smit, Kristin Plessner, Andreas Kislak and Holger Schrumph. Thank you for our time together, for all the helpful discussions and the friendship that has developed. Unbelievable that you made me go running. Without you it would not have been the same.

## 11 Declaration

I declare that this thesis was composed by myself and that I exclusively used the indicated literature and resources. The thoughts taken directly or indirectly from external sources are properly marked as such.

Ich versichere an Eides Statt, dass die Dissertation von mir selbständig und ohne unzulässige fremde Hilfe unter Beachtung der „Grundsätze zur Sicherung guter wissenschaftlicher Praxis an der Heinrich-Heine-Universität Düsseldorf“ erstellt worden ist.